

---

Electronic Thesis and Dissertation Repository

---

1-30-2020 2:00 PM

## Preparation of Intra-articular Drug Delivery Systems for the Treatment of Osteoarthritis

Ian Villamagna, *The University of Western Ontario*

Supervisor: Gillies, Elizabeth R., *The University of Western Ontario*

Co-Supervisor: Beier, Frank, *The University of Western Ontario*

A thesis submitted in partial fulfillment of the requirements for the Doctor of Philosophy degree in Biomedical Engineering

© Ian Villamagna 2020

Follow this and additional works at: <https://ir.lib.uwo.ca/etd>



Part of the [Biomaterials Commons](#)

---

### Recommended Citation

Villamagna, Ian, "Preparation of Intra-articular Drug Delivery Systems for the Treatment of Osteoarthritis" (2020). *Electronic Thesis and Dissertation Repository*. 6956.

<https://ir.lib.uwo.ca/etd/6956>

This Dissertation/Thesis is brought to you for free and open access by Scholarship@Western. It has been accepted for inclusion in Electronic Thesis and Dissertation Repository by an authorized administrator of Scholarship@Western. For more information, please contact [wlsadmin@uwo.ca](mailto:wlsadmin@uwo.ca).

## Abstract

Osteoarthritis (OA) is a degenerative disease of the articular joints that affects over 240 million people globally. Despite its overwhelming prevalence, there is no disease modifying agent currently available to treat the disease, and many treatment options remain palliative in nature. Potentially effective treatments for OA are limited by probable systemic side effects. Intra-articular drug delivery systems present a new opportunity for the treatment of OA; encapsulated therapeutics can be injected directly into the joint, at the area of injury, thereby bypassing systemic administration and diminishing the chance for side effects. This thesis describes the research and development of novel polymeric drug delivery systems for intra-articular administration. Initially, a polymer particle delivery platform using poly(ester amide) (PEA) was developed to encapsulate the non-steroidal anti-inflammatory drug celecoxib. Drug-loaded particles were successfully prepared, and were characterized physicochemically and biologically using *in vitro* and *in vivo* techniques. Drug was released *in vitro* from particles over a period of months, and no cellular toxicity from treatment with the particles was observed. The particles elicit a favorable host response *in vivo* when tested in an ovine model. The PEA particle delivery platform was further developed to encapsulate and deliver the small molecule, GSK3787, which had been previously implicated as a potential disease modifying agent for OA. The physicochemical properties of the particles were characterized including the measurement of the mechanical properties of individual particles by atomic force microscopy, and it was found that the modulus was in the range of articular cartilage. The drug-loaded and empty particles exhibited low toxicity to mammalian cells. In order to establish an even more prolonged release, and greater control over the system, a hybrid drug delivery system consisting of GSK3787-loaded PEA particles embedded within a thermally-responsive hydrogel was prepared. This system was evaluated to understand the effects of particle and drug incorporation on the gel properties including syneresis, Young's modulus, degradation, and toxicity. The release of GSK3787 from the hybrid system was slower *in vitro* than from hydrogel into which drug was directly loaded without particles. The hybrid system is promising for further *in vivo* evaluation. Overall, this thesis furthered the understanding of polymer drug delivery systems for intra-articular use, and led to the development of three new systems for potential use in treating OA.

Furthermore, for the first time, a means to deliver the potential disease modifying agent GSK3787 was developed.

## Keywords

Intra-articular, Drug delivery, Nanoparticle, Hydrogel, Osteoarthritis (OA), Emulsification, Scanning electron microscopy (SEM), Atomic force microscopy (AFM), Dynamic light scattering (DLS), Cell culture, Ovine, GSK3787, Celecoxib

## Summary for Lay Audience

Osteoarthritis (OA) is a degenerative disease of the joints that affected over 5 million Canadians in 2019, or 1 in 6 people in the country. The prevalence of the disease is continuing to rise, and it is estimated that 1 in 4 Canadians will be affected by OA in 2035. Despite its prevalence, non-surgical treatment options remain only modestly effective. Drug treatments for the disease are greatly limited by their systemic side effects. Non-steroidal anti-inflammatory drugs for instance, have proven effective at treating the pain associated with the disease, but have well documented gastrointestinal and cardiovascular side effects. While no disease modifying agents are currently used for OA treatment, there are a number of potential agents that cannot be given as traditional oral drugs due to potential negative side effects. In order to reduce these side effects and to open up the potential of using new disease modifying agents, drug delivery systems have been proposed. These systems are made from polymers that are well tolerated in the body, and are designed to encapsulate drug, then to be injected directly into the joint where they will begin to degrade, and slowly release the drug to the affected tissue over time. This thesis describes the research and development of three new drug delivery systems. All of the systems were developed to be injectable, and were tested for their physical, chemical and biological characteristics, to determine if they were suitable systems for the delivery of therapeutics in the treatment of OA. The three drug delivery systems developed in this work have the potential to alter the way that OA is treated, and increase the feasibility of curing the disease.

## Co-Authorship Statement

The work described here is the product of a collaborative effort between multiple parties across different universities. The individual contributions by chapter are listed below.

Chapter 1 was written by the author, and was edited by Dr. Elizabeth Gillies and Dr. Frank Beier.

Chapter 2 describes a study that was designed by the author, Dr. Elizabeth Gillies, and Dr. Mark Hurtig, a veterinarian at the University of Guelph. Experimentation was performed primarily by the author. Trent Gordon assisted with polymer synthesis, as well as particle preparation and characterization as a fourth year research project student that I mentored. Dr. Mark Hurtig performed intra-articular injections, synovial fluid and plasma sampling in animals, as well a histology. The manuscript was written by the author and was edited by Dr. Elizabeth Gillies, Dr. Frank Beier, and Dr. Mark Hurtig.

Chapter 3 describes a study that was designed by the author, Dr. Gillies, and Dr. Beier. Experimentation was primarily completed by the author, with assistance from Danielle McRae who was responsible for the designing and running atomic force microscopy (AFM) studies, and Aneta Borecki, who developed chromatography methods for drug quantification. The manuscript was primarily written by the author, except for the AFM procedure, which was written by Danielle McRae and edited by Dr. Francois Lagugné-Labarthe. The remainder of the manuscript was edited by Dr. Elizabeth Gillies and Dr. Frank Beier.

Chapter 4 describes a study designed by the author, David Andy Prince, and Dr. Elizabeth Gillies. Experimentation was completed by the author. David Andy Prince assisted in the synthesis of polymers, and Aneta Borecki was responsible for the development of chromatographic drug quantification methods. The manuscript was written by the author and edited by Dr. Elizabeth Gillies and Dr. Frank Beier.

Chapter 5 was written by the author and edited by Dr. Elizabeth Gillies and Dr. Frank Beier.

## Acknowledgments

This work was made possible through a CONNECT! NSERC Create training grant, as well as Western University's Bone and Joint Institute, and the School of Biomedical Engineering for providing funding and financial support.

I would like to thank my supervisors, Dr. Elizabeth Gillies and Dr. Frank Beier, for their roles in my training. I feel extremely fortunate to have supervisors who were not only great mentors, but also great people, who always had my best interest in mind, and supported a student with a young family.

Thank you to my committee members, Dr. Cheryle Seguin and Dr. Lauren Flynn for joining my supervisors to form an amazing, and immensely helpful team that I could lean on.

Thank you to Dr. Mark Hurtig, for being an excellent teacher and for allowing me to see a side of this work that I did not think I'd get to play a part in.

I would like to thank both the numerous Gillies and Beier lab members who I shared labs with over my time at Western. Special regards to Aneta Borecki and Dawn Bryce for all of their assistance.

Thank you to my siblings, Holly and Sean; I have always felt that I was the least intelligent of the three of us, and I still do for the most part, but now I can use Excel, so maybe the tides are changing.

I would not have made it to this point without my parents affording me the opportunities that I had. Thank you for everything you have done, and for your continued support of myself and my family.

My wife, the person who didn't think twice when I asked to move to a city in Canada that she'd never heard of. The person who willingly got into a dilapidated Jeep that could barely get out of first gear, and drove across the country with me. The person who has taken every twist and turn throughout this, and handled it all with a grace and poise that I can only strive to achieve. Thank you for everything, but mostly thank you for being you.

Finally, to my children, Lana and Cara. I could spend a lifetime, and I would not be able to articulate my gratitude to you both. People ask me all the time how I managed children while getting my degree, but the truth is I can't imagine it any other way; because at the end of the day I wasn't a student, or a scientist, nor was I an engineer, or a candidate. I was just your dad, and that's all I ever wanted to be. I could get ten more degrees, and any pride would pale in comparison to the pride I feel from simply being your dad.

# Table of Contents

Abstract.....	ii
Summary for Lay Audience.....	iv
Co-Authorship Statement.....	v
Acknowledgments.....	vi
Table of Contents.....	viii
List of Tables.....	xiv
List of Figures.....	xv
List of Appendices.....	xx
List of Abbreviations.....	xxi
Chapter 1.....	1
1.1 Introduction.....	1
1.2 OA: Definition, Prevalence, Cost and Impact.....	2
1.2.1 The disease.....	2
1.2.2 Prevalence of OA.....	3
1.2.3 Risk Factors.....	4
1.3 Costs of OA.....	5
1.4 Joint physiology and OA pathophysiology.....	6
1.4.1 Articular cartilage physiology.....	6
1.4.2 Pathophysiology of articular cartilage in OA.....	7
1.4.3 Subchondral bone physiology.....	8
1.4.4 Pathophysiology of subchondral bone in OA.....	9
1.4.5 Physiology of synovial membrane.....	10
1.4.6 Pathophysiology of synovial membrane in OA.....	11
1.4.7 Physiology of synovial fluid.....	12

1.4.8	Pathophysiology of synovial fluid in OA .....	12
1.5	Disease onset, diagnosis and progression .....	12
1.6	Current treatments.....	13
1.6.1	Non-Pharmacologic treatment .....	14
1.6.2	Pharmacologic therapy.....	14
1.6.3	Systemic pharmacologic treatment.....	15
1.6.4	Intra-articular injections.....	16
1.6.5	Joint replacement .....	16
1.7	Potential disease modifying agents.....	17
1.7.1	Disease Modifying Agents Targeting Pain.....	17
1.7.2	Ion Channels .....	18
1.7.3	Nerve Growth Factor .....	19
1.7.4	Other pain receptor targeted disease modifying agents .....	19
1.7.5	Disease Modifying Agents targeting Inflammatory Modulation.....	20
1.7.6	Cytokines .....	20
1.7.7	Other Inflammatory Pathways as Potential Disease Modifying Agent Targets.....	21
1.8	PPAR $\delta$ Antagonists as a DMA for OA treatment .....	22
1.9	Intra-articular drug delivery systems .....	23
1.9.1	Liposomes.....	24
1.9.2	Nanoparticles .....	26
1.9.3	Microparticles .....	28
1.9.4	Hydrogels.....	32
1.10	Project overview .....	40
1.10.1	Hypothesis.....	41
1.10.2	Specific Aims.....	42

1.11	References .....	42
Chapter 2 .....		62
2	Poly(ester amide) particles for controlled delivery of celecoxib .....	62
2.1	Introduction.....	62
2.2	Materials and Methods.....	62
2.2.1	General materials and procedures .....	64
2.2.2	Tensile testing.....	64
2.2.3	Contact angle measurements.....	64
2.2.4	Preparation of particles .....	65
2.2.5	Scanning electron microscopy (SEM) .....	65
2.2.6	Determination of drug loading and encapsulation efficiency .....	65
2.2.7	<i>In vitro</i> release of CXB .....	66
2.2.8	<i>In vitro</i> degradation of particles in PBS.....	67
2.2.9	Cell culture.....	67
2.2.10	<i>In vitro</i> toxicity .....	67
2.2.11	<i>In vivo</i> host response.....	68
2.3	Results.....	64
2.3.1	Particle preparation and characterization.....	68
2.3.2	<i>In vitro</i> release of CXB and particle degradation .....	73
2.3.3	<i>In vitro</i> and <i>in vivo</i> studies .....	75
2.4	Discussion.....	79
2.5	Conclusions.....	85
2.6	References.....	68
Chapter 3.....		90
3	Preparation and Characterization of Poly(ester amide) Particles Loaded with the PPAR $\delta$ Antagonist GSK3787 .....	90

3.1	Introduction.....	90
3.2	Materials and Methods.....	92
3.2.1	General materials and procedures.....	92
3.2.2	GSK3787 loaded particle preparation (PBSe-GSK3787).....	93
3.2.3	Non-drug-loaded particle preparation (PBSe-NDL).....	94
3.2.4	Dye-labeled particle preparation.....	94
3.2.5	Scanning electron microscopy (SEM) .....	94
3.2.6	Determination of drug loading and encapsulation efficiency .....	94
3.2.7	Atomic force microscopy of PBSe-GSK3787 and PBSe-NDL.....	95
3.2.8	<i>In vitro</i> release of GSK3787 .....	96
3.2.9	Primary chondrocyte harvest and culture .....	96
3.2.10	Cytotoxicity of GSK3787 to IMAC cells .....	97
3.2.11	Cytotoxicity of PBSe-GSK3787 and PBSe-NDL to IMAC cells.....	98
3.2.12	Brightfield imaging of IMAC cells treated with PBSe-GSK3787 particles .....	98
3.2.13	IMAC staining and confocal microscopy .....	98
3.2.14	<i>Ex vivo</i> intra-articular injection of PBSe-GSK3787-IR.....	99
3.3	Results and Discussion .....	99
3.3.1	Preparation and characterization of PBSe particles.....	99
3.3.2	<i>In vitro</i> release of GSK3787 .....	104
3.3.3	Cytotoxicity of GSK3787, PBSe-GSK3787, and PBSe-NDL on primary cell cultures .....	105
3.3.4	<i>Ex vivo</i> intra-articular injections .....	108
3.4	Conclusions.....	109
3.5	References.....	90
	Chapter 4.....	118

4	Thermo-responsive hybrid particle in hydrogel delivery system for intra-articular drug delivery.....	118
4.1	Introduction.....	118
4.2	Materials and Methods.....	120
4.2.1	General materials and procedures.....	120
4.2.2	Preparation of hydrogels.....	121
4.2.3	Scanning electron microscopy (SEM).....	121
4.2.4	Measurement of hydrogel syneresis.....	122
4.2.5	Hydrogel degradation.....	122
4.2.6	Measurement of Young's moduli under compression.....	122
4.2.7	<i>In vitro</i> release of GSK3787 from hydrogels in PBS.....	123
4.2.8	Primary articular chondrocyte harvest and culture.....	123
4.2.9	Toxicity assays on IMAC cells.....	123
4.2.10	Statistical Analyses.....	124
4.3	Results and Discussion.....	124
4.3.1	Preparation of materials.....	124
4.3.2	Preparation and characterization of hydrogels.....	125
4.3.3	Primary cell toxicity from hydrogel systems.....	131
4.4	Conclusions.....	132
4.5	References.....	133
Chapter 5	.....	139
5	Conclusions and Future Work.....	139
5.1	Conclusions.....	139
5.1	Future Directions.....	143
5.2	References.....	145
6	Appendices.....	148

6.1 Appendix A: Supplemental Information for Chapter 2 .....	148
6.2 Appendix B: Supplemental Information for Chapter 3.....	154
6.3 Appendix C: Supplemental Information for Chapter 4.....	158
6.4 Appendix D: Permissions .....	163
Curriculum Vitae .....	168

## List of Tables

Table 2.1: Average diameters of the PEA-based particles obtained by DLS and SEM and CXB loading and encapsulation efficiency measured by NMR spectroscopy. Errors correspond to the standard deviations on triplicate measurements of three different particle compositions. ....	71
Table 2.2: Young's moduli and ultimate tensile strengths of the polymers and their blends with CXB, as measured by tensile testing in water at 37 °C and contact angles of polymer films. Errors on the measurements correspond to the standard deviations of triplicate samples.....	73
Table 3.1: Physiochemical characteristics of PBSe-GSK3787 and PBSe-NDL particles....	102
Table 4.1: Hydrogel preparations and their physiochemical properties. ....	125

# List of Figures

Figure 1.1: The relationship between abnormal mechanical stress and abnormal physiological factors in OA. Adapted with permission from reference 12. Copyright 2011, Elsevier..... 3

Figure 1.2: The structure of articular cartilage. Reproduced with permission. Copyright Mary Ann Liebert, 2018. .... 7

Figure 1.3: Illustration of articular cartilage and subchondral bone. Reproduced with permission from Karsdal et al. Copyright Elsevier, 2008..... 9

Figure 1.4: Histological preparation of the synovial membrane. Reproduced with permission. Copyright 2011, Bentham Open. .... 10

Figure 1.5: An outline of the current treatments for OA. .... 13

Figure 1.6: The structure of a liposome. .... 24

Figure 1.7: The structure of a solid core polymer nanoparticle. .... 26

Figure 1.8: Hydrogel networks with varying gelation mechanisms. (A) Shows physical crosslinking with two proposed mechanisms: bridging of hydrophilic chains (top left), and micelle agglomeration (bottom left). (B) Shows a covalently crosslinked network before and after gelation is induced. Polymer chains seen in blue have covalently crosslinkable groups on their backbone (green). .... 32

Figure 1.9: PCLA-PEG-PCLA structure. .... 34

Figure 1.10: The mixture of Pluronic F127 and Hyaluronic acid to form a hydrogel. Reproduced with permission from reference 157. Copyright 2017, Elsevier..... 36

Figure 1.11: Chemical structure of DPGS and hydrogel formation. Reproduced with permission from reference 162. Copyright 2017, Elsevier. .... 39

Figure 2.1: Chemical structures of the polymers PBSe and POSe. .... 69

Figure 2.2 Size and Morphology of Celecoxib particles. A) DLS diameter distributions by volume % for CXB and non-drug-loaded particles made from either PBSe or POSe; B-E) SEM micrographs of prepared particles showing their spherical structures and size distributions: B) PBSe-NDL; C) PBSe-CXB; D) POSe-NDL; E) POSe-CXB. Material surrounding the particles in B and D is likely PVA..... 70

Figure 2.3 DSC thermograms of drug-loaded and non-drug-loaded particles. DSC traces showing that the T<sub>g</sub> was increased through CXB incorporation only for PBSe. A subtle transition corresponding to PVA was observed at 60 – 70 °C but no melting temperature was observed for CXB. .... 72

Figure 2.4: CXB release from PBSe-CXB particles and POSe-CXB particles performed in pH 7.4 PBS containing 2 wt% Tween 20 showing slower release of CXB from the PBSe-CXB particles. The release of insoluble free CXB through the dialysis membrane was also measured as a control to show that the release rate was not limited by the drug dissolution rate..... 74

Figure 2.5: Degradation of PEA particles in pH 7.4 PBS at 37 °C. A-C) PBSe-CXB particles after A) 14, B) 30 and C) 60 days; D-E) POSe-CXB particles after D) 7 and E) 14 days. All images were obtained at the same magnification. While particles were still observed for PBSE-CXB at 60 days, most of the POSe-CXB particles were rapidly eroded. .... 75

Figure 2.6: Metabolic activity of ATDC5 cells as treated with increasing concentrations of CXB. As measured by MTT assay. Metabolic activity reported as an average percentage of control cells (mean ± SD), N=4. .... 76

Figure 2.7 Metabolic activity of C2C12 cells as treated with increasing concentrations of CXB. As measured by MTT assay. Metabolic activity reported as an average percentage of control cells (mean ± SD), N=4. .... 76

Figure 2.8: Metabolic activity of cells treated with particles. A) ATDC5 cells and B) C2C12 cells as measured by an MTT assay after a 48 h incubation with PBSe-CXB or PBSe-NDL particles. Reported as mean ± SD. (N = 4). .... 77

Figure 2.9: Synovial fluid analysis of injected sheep joints. A) Protein levels in synovial fluid at days 0, 8 and 15. \* Indicates a significant difference between day 0 and day 8. (ANOVA  $p = 0.04$ ) B) WBC levels at days 0, 8 and 15. \* Indicates a statistically significant difference between day 0 and day 8 (ANOVA  $p = 0.0001$ ).  $N = 4$  at days 0 and 8 and  $N = 2$  at day 15. 78

Figure 2.10: Immunohistochemical analysis of the synovial membrane of an injected sheep 15 days post injection. Hematoxylin and eosin staining was performed on sections of sheep synovium. Particles are visible within the membrane (indicated with red arrows). ..... 79

Figure 3.1: Chemical structures of PBSe and GSK3787. .... 100

Figure 3.2: Scanning electron micrographs of particles (A) PBSe-GSK3787 and (B) PBSe-NDL particles showing their spherical morphologies and diameters in the solid state; (C) DLS diameter distributions by volume % of PBSe-GSK3787 and PBSe-NDL particles showing the smaller diameters of the drug-loaded particles. .... 101

Figure 3.3: Differential scanning calorimetry of GSK3787, PBSe-NDL, and PBSe-GSK3787. DSC shows a  $T_m$  for the drug and for phase separated drug in the particles. Particles both with and without drug had very similar  $T_g$  values, again suggesting phase separation of the drug in the particles. .... 103

Figure 3.4: AFM image of a PBSe-GSK3787 particle. (A) showing the grid corresponding to the measurement of the modulus taken at 100 different points on a particle. (B) Representative approach and withdrawn curves that were used to calculate the modulus... 104

Figure 3.5: Cumulative release of GSK3787 at 37 °C in PBS containing 2 wt% polysorbate 80. Slower release of GSK3787 was observed from PBSe-GSK3787 particles compared to the free drug. Error bars correspond to the standard deviations on three separate particle populations in dialysis bags. .... 105

Figure 3.6: Metabolic activity of IMAC cells, as measured by MTT assay. 48 h after treatment with A) increasing concentrations of the PPAR $\delta$  inhibitor, GSK 3787 and B) PBSe-GSK3787 and PBSe-NDL particles. No significant toxicity was observed for the free drug or for PBSe-NDL. However, a trend towards higher toxicity was observed for PBSe-GSK3787 particles. Error bars correspond to standard deviations ( $N = 4$ ). .... 106

Figure 3.7: Brightfield images of live IMAC cells. Treated with A) no particles; B) 150  $\mu\text{g}/\text{mL}$  of PBSe-GSK3787 particles; C) 1000  $\mu\text{g}/\text{mL}$  of PBSe-GSK3787 particles. The particles agglomerated and adhered to the outsides of the cell membranes. Healthy cell morphologies were observed for cells treated with 150  $\mu\text{g}/\text{mL}$ , whereas the cells were almost completely coated with particles at 1000  $\mu\text{g}/\text{mL}$ . ..... 107

Figure 3.8: Confocal microscopy images of IMAC cells. Treated with 100  $\mu\text{g}/\text{mL}$  PBSe-GSK3787-NR particles (red) for 48 h, then stained with AlexaFluor 488 Phalloidin (green, cytoskeletons) and DAPI (blue, nuclei): A) 2D image showing agglomerates of particles on the cells; B) 3D rendering of cells showing particles localized at the cell surface and not taken up by the cells. .... 108

Figure 3.9: Representative knee joint explant from a C57BL/6 mouse that was injected with 5  $\mu\text{L}$  of a 100  $\text{mg}/\text{mL}$  suspension of PBSe-GSK3787-IR particles. Upon resection of the limbs, images were taken with a stereoscope to determine injectability and localization of particles. Images taken 7 days post injection of (A) Knee joint at 7.3x magnification; (B) Knee joint at 1.6x magnification; (C) Particles as visualized in the joint under fluorescence microscopy, 1.6x magnification. .... 109

Figure 4.1: Schematic illustrating the proposed particle in hydrogel hybrid drug delivery system ..... 120

Figure 4.2: Chemical structures and particle SEM. A) Chemical structure of PBSe; B) Representative SEM image of PBSe-GSK3787 particles; C) Chemical structure of PCL-PEG-PCL. .... 125

Figure 4.3: SEM micrographs of: A) Control hydrogel; B) GSK3787 hydrogel; C) PBSe-GSK3787 particles in hydrogel. .... 127

Figure 4.4: DSC thermograms for control hydrogel, GSK3787 hydrogel, and PBSe-GSK3787 hydrogel. Direct incorporation of GSK3787 disrupts packing of the caprolactone domains, resulting in disappearance of the melting endotherm, while the incorporation of PBSe-GSK3787 particles does not greatly affect the thermal properties relative to the control, likely

due to their incorporation into the aqueous domains of the hydrogel. A small exotherm at  $-35$  °C in the PBSe-GSK3787 hydrogel likely corresponds to cold crystallization..... 127

Figure 4.5: Syneresis of hydrogel systems. Measurement of the water loss from the hydrogels showing less than 10% syneresis for the control, drug-loaded, and particle-loaded hydrogels over 24 h. The Measurements were performed in triplicate and the error bars correspond to the standard deviations..... 128

Figure 4.6: Percent mass remaining over time for hydrogel systems at 37 °C, in PBS. Incorporation of GSK3787 or PBSe-GSK3787 particles resulted in more rapid degradation of the gels. All measurements were performed in triplicates, and the error bars correspond to the standard deviations. Error bars on the control hydrogel are too small to be visible..... 129

Figure 4.7: Stress-strain curves of three hydrogel systems, as measured in PBS at 37 °C. All measurements were performed in triplicates, and the error bars correspond to the standard deviations. .... 130

Figure 4.8: Release of GSK3787 from GSK3787 hydrogel and PBSe-GSK3787 hydrogel in PBS at 37 °C. Slower release from the particle in hydrogel system is noted. The experiments were performed in triplicate and the error bars correspond to the standard deviations..... 131

Figure 4.9: Metabolic activity of IMAC cell cultures when treated with leachate media from three different hydrogel preparations. Control hydrogel, GSK3787 hydrogel and PBSe-GSK3787 were soaked in media for 14 days before being added to cells for 48 hours. Metabolic activity was tested by MTT assay. All samples were performed with three biological replicates, and six technical replicates per plate. Plotted as mean absorbance  $\pm$  standard error (N = 4). .... 132

## List of Appendices

Appendix A: Supplemental Information for Chapter 2.....	145
Appendix B: Supplemental Information for Chapter 3.....	151
Appendix C: Supplemental Information for Chapter 4.....	156
Appendix D: List of Permissions.....	162

## List of Abbreviations

ACLT	Anterior cruciate ligament transection
AFM	Atomic force microscopy
BSA	Bovine serum albumin
CBD	Cannabidiol
CDC	Center for disease control
CL	Caprolactone
COX	Cyclooxygenase
CS	Chondroitin sulfate
CT	Computed tomography
CXB	Celecoxib
DAPI	4',6-diamidino-2-phenylindole
DGPS	Dendritic poly (glycerol sulfate)
DI	Deionized
DL	Drug loading
DLS	Dynamic light scatter
DMA	Disease modifying agent
DMEM	Dulbecco's modified eagle medium
DMF	Dimethylformamide
DMSO	Dimethyl sulfoxide
DSC	Differential scanning calorimetry
ECM	Extracellular matrix
EE	Encapsulation efficiency
FBS	Fetal bovine serum
FDA	Food and Drug Administration
GAG	Glycosaminoglycan

GSK	GlaxoSmithKlein
HA	Hyaluronic acid
HPLC	High performance liquid chromatography
IA	Intra-articular
IL	Inter-leukin
IMAC	Immature murine articular chondrocytes
IQR	Interquartile range
ITS	Insulin transferrin selenium
KPS	Potassium persulfate
LA	Lactic acid
MAPK	Mitogen-activated protein kinase
MEM	Minimum essential media
MMP	Matrixmetalloproteinase
MRI	Magnetic resonance imaging
MTT	3-(4,5-dimethylthiazol-2-yl)-2,5-diphenyltetrazolium bromide
NAV	Sodium channel voltage gated
NDL	Non-drug loaded
NF-kb	Nuclear factor kappa beta
NGF	Nerve growth factor
NMR	Nuclear magnetic resonance
NR	Nile red
NSAID	Non-steroidal anti-inflammatory drug
OA	Osteoarthritis
OARSI	Osteoarthritis Research Society International
OTC	Over the counter
PBS	Phosphate buffered saline

PBSe	Phenylalanine butane diol sebacate
PCLA	Poly(caprolactone- <i>co</i> -lactide)
PDA	Photodiode array
PDI	Polydispersity index
PEA	Poly(ester amide)
PEG	Poly(ethylene glycol)
PF	Pluronic F127
PFA	Paraformaldehyde
PLA	Poly(lactic acid)
PLGA	Poly(lactic- <i>co</i> -glycolic acid)
PMMA	Poly(methyl methacrylate)
PMMX	Partial medial meniscectomy
POSe	Phenylalanine octanediol sebacate
PPAR	Peroxisome proliferated activated receptor
PTOA	Posttraumatic osteoarthritis
PVA	Poly(vinyl alcohol)
PX	Piroxicam
SDS	Sodium dodecyl sulfate
SEC	Size exclusion chromatography
SEM	Scanning electron microscopy
SNRI	Serotonin-norepinephrine reuptake inhibitor
TA	Triamcinolone acetonide
TEMED	Tetramethylethylenediamine
TG	Triglycerol monostearate
TNF	Tumor necrosis factor
TrkA	Tropomyosin receptor kinase A

TRPV1	Transient receptor potential cation channel subfamily V member 1
UV	Ultraviolet
WBC	White blood cell

# Chapter 1

## 1.1 Introduction

Osteoarthritis (OA) is a leading cause of chronic disability in Canada, with annual costs projected to reach \$7.6 billion by 2031.<sup>1</sup> More than 3 million Canadians, and 27 million Americans currently suffer from this disease, which dramatically reduces mobility, independence, and quality of life for affected patients.<sup>2,3</sup> OA is also a significant risk factor for many other diseases such as cardiovascular and metabolic diseases, as well as depression.<sup>4</sup> It is a progressive disease, involving the breakdown of joint cartilage, synovium, and bone. Currently, no disease modifying agents are available to treat OA, and care remains mostly palliative. While medications such as anti-inflammatory drugs can be taken to manage pain and improve joint function, they suffer from significant side effects and do not alter the disease progression.<sup>5</sup> Joint replacement as a treatment for end-stage disease also comes with limitations such as risk of infection, potential implant failure, and altered biomechanics that can cause degenerative changes in other parts of the body.<sup>6</sup>

In an effort to elucidate new disease modifying agents (DMA) to treat OA, increasing research has been performed studying the underlying mechanisms and molecular processes that take place in OA. Recent studies have identified the peroxisome proliferator-activated receptor  $\delta$  (PPAR $\delta$ ), as a potential target for slowing or halting the disease.<sup>7,8</sup> The inhibition of PPAR $\delta$  has shown strong potential to provide protective effects for OA in animal models, as further discussed in section 1.8 of this review.<sup>9</sup> Commercial PPAR $\delta$  antagonists are available, however they remain clinically unsuitable for use. PPAR $\delta$  receptors are present in a multitude of tissues in the body, and play important roles in fat oxidation and brain function.<sup>10,11</sup> As such, there is a potential for adverse side effects resulting from systemic administration of PPAR $\delta$  antagonists. As with many other potential DMAs, PPAR $\delta$  antagonists could benefit from injection directly into the joint, where drug levels could be high enough to elicit a response, without causing systemic side effects. Delivery of medications directly into the joint

however is subject to rapid clearance by the lymphatic system of the joint. As such, the need for a drug delivery system becomes apparent for intra-articular (IA) administration of a number of different drugs. These systems would provide a prolonged release of drug, in a high dosage, directly to the area of injury, but would not be subject to clearance due to their larger size. This chapter aims to provide a comprehensive review of drug delivery systems for IA use, through understanding OA as a disease, its pathophysiology, potential DMAs, and different examples of IA drug delivery systems.

## 1.2 OA: Definition, Prevalence, Cost and Impact

### 1.2.1 The disease

OA is a degenerative disorder of the joints that is the most common form of clinically presented arthritis.<sup>1</sup> The disease is multi-faceted, and affects all of the different tissues that make up joints, including cartilage, synovium, and bone.<sup>12</sup> The disease can present in one or multiple joints. OA can occur in weight-bearing joints, such as the knees or hips, but can also be found in non-weight-bearing joints, such as those within the hand.<sup>13</sup> For many years the disease was categorized as a mechanical disease, caused by wear and tear of joints and joint tissues over time. While it is understood that mechanical forces play an important role in the development and progression of OA, more recently, molecular mechanisms have been studied in an attempt to better understand the pathophysiology of the disease. The upregulation of pro-inflammatory cytokines, which can lead to increases in matrix metalloproteinases, has been shown to lead to the increase in catabolism of joint tissues, and the decrease of anabolic processes that can repair these tissues.<sup>14</sup> The relationship between mechanical and molecular factors in OA is becoming increasingly understood, as it is believed that both can play an active role in the disease. An altered mechanical loading of the joints can lead to abnormal stresses, which can change the physiology of the joint, whereas an altered physiology, such as inflammation, can cause an altered mechanical loading, furthering the progression of the disease activity.<sup>15</sup> Figure 1.1 shows the relationship between mechanical and molecular factors in OA.

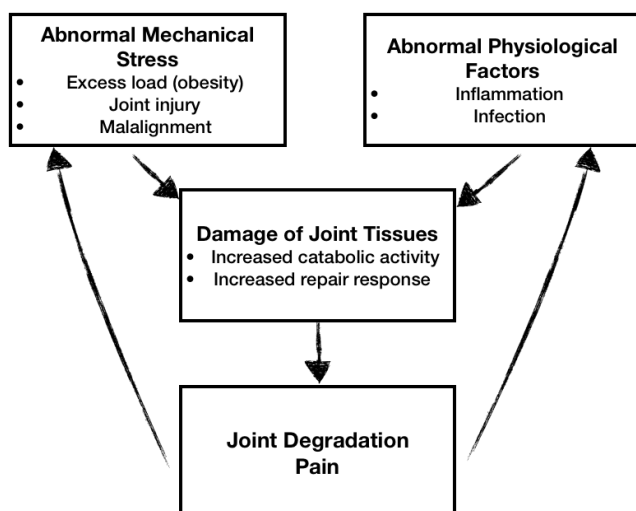


**Figure 0.1: The relationship between abnormal mechanical stress and abnormal physiological factors in OA.** Adapted with permission from reference 12. Copyright 2011, Elsevier.

### 1.2.2 Prevalence of OA

OA is an extremely common disease and continues to be a major challenge for healthcare systems as the prevalence continues to rise. In 2019, a study published by Zhao *et al.* reported on the prevalence of OA based on patients who sought treatment for the disease, and it was estimated that the prevalence of OA in the United States was 10.5% of the population, or 26.5 million people.<sup>4</sup> Over the age of 75, it was estimated that the percentage of people with OA in the US was higher than 25%. In Canada, it was estimated in 2014 that OA affects 10% of the population over the age of 15, and that over 45% of people over the age of 65 reported the disease in at least one joint.<sup>16</sup> Furthermore, Canadian studies estimated that the average onset age of the disease was in the late 40s, but that patients went an average of over 7 years before actual diagnosis of the disease by a physician.<sup>16</sup> The rising prevalence of OA shows no signs of slowing, with the Center for Disease Control (CDC) projecting that by 2030, 67 million adults, corresponding to 25% of the population over 18 will have OA.<sup>17</sup> This is compared with the 52.5 million adults in 2010-2012.

While the overall numbers of patients with clinically diagnosed OA can be overwhelming, one of the more prevalent recent statistics is the emerging population developing OA at a younger age. The rise in prevalence has been a long-standing issue, with studies suggesting in 2017 that OA prevalence had doubled since the mid 20<sup>th</sup> century, attributing it to a number of different factors.<sup>18</sup> This increase in younger populations being affected by OA has also resulted in sharp increases in younger populations receiving joint replacement surgeries, burdening the healthcare systems with extremely high costs.<sup>5,19,20</sup>

### 1.2.3 Risk Factors

OA has been associated with a number of different risk factors. These include, but are not limited to, age, genetic susceptibility, obesity, gender, trauma, muscle weakness, repetitive motions and meniscal or ligament damage.<sup>19</sup> It is well known that age is the largest risk factor that contributes to OA. It has been hypothesized that the increased prevalence of OA with age is tied to normal biological factors and changes in tissues that also increase naturally with age.<sup>2</sup> The thinning of cartilage, loss of muscle mass, and oxidative damage all occur more frequently in older populations, and can make joints more susceptible to damage from other risk factors, such as mechanical damage.

Obesity is another risk factor that has an overwhelming prevalence in OA. It is believed that obesity plays both mechanical and metabolic roles that lead to the onset and progression of the disease.<sup>20,21</sup> Increased loading of the joint due to extra weight is a likely mechanism by which OA occurs due to obesity. Simply overloading of the joint however is not believed to be the sole cause of obesity induced OA, with failure of ligamentous and other structural support believed to cause further joint damage and play a key role in disease development. A recent meta-analysis of studies that looked at weight loss in OA showed a 5% weight reduction was sufficient to improve symptoms of the disease.<sup>22</sup>

Genetic factors have also been shown to play a role in the development of OA. Studies performed on twins, and closely related family members have shown that there is an inheritable component of OA, and that there is a larger genetic influence for joints that

are less affected by mechanical forces, such as hand OA.<sup>23</sup> Furthermore, genome-wide association studies have recently identified specific loci on chromosomes that have been tied to an increased prevalence of hand and knee OA.<sup>24</sup>

A number of other risk factors exist for OA, such as joint injuries, bone diseases, metabolic disorders, repeated stresses, and infections. Injuries to joints have been increasingly studied and accepted as a means to induce OA. A number of studies have recently tied injuries that occur from sports, or work-related injuries to the development of OA. One specific subset of the disease, posttraumatic OA (PTOA), develops after injuries to the joint. PTOA has been found to account for roughly 10% of all new cases of OA, and can occur after any number of injuries to the tissues of the joint.<sup>25</sup>

### 1.3 Costs of OA

The direct healthcare costs associated with OA to various healthcare systems in the world can vary greatly due to the population, as well as the way healthcare is managed in the respective countries. Direct costs for OA can include, but are not limited to, pharmaceuticals, hospitalization, diagnostics, physician visits, rehabilitation, transport and physiotherapy.<sup>5,8,21</sup> In the United States, it was estimated in 2019 that the overall cost of OA on the healthcare system was over \$190 billion US.<sup>4</sup> The out of pocket costs for healthcare in OA patients was reported to be roughly \$1400 per year in the United States, more than double what non-OA sufferers pay. The use of informal care, such as trips to the pharmacy, over-the-counter (OTC) medications or other treatments can be high for OA patients, though it is not as often reported, and is hard to fully tabulate.<sup>25</sup>

Countries with smaller populations, such as Canada, do not have overall charges at the same magnitude of the US, but still carry a significant burden from the direct costs of OA. It was estimated that in 2010, the direct cost of OA to the Canadian healthcare system was \$2.1 billion, but that it was expected to rise to \$7.9 billion by 2030.<sup>8</sup> OA is also associated with a high number of indirect costs as well. These can be things such as absenteeism from a workplace for an OA patient, or the lack of productivity due to the illness.<sup>22,23</sup> Premature retirement and even the increased risk of mortality accounts for another loss of potential income for OA patients.<sup>24</sup>

## 1.4 Joint physiology and OA pathophysiology

OA is a disease of the entire joint, with each of the different tissue types that make up the joint affected by the disease in different ways. Synovial joints make up the majority of human joints and allow for free movement. These are the joints that are affected by OA, and are mainly comprised of subchondral bone, synovium, cartilage, and have a viscous synovial fluid that fills the joint space.

### 1.4.1 Articular cartilage physiology

The two bones that make up a joint are covered with articular cartilage. When healthy, articular cartilage has a smooth surface that exhibits a low coefficient of friction—allowing the bones that make up joint to move freely and smoothly.<sup>13</sup> It is viscoelastic and is designed to distribute loads across the joint evenly. A 2009 review by Fox *et al.* described the components and cellular make-up of articular cartilage.<sup>26</sup> The cells within cartilage, chondrocytes, produce extra cellular matrix (ECM), which has two major components in cartilage: collagen type 2 and proteoglycans. Proteoglycans consist of a core protein and multiple glycosaminoglycan (GAG) chains. GAGs are polysaccharides that have negative charges and are used to form proteoglycans which are highly negatively charged molecules. The negative charge of the GAGs allows for the movement of charged molecules into the joint, and creates an environment in which water can fill, thereby swelling the cartilage tissue.<sup>27</sup> The swelling with water is what allows the cartilage to be load bearing, and to dissipate the forces that occur from the compression of the joint by the subchondral bone. The two GAGs found in the joint are chondroitin sulfate (CS) and hyaluronic acid (HA).

Articular cartilage is typically 2-4 mm thick, and is comprised of distinct layers, each with different properties (Figure 1.2). In each of these zones, cells have different morphologies, activities, and arrangements, and there are differing chemical and physical compositions. The first zone in cartilage typically consists of flattened cartilage cells, or chondrocytes, that make up a dense superficial layer. This layer comes into contact with the synovial fluid, and shear forces of the joint. This first layer is also described as having

collagen fibers that are tightly packed, and horizontally aligned. Immediately below the superficial zone of cartilage is the middle zone. This area makes up the bulk of the cartilage volume and it contains proteoglycans and thicker collagen fibrils. In this layer, the collagen is not organized horizontally, and packs less closely than in the superficial zone. Chondrocytes in this zone are at a lower density and are spherical. This zone is required for absorbing the immediate mechanical forces on the cartilage tissue. The deep zone of the cartilage has collagen fibers and chondrocytes that are arranged perpendicular to the surface of the cartilage, and absorb the bulk of the load that is exerted on cartilage tissue. Finally, the calcified zone is a dense bottom layer that has the highest proteoglycan and collagen content of the tissue, in addition to chondrocytes which are densely packed in vertical formation.

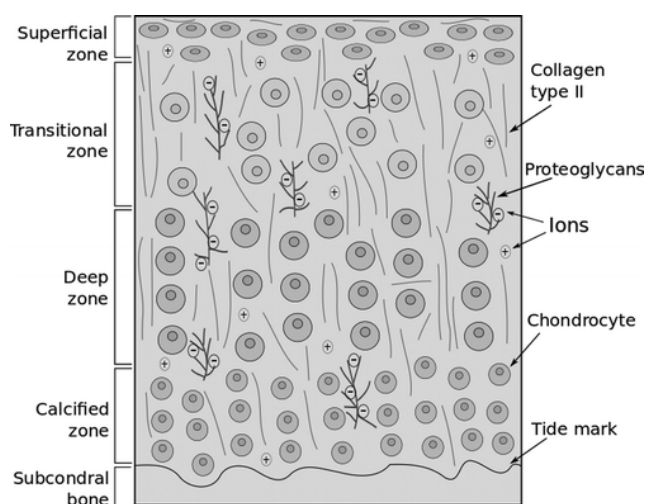


**Figure 0.2: The structure of articular cartilage.** Reproduced with permission.

Copyright Mary Ann Liebert, 2018.

#### 1.4.2 Pathophysiology of articular cartilage in OA

The cartilage is often thought of as one of the most altered tissues in OA. Radiographic imaging can show the degradation of cartilage, as well as overall thinning of the tissue.<sup>28</sup> It is well documented that an increase in catabolic factors and decrease in anabolic factors leads to damage of cartilage in OA.<sup>14</sup> The change in the balance of anabolism to catabolism has been increasingly studied, however, the overall reasons and causes behind

this change remain unclear. Once the breakdown of cartilage has begun, it is extremely difficult to repair. Cartilage is not known for its self-healing capacity, because chondrocytes typically have a very low proliferation rate.<sup>29</sup> Furthermore, the cartilage tissue is avascular, meaning it is difficult for new growth factors or repair molecules to make their way to the tissue. The leaking of proteoglycans from the damaged cartilage have been shown to cause synovial inflammation, thereby leading to further progression of the disease.

Mechanical degradation of cartilage plays a large role in the pathophysiology of OA as well. While normal physiologic loading in joints is protective, and actively required to maintain proper cartilage thickness, the unphysiological loading can cause damage to joints. In 2018 Cooke *et al.* showed that the dynamic loading of human cartilage tissue led to an increase in the surface roughness and cartilage degradation.<sup>30</sup> While the change was noted in healthy cartilage tissue, it was largely altered in tissue that had been previously diagnosed with OA. Histological preparations showed visible damage in cartilage after dynamic loading as well, and the damage was once again much worse in OA patients. The work suggested that mechanical damage can cause cartilage degradation, and once there is already degradation, the tissues are far more susceptible to further damage.

### 1.4.3 Subchondral bone physiology

Subchondral bone refers to the bone that forms an interface between the calcified cartilage and the trabecular bone (Figure 1.3).<sup>31</sup> To date, the exact definition has been slightly ambiguous with different researchers having different interpretations of the components of the bone, as well as its depth. The bone is typically described as having a plate where there is an immediate separation from cartilage, followed by subchondral trabecular bone underneath.<sup>31</sup> The subchondral bone plays an important role in the function of a healthy joint, and acts primarily as a shock absorber for forces that are placed upon the joints during normal movement.<sup>32</sup> Subchondral bone is much more stiff than articular cartilage, and as such it works to absorb a large amount of the mechanical forces in the joint. Subchondral bone has also been implicated for its role in nutrient

supply, metabolism and remodeling, supplying the tissues of the joint with nutrients that are necessary to maintain homeostasis.<sup>31</sup> All of these factors affect the normal activity of the articular cartilage, thereby allowing it to continue to function normally.<sup>31</sup>

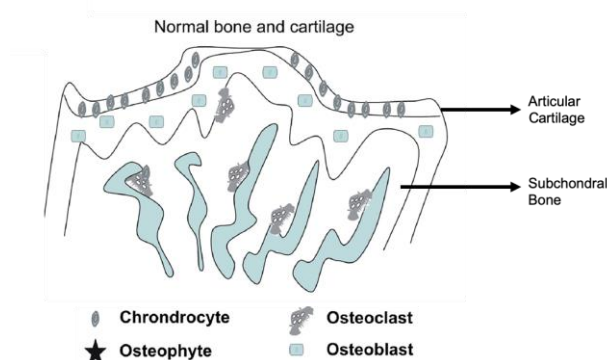


**Figure 0.3: Illustration of articular cartilage and subchondral bone.** Reproduced with permission from Karsdal *et al.* Copyright Elsevier, 2008.

#### 1.4.4 Pathophysiology of subchondral bone in OA

Due to the close connection between the subchondral bone and the articular cartilage, the subchondral bone plays an intricate role in the metabolism of articular cartilage, and damage to the bone can cause major metabolic changes in cartilage.<sup>33</sup> It has been noted that in early progression of OA, the interface between the subchondral bone and articular cartilage undergoes distinct remodeling, especially in areas that cartilage damage is present.<sup>34</sup> This remodeling results in increased bone proliferation, thereby increasing the thickness of the subchondral bone. The mechanism by which bone turnover and structural degradation of the bone is increased in early stage OA is not fully understood, but a number of different possibilities have been studied. Repair of microdamage to the surface of the bone, an increased vascularity of the bone, and a widening porosity, which can increase the crosstalk between bone and cartilage, have all been studied, and are believed to play a role.<sup>34</sup> As OA progresses, a decrease in mineralization and reduced bone stiffness are noted, which are believed to be a result of the accelerated bone turnover.

To date, a number of different therapeutic options to treat the subchondral bone and its role in OA have been studied. Hormonal therapy to block the bone remodeling process,

bisphosphonate and calcitonin use, or bone formation agents have all been studied as potential options for treatment.<sup>35</sup> Many of these therapies appear to have promising results in animal models, but have either failed to provide reproducible results in humans, or remain inconclusive.

#### 1.4.5 Physiology of synovial membrane

The synovial membrane is a soft tissue that lines synovial joints and tendons, and forms the fat pad and bursae. The synovial membrane is made up of two distinct layers: the intima, which is a layer made up of macrophages and fibroblast cells, and the subintima which is made up of blood and lymphatic vessels, resident fibroblasts as well as infiltrating cells, embedded into a collagenous extracellular matrix. The intimal layer of the synovial membrane is typically 20-40  $\mu\text{m}$  thick in cross-section, while the subintima can be up to 5 mm in thickness.<sup>36</sup> The synovial membrane serves as a barrier to the joint space, but is not entirely closed off from the rest of the joint. Cells form an imperfect layer to make up the membrane, meaning there can be transport into and out of the membrane. A histological preparation of the synovial membrane is seen in Figure 1.4.

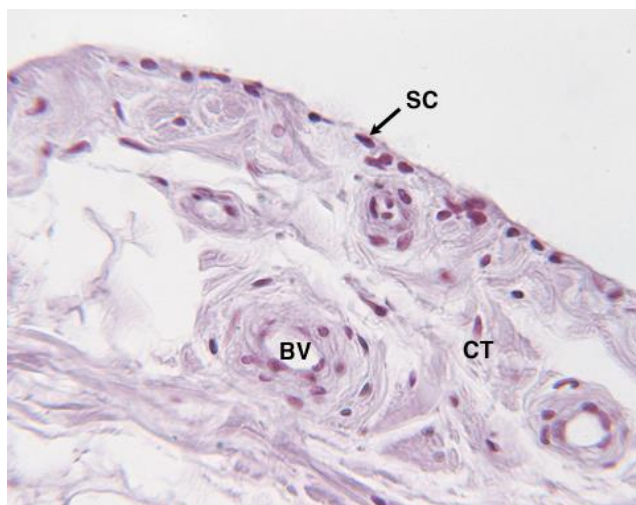


**Figure 0.4: Histological preparation of the synovial membrane.** Image shows synovial cells (SC), blood vessels (BV) and connective tissue (CT). Reproduced with permission. Copyright 2011, Bentham Open.

The synovial membrane provides a barrier that still allows for the movement of materials to the adjacent tissues of the joint. To retain synovial fluid, the intimal layer of the synovial membrane exhibits a free exchange of proteins and molecules, while inhibiting the transit of the hyaluronan that is an important component of the joint fluid. Through this free movement, the cell types that make up the intimal and subintimal layers work together to control the volume of the synovial fluid within the joint. The synovial membrane also plays an integral role in the lubrication of cartilage through the secretion of lubricin. The synovial membrane also secretes molecules that are imperative for the nutrition of the joint cells and tissues, through utilization of the blood vessels that lie within it.

#### 1.4.6 Pathophysiology of synovial membrane in OA

In OA, the most common change in the synovial membrane involves the inflammation and enlargement of the tissue, known as synovitis. Synovitis is believed to be the largest driving factor behind the pain associated with OA. This inflammatory response is hallmarked by an influx of white blood cells to the tissue, which are responding to pro-inflammatory cytokines that are secreted by cells while the disease occurs. An influx of macrophages into the tissue is a hallmark of synovial inflammation. It has been hypothesized that as cartilage begins to break down as a result of OA, the byproducts are released into the synovial fluid, which are then phagocytosed by synovial cells. This action amplifies the synovial inflammation. The inflamed synovial membrane further produces catabolic and pro-inflammatory cytokines, leading to a production of enzymes which break down the cartilage further. On a macroscopic scale, synovitis as a result of OA is easily visualized by magnetic resonance imaging (MRI), in which synovial hypertrophy, and synovial fluid volume can be easily seen in patients that have OA. Contrast enhanced MRI has been found to be extremely well correlated with radiographic OA as measured by X-Ray.<sup>37</sup>

### 1.4.7 Physiology of synovial fluid

The synovial fluid is a viscous solution that is an important component of the joint. Synovial fluid is typically a clear, beige-coloured, viscous liquid. The typical volume of synovial fluid in a human knee joint is roughly 1 mL.<sup>38</sup> The synovial fluid has a number of different roles in the normal function of a joint. Its main function is to reduce the friction between the articular cartilage of the joint during movement, with the main component that imparts the lubricating qualities being hyaluronan.<sup>39</sup> Hyaluronan plays an important role in cartilage protection and the nutrient transport to cartilage. In addition, the fluid acts as a biochemical reservoir for a number of different proteoglycans<sup>40</sup> and surface active phospholipids<sup>41</sup> that also play a key role in giving the synovial fluid lubricating qualities. Furthermore, the synovial fluid contains molecules that mediate communication between cell populations in the joint.<sup>38</sup>

### 1.4.8 Pathophysiology of synovial fluid in OA

There is a marked increase in catabolic and pro-inflammatory cytokines that are present in the synovial fluid of a joint affected by OA. It has been hypothesized that this increase in cytokines can lead to further degradation of cartilage. In addition, the level of proteins and overall volume of synovial fluid increase in OA, which can lead to further inflammation of the joint.<sup>38</sup>

## 1.5 Disease onset, diagnosis and progression

Patients that are suffering from OA typically present with common symptoms. Joint pain that is chronic is the most common complaint, but loss of function or natural range of motion, as well as joint effusions are also commonly described by patients.<sup>19</sup> After the completion of a physical exam, radiographic screening of patients with X-ray remains the gold standard in OA diagnosis, however MRI can be utilized for a more wholistic view of the entire joint and all the tissues involved in OA.<sup>42</sup> Despite the success X-ray technology has had in OA diagnosis, it remains imperfect. In many cases patients can present with radiographic findings of joint space narrowing, but report little to no clinical symptoms. The opposite can also hold true, with some patients reporting a decrease in the ability to

use the joint, as well as intense pain, but can show no major changes radiographically.<sup>43</sup> Just as the radiographic findings of the disease can differ for patients, the progression of the disease can widely vary between patients. Progression in some individuals may be slow, while other patients have reported rapid progression of the disease. Severity can limit the abilities of patients on a day to day basis, with part of the affected population not being able to perform normal movements, like standing and walking.<sup>17</sup> The disease is typically monitored by physicians using continued radiographic imaging, alongside clinical findings and patient reported abilities.<sup>28, 42</sup>

## 1.6 Current treatments

The treatment of OA remains variable from patient to patient, and despite the prevalence of the disease, there remains no gold standard for the treatment of OA, nor is there a disease modifying agent available. The treatment of OA is typically dictated by the progression and the stage of the disease, as well as individual patient preferences (Figure 1.5). Joint replacement surgery can be used for a subset of patients that have severe OA that is deemed to have a distinct effect on quality of life. Though the surgery is typically reserved as a final option, the number of total joint replacements is growing, with more than 600,000 knee replacements performed in the United States last year.

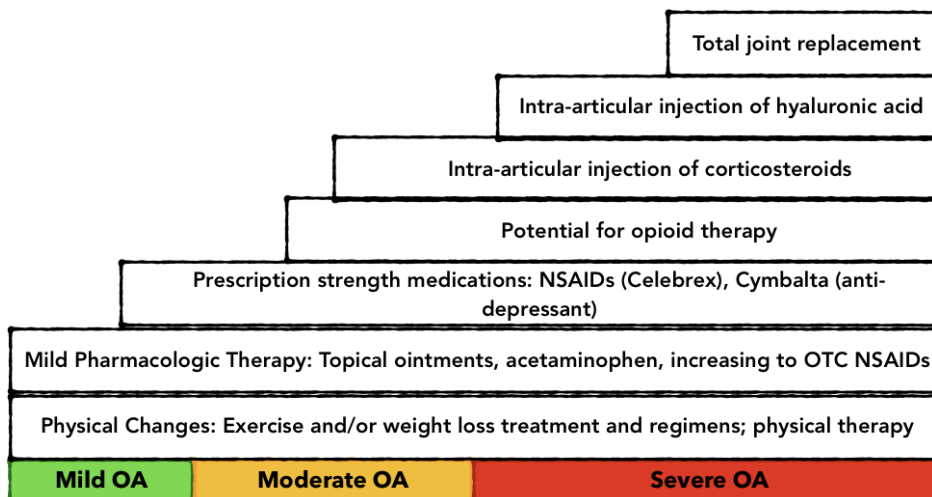


**Figure 0.5: An outline of the current treatments for OA.**

### 1.6.1 Non-Pharmacologic treatment

Due to the costs associated with OA, and its overall prevalence, it is becoming increasingly common for physicians treating OA patients to use non-pharmacologic therapy as a first line treatment method.<sup>44</sup> These therapies are typically intended to control the symptoms before pharmaceutical intervention is required, thereby limiting the amount of medications required by patients. Many different types of non-pharmacologic therapies have been suggested for OA treatment, including exercise,<sup>45-48</sup> physical therapy,<sup>49</sup> the use of mobility assistance devices such as braces or splints,<sup>50</sup> acupuncture,<sup>51</sup> nutraceuticals,<sup>52-54</sup> weight loss,<sup>21, 55-57</sup> and ultrasound.<sup>58</sup>

Of the current non pharmacologic treatments that are used for OA therapy, exercise and weight loss are the most commonly utilized therapies. By reducing the overall weight of patients, the overall load on the joint, and thereby on the damaged tissues, can be reduced. Weight reduction has shown favorable patient reported outcomes of the disease, as well as to increase patient reported quality of life.<sup>56</sup> Recent studies have looked at the effect of diet-based weight loss in OA patients,<sup>17, 53</sup> as well as exercise-induced weight loss of OA patients,<sup>45</sup> and in both cases have found that the reduction of weight is beneficial in the management of the disease. Recently, numerous studies have reported that there is a beneficial effect on the disease from exercise, regardless of weight loss.<sup>46, 48, 59, 60</sup>

### 1.6.2 Pharmacologic therapy

Though the non-pharmacologic therapies are gaining momentum in the treatment of OA, pharmacologic therapies are still commonly used. The history of pharmacologic therapy for OA is well documented, and the medications that are used in OA treatment have inherent risks associated with them. The drug rofecoxib, for example, was once believed to be a gold standard for OA treatment: the potent COX inhibitor was extremely effective at mitigating pain associated with the disease. However, in 2004 it was voluntarily pulled from the market because of safety concerns, specifically an increased risk of cardiac infarctions—a fate that has been common in drugs designed for OA over the years.<sup>61</sup>

### 1.6.3 Systemic pharmacologic treatment

Most pharmacologic therapy associated with OA is taken systemically. Oral medications, such as acetaminophen, or non-steroidal anti-inflammatory (NSAID)s are typically used, as they are effective at lowering the pain and inflammation associated with the disease. These medications are non-specific, and while they are effective, they must be utilized at high doses to reach beneficial effect in OA treatment. Prescription strength NSAIDs have been developed as more selective anti-inflammatory agents. Celecoxib and meloxicam, are two selective COX-2 inhibitors that have been used in OA treatment.<sup>62</sup> The potential side effects of NSAID usage for OA treatment is well documented, and remains an issue. The link between NSAID therapy and gastrointestinal disorders has been widely studied and corroborated,<sup>63</sup> a problem which is amplified for older patients who are more susceptible to gastrointestinal side effects, and OA. Furthermore, NSAIDs have documented cardiovascular side effects,<sup>64</sup> making the long term use of NSAIDs problematic in some patients. More recently, serotonin and norepinephrine reuptake inhibitor (SNRI)s have been studied as a pharmacologic option for the treatment of OA. Sold under the brand name Cymbalta, duloxetine has shown promising results in stopping the pain that is associated with OA, but only treats the symptom, and does not actually alter the pathophysiology of the disease. Side effects do remain due to treatment with duloxetine, and it is not currently recommended as a first line therapeutic for OA treatment.<sup>65</sup>

Other systemic options for the treatment of OA include topical ointments. Topical ointments typically have better safety profiles than orally ingested counterparts, and have the ability to deliver a number of different drugs to the area of injury, such as NSAIDs<sup>66</sup>. While topical administration is safer, it has also been noted that the therapeutic benefit of topically delivered NSAIDs is far less than when delivered orally. Other topical agents that can be used serve primarily as pain relief agents, such as capsaicin gel, and while there have been studies showing benefits to using these types of treatment when compared to placebo, the actual clinical benefits remain unclear.<sup>62, 67</sup>

### 1.6.4 Intra-articular injections

In an attempt to increase the amount of bioavailable drug molecules at the area of injury, while mitigating the side effects that are seen from systemically administered drugs, IA injections can be utilized. IA injections have been used in the treatment of OA for over 50 years, and have generally good safety profiles.<sup>68</sup> The most common IA injection used for the treatment of OA is the injection of corticosteroids.<sup>69</sup> Methylprednisolone, triamcinolone and dexamethasone are all commonly used steroids.<sup>69</sup> IA injection allows for a higher dose to be localized at the damaged tissues than could be delivered systemically.<sup>70, 71</sup> Furthermore, the use of an IA injection of allows for the steroids to be compounded with other molecules to slow their clearance from the joint.<sup>72</sup> Adverse events from corticosteroid injection are documented, but are considered mild or moderate in most cases.<sup>73</sup> However, current steroid injections provide only a short-term benefit and do not alter the disease course long-term, so there is a hesitance to continue repeated IA injections.<sup>73</sup>

Viscosupplementation is a means of replacing naturally occurring molecules within the joint that are either damaged or lost when OA progresses. These injections are typically comprised of HA or its derivatives, or chondroitin sulfate.<sup>62, 74</sup> It is hypothesized that these injections improve the viscoelastic properties of the synovial fluid, which helps to dissipate the mechanical load on joints, and provide better lubrication. There are no major safety concerns of viscosupplementation, outside of the typical risks associated with the injection, though the clinical efficacy remains questioned.<sup>75</sup>

### 1.6.5 Joint replacement

Depending on the joint affected, the response to the aforementioned therapies, and other patient specific factors, total joint replacement therapy can be performed. Joint replacement therapy for OA is typically reserved for extreme cases of the disease, in which mobility is significantly impaired, or quality of life has diminished severely.<sup>76</sup> In recent years, there has been a growing demand for total joint replacements in both the knee and the hip, but at the same time there is an anticipated shortage in surgeons that are willing to perform these operations.<sup>76</sup> The risks of joint replacement surgery are well

documented. Adverse reactions to implants, or infections associated with the surgeries are known issues, and the failure of the implant begins to occur naturally over the lifetime of the implant with increased usage, necessitating a new joint replacement, and subsequent surgeries.<sup>77,78</sup> Recent studies have looked at a minimally invasive procedures compared to a more traditional approaches, and while there were promising results, there is still no general consensus on a gold standard for joint replacement surgery.<sup>79</sup> Due to the costs associated with the replacement of joints, and the need for continuous care of implants, the surgeries typically remain an option that can only be utilized in cases where the disease has progressed, and is causing major mobility and quality of life issues for patients.<sup>78</sup>

## 1.7 Potential disease modifying agents

While the complete pathophysiology of OA is not yet fully understood, there is an undeniable need to develop disease modifying agents that can alter the progression of the disease, rather than solely treating its symptoms. Recent research as begun to study the many different molecular pathways that are involved in the onset and progression of OA, and through the understanding of these pathways, new potential DMAs have been proposed. These potential DMAs can have a number of different targets and mechanisms that work to alter the pathophysiology of the disease, such as pain attenuation or inflammation inhibition. Recently, newer targets have emerged that could serve to alter the tissues and their molecular processes, thereby slowing or halting the progression of OA. Below, potential OA therapeutics are categorized by their classes, and are discussed.

### 1.7.1 Disease Modifying Agents Targeting Pain

Pain is one of the most commonly associated pathways that is studied for the development of a potential OA therapeutic. The pain that is associated with OA is often early onset in the disease, where it is related to initial tissue injury, inflammation, and increased sensitivity in the tissues around the joint.<sup>80</sup> As the disease progresses, increased pain around the area of injury is associated with the disease, and unlike in other diseases, the pain that is associated with the initial injury in OA does not subside with time. Due to

the widespread and variable nature of pain in OA, a number of different mechanisms have been studied. Despite the overwhelming prevalence of pain in OA, the targeting of pain as a potential for modification of the disease has been contested in the research community. However, as the underlying mechanisms of pain in OA become increasingly understood, a means to halting the processes driving pain can be developed. Recently, the synergistic relationships between the modification of pain mechanisms and inflammation, or structural alteration within the joint have been researched, leading to the belief that pain is indeed a potential drug target that can modify disease.<sup>77</sup>

### 1.7.2 Ion Channels

One pathway that has been studied for its effect on pain in OA is the activity of ion channels; a number of different ion channels have been implicated for their roles in OA. For example, the TRP Vanilloid 1 (TRPV1) receptor was the target of a new molecule developed by Centrexion Therapeutics, known as CNTX-4975.<sup>81</sup> The TRPV1 receptor had been initially identified in 2013 as a potential target.<sup>82</sup> This molecule is a TRPV1 agonist—a capsaicin derivative that stimulates unmyelinated C-fiber afferents, resulting in the secretion of Substance P, which provides a desensitization of pain fibers.<sup>83</sup> In 2019 CNTX-4975 advanced into phase IIb clinical trials with the US FDA, and has shown a distinct reduction in pain over 24 weeks of use. Though some of the TRPV1 antagonists have had their trials ultimately stopped for safety concerns, a number of these molecules are still currently being researched and appear promising. Negative side effects and safety concerns have still been noted, and it has been recommended that many of these TRPV1 antagonists utilize a non-systemic mode of administration to mitigate potential side effects.<sup>82, 84, 85</sup> NAV 1.8 is a voltage gated sodium channel that has been implicated in the mechanotransduction in pain in OA. It was found in a recent study that the application of a selective NAV 1.8 blocker of the sodium channel was helpful in decreasing the nociceptive transmission from the tissues of the joint, thereby leading to a reduction in overall pain.<sup>86</sup> The pathway has been tested in local, topical, and oral administration routes thus far, and has shown promising safety results.<sup>86</sup>

### 1.7.3 Nerve Growth Factor

Nerve growth factor (NGF) is a neuropeptide that is released during injury or inflammation, and has been implicated as a main cause of pain in OA. NGF has been shown to bind to Tropomyosin Kinase A (TrkA), which can then lead to an enhanced perception of pain, as well as a triggering of the initial pain response. It has been hypothesized that through the inhibition of the NGF signaling pathway, there may be a decreased sensitization to pain from both inflammatory and non-inflammatory sources.

The inhibition of the NGF signaling pathway has been studied through different mechanisms. One such example is the use of monoclonal antibodies, which had been studied and deemed efficacious in preclinical studies. In clinical trials however, safety concerns became quickly apparent, and these findings brought the initial clinical research of NGF targeting monoclonal antibodies for OA to a near standstill.<sup>87</sup> In recent years however, new research on the use of human monoclonal antibodies as well as NSAID combination therapy have emerged, and appear to be promising avenues that could potentially deliver a new treatment of OA.<sup>88, 89</sup> Small molecules have also been investigated as a means to block NGF pathways, but to date none have emerged as usable candidates.<sup>90</sup>

### 1.7.4 Other pain receptor targeted disease modifying agents

Opioid receptors have been studied for the treatment of OA pain. The use of opioids in OA treatment remains a widely debated topic, due to the associated side effects with opioid treatment, including dependence. In an attempt to make opioid use more applicable to OA patients and mitigate side effects, new research has been performed with attempts to change the mechanisms of action of the drugs. Alterations in the drugs have allowed for the development of opioids that act peripherally, rather than centrally, which are believed to be safer methods of opioid use, while still maintaining the efficacy.<sup>91</sup>

Recent work in 2015 by Sophocleous *et al.* studied the effect of a CB2 agonist to the type II cannabinoid receptor. Studies appeared initially promising in preclinical animal models, but the results were not reproducible in human models of OA.<sup>92</sup> Despite these

results, the use of cannabidiol (CBD) remains a widely studied area in OA, with more recent work in 2017 by Philpott *et al.* showing that the administration of CBD in rat models of OA worked to attenuate the progression of OA, through a reduction in joint inflammation.<sup>93</sup> The decrease in inflammation was coupled with lower pain measurements in the animals. Similar results using CBD were shown in 2016 by Hammell *et al.*, where CBD was administered topically, and led to significantly reduced joint swelling as well as the absence of pain in animals treated.<sup>94</sup>

### 1.7.5 Disease Modifying Agents targeting Inflammatory Modulation

It is widely understood that inflammation plays a role in the progression of OA; an increase in inflammatory modulators has can lead to an increase in pain, as well as degradation of the joint tissues.<sup>12</sup> As such, a number of recent studies have focused on controlling the inflammatory signaling cascades through the control of cytokines.

### 1.7.6 Cytokines

A number of pro-inflammatory cytokines have been associated with OA. As reviewed in 2011 by Kapoor *et al.* cytokines such as interleukin (IL)-1 $\beta$ , IL-6, IL-1 $\alpha$ , IL-15 have all been found to be increased in the synovial fluid of joints affected with OA.<sup>33</sup>

Furthermore, tumor necrosis factor (TNF)- $\alpha$ , has been identified as a major proinflammatory cytokine that is associated with the progression of OA.<sup>33</sup> TNF- $\alpha$  and IL-1 $\beta$  are believed to play a role in the signaling of NGF, thereby leading to not only inflammation, but an increased pain response as well.<sup>95</sup>

Due to their overwhelming presence in OA, IL-1  $\alpha$  and IL-1 $\beta$  are common targets for inflammatory modulation. IL-1 stimulates neutrophil migration in OA, and activates articular cells to produce mediators that are involved in joint inflammation and destruction.<sup>96</sup> Furthermore, IL-1 has inhibitory actions on the production of new extracellular matrix components.<sup>97</sup> The two aforementioned cytokines both bind to the same receptor, (IL-1R1) making receptor antagonism of IL-1R1 a common target for drug development. Anakinra for instance, is an IL-1R1 receptor antagonist that has shown clinical promise for treatment in OA patients. A 2017 study showed a beneficial

effect of using anakinra for treatment in large joints, but it was recommended that only patients who had failed first line therapy receive the medication.<sup>98</sup> These results have been directly contradicted in the past by other studies though, leaving the clinical recommendations regarding anakinra in a state of flux. Other attempts have been made using antibodies, such as lukitizumab, to control the activity of IL-1R1.<sup>99</sup> The effects of lukitizumab have been highly variable in different trials, and it is not currently being used to treat OA.

Tumor Necrosis Factor (TNF)- $\alpha$  is another common target cytokine for the treatment of inflammation in OA. Anti-TNF- $\alpha$  therapies have been developed and clinically available for a number of years in inflammatory conditions such as rheumatoid arthritis, inflammatory bowel disease, and psoriasis. A 2012 paper reported on the efficacy of anti-TNF- $\alpha$  administration in the treatment of OA, and while it concluded that there were promising results in initial human trials, more work has to be done to complete full trials with correct controls and appropriate patient levels.<sup>100</sup>

A number of other cytokines have been identified as potential targets for OA treatment, such as IL-10, IL-6, and interferon  $\beta$ . All of these are currently within studies in the FDA to determine the efficacy and safety of treatment, though no results have been posted to date, and their future as potential candidates for DMAs remain unclear.<sup>14</sup>

### 1.7.7 Other Inflammatory Pathways as Potential Disease Modifying Agent Targets

Certain molecular pathways in the body have been determined to play a role in the production of inflammatory cytokines, and other mediators of inflammation. For example, the nuclear factor- $\kappa$ B (NF- $\kappa$ B) is integral to the production of pro-inflammatory cytokines, and has been implicated recently in OA. The inhibition of (NF- $\kappa$ B) was targeted by a compound called SAR113945 in 2017. In administration of this inhibitor, it was noted in phase I trials that there were beneficial effects, however phase II trials have failed to demonstrate similar responses.<sup>101</sup>

P38 mitogen activated protein kinase (MAPK) is another example of a potential target for a disease modifying agent in OA. P38 MAPK is a pathway that is associated with the synthesis of pro-inflammatory cytokines, and the inhibition of p38 MAPK has been targeted as a means to attenuate the progression of these cytokines. Much like molecules targeting the NF- $\kappa$ B pathway, the treatments associated for p38 MAPK have been mostly underwhelming, with one report of a clinical reduction of pain for 4 weeks post-injection, but no clinically approved p38 MAPK molecule to date.<sup>102</sup>

## 1.8 PPAR $\delta$ Antagonists as a DMA for OA treatment

In 2015, Ratneswaran *et al.* showed that activation of PPAR $\delta$  resulted in the degradation of cartilage extracellular matrix in explant culture of rat limbs.<sup>9</sup> Furthermore, cartilage-specific PPAR $\delta$  knockout mice were protected in a PTOA model involving destabilization of the medial meniscus surgery, suggesting that PPAR $\delta$  promotes PTOA.<sup>9</sup> It was elucidated from these studies that PPAR $\delta$  antagonists could potentially provide a protective or even therapeutic effect for OA.

PPAR $\delta$  antagonists are known, and are commercially available. GSK0660 was first developed in 2009, and was found to have an IC<sub>50</sub> of 155 nM against PPAR $\delta$  and nearly 10-fold selectivity over other PPAR subtypes. However, the molecule had poor bioavailability, so was not further explored by Glaxo Smith Kline (GSK).<sup>103</sup> This led to the development of GSK3787, a second PPAR $\delta$  antagonist that was demonstrated to antagonize PPAR $\delta$  *in vivo* with high specificity through covalent binding to Cys 249 in the PPAR $\delta$  binding site.<sup>104</sup>

In 2017, Ratneswaran *et al.* performed a pilot study to demonstrate the potential for PPAR $\delta$  antagonists to inhibit OA progression. Sprague-Dawley rats underwent anterior cruciate ligament transection and partial medial meniscectomy (ACLT/PMMX) surgery followed by treatment with DMSO (vehicle control) or GSK3787 administered subcutaneously for 30 days at 1 mg/kg/day. Over the 4 weeks post-surgery, rats that underwent ACLT/PMMX with DMSO treatment got progressively worse, with functional impairments in mobility including increased rest time, decreased movement time, and

decreased vertical activity episode counts. These rats also demonstrated decreased loading of the operated limb, while PPAR $\delta$  inhibitor-treated rats did not experience similar declines in functional activity and limb loading. This data suggested that PPAR $\delta$  inhibition prevents functional limitations induced by damage in part, indicating its strong potential as a therapeutic agent in OA.

PPAR $\delta$  receptors are prevalent throughout the body, where they play important roles.<sup>10,</sup>  
<sup>105</sup> PPAR $\delta$  agonists have been investigated for the treatment of metabolic diseases, such as diabetes and obesity, as it has been shown that activating PPAR $\delta$  can increase fatty acid metabolism, improve insulin sensitivity, and decrease serum glucose.<sup>106-109</sup>

Furthermore, PPAR $\delta$  is the predominant PPAR subtype in the brain, where it plays a role in cognitive function.<sup>110, 111</sup> In the short-term pilot study of GSK3787, metabolic effects, as measured by abnormalities in weight gain, liver weight, or blood glucose were not observed, but a detailed toxicology study was not performed, and daily systemic administration of this drug is not feasible over the long-term due to the high risk of side effects. For use in OA, the direct delivery of the drug into the joint would allow for levels of GSK3787 required for efficient PPAR $\delta$  inhibition in the joint. To date, no study has examined the effect of IA injections of GSK3787 for the treatment of OA.

## 1.9 Intra-articular drug delivery systems

IA administration of drugs to treat OA remains paradoxical in nature. Injection of drug molecules directly to the site of injury can potentially allow for high concentrations of drug to reach the target tissues. The joint however, is extremely efficient at clearing small molecules from the synovial fluid, meaning the high drug concentrations are not likely to last for a prolonged time. Free drugs are removed from the IA space by lymphatic drainage within a few hours, so they often cannot reach their targets at sufficient levels over the required period of time to achieve a therapeutic effect.<sup>112</sup> Many drugs that have been studied with IA injections have shown half-lives in the synovial fluid of 1-5 hours.<sup>113</sup> The short half-life of drug molecules that are injected into the joint can be explained, at least partially by the make-up of the synovial lining. Synoviocytes have the ability to synthesize HA. Macrophages within the synovial membrane work to clear the

joint fluid of debris. Furthermore, the lining of the synovium is discontinuous; there are gaps 0.1-5 microns in diameter, through which any free drugs that are injected can easily flow, ultimately reaching the blood circulation.<sup>114-116</sup>

Given the rapid clearance of free drugs after IA injection, many OA therapeutics would benefit from encapsulation into delivery systems that provide prolonged release. These systems would not only afford the opportunity to deliver drugs to the affected tissue at higher doses than what could be delivered systemically, but would decrease the required frequency of IA injections, so discomfort for patients as well as potential complications associated with injection would be minimized.<sup>117, 118, 119</sup> A number of delivery systems have been explored for the IA delivery of OA drugs.<sup>120</sup> Examples of IA drug delivery systems, their potential benefits and limitations, as well as results of studies, are described below.

### 1.9.1 Liposomes

Liposomes are a common class of drug delivery system composed of a phospholipid membrane encapsulating an aqueous core (Figure 1.6). Drugs can be loaded into the membrane or aqueous core. Liposomes are generally designed to slowly release drugs via diffusion through or out of the phospholipid membrane. A number of liposome systems have been developed and used for IA use.

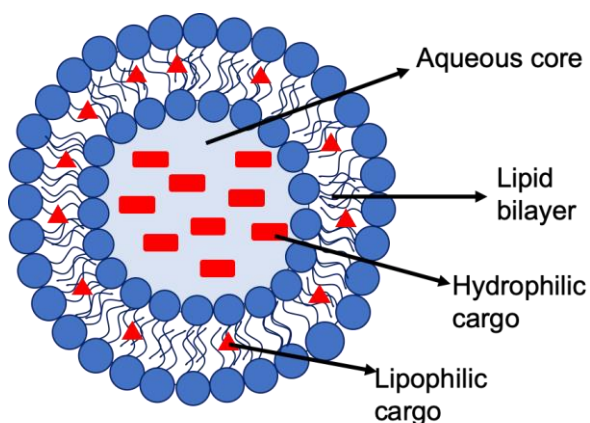


**Figure 0.6: The structure of a liposome.**

In a 2013 study by Dong *et al.*, cholesterol and soybean phosphatidylcholine were combined with the NSAID celecoxib, and liposomes were synthesized using a film hydration technique.<sup>121</sup> Film hydration involves dissolving the lipids and drugs in a common solvent before evaporating the solvent leaving a film. Upon resuspension in water, lipids form a natural bilayer, thereby entrapping drugs.<sup>122</sup> In the study, liposomes were found to have high encapsulation efficiencies, of roughly 99%. Though the authors showed that they could slow the release of celecoxib through the addition of HA to the liposome, nearly 100% of the loaded cargo was still released after just 48 hours. *In vivo* testing in a rabbit model showed that the liposomes provided a more beneficial effect than the injection of free drug, though measurements were taken only once at two weeks post-administration.

In other cases, liposomal formulations developed for IA use provided a more prolonged drug release than 48 hours. In 2015, Pradal *et al.* studied the loading of a p38 MAPK inhibitor, VX-745, into a liposomal delivery vehicle.<sup>102</sup> In this study, cholesterol was again used with dipalmitoylphosphatidylglycerol and distearoylphosphatidylcholine to prepare the liposomes. The system was developed to overcome solubility issues and the rapid recrystallisation of the drug when in contact with an aqueous physiological environment. One key finding from the study was the improved drug resident time when compared to an injection of free drug alone, showing promise for the administration of IA liposomes.

Edwards *et al.* continued to work on liposomal formulations for IA use. A liposome was developed using 1,2-dipalmitoyl-sn-glycero-3-phosphocholine. Iohexol, a CT contrast agent, was used as a model drug, and it was determined that when encapsulated within a liposome, the half-life was 124 hours in the joint, compared to 3 hours when injected without the use of a liposome.<sup>123</sup>

While liposomes have an ability to encapsulate drugs, and due to their larger size, should prolong joint residence time, there are a number of drawbacks that make the use of liposomes for IA use extremely difficult. In particular, liposomes have a high water

content, and as such their mechanical properties are typically insufficient to survive the mechanical forces within the joint.

### 1.9.2 Nanoparticles

Nanoparticles have been widely used as drug delivery platforms for IA use,<sup>124</sup> cancer treatment,<sup>125</sup> ophthalmic treatments<sup>126</sup> and other areas. For use in drug delivery applications, nanoparticles are typically synthesized from biodegradable polymers, and have the ability to encapsulate a variety of drugs. As nanoparticles degrade, the loaded drug is released from the system or it may diffuse out prior to degradation. Due to the relative ease of synthesis, and diversity of nanoparticles, a number of different types have been developed for IA use. Nanoparticles can fall into a few different categories, and are closely related to larger sized microparticles. A nanoparticle is typically described as 100-500 nm in size, whereas microparticles are larger, above 1  $\mu\text{m}$  in size. The structure of particles, either nano or micro, is depicted in figure 1.7. Typically, IA nanoparticle formulations that have been developed can be broken down into two main subcategories: nanoparticles for the delivery of drugs into the synovial fluid, and nanoparticles that are designed to diffuse throughout the surrounding tissues.

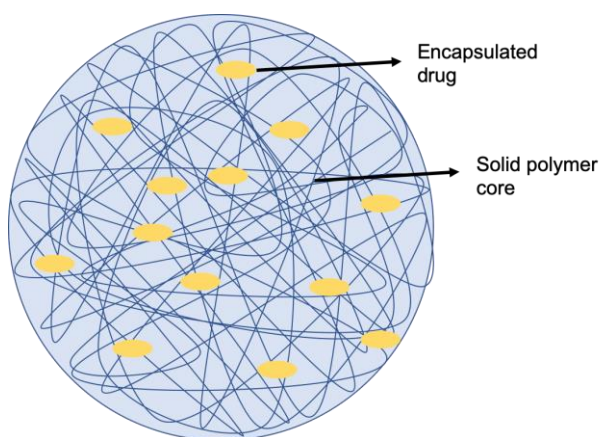


**Figure 0.7: The structure of a solid core polymer nanoparticle.**

In 2007, Thakkar *et al.* developed an IA nanoparticle delivery system that encapsulated the NSAID celecoxib. Here, glycerol was used to create solid lipid nanoparticles. The

average diameter was reported to be roughly 250 nm, and a drug loading percentage just over 4% was achieved. They measured the *in vitro* drug release from the nanoparticles and found that after 7 days 95% of the loaded celecoxib had been released.

Natural polymers have also been used to make nanoparticle formulations for IA use. HA and chitosan were used by Ryan *et al.* in 2013 to develop a nanoparticle that encapsulated salmon calcitonin.<sup>127</sup> The diameter of the nanoparticles was 163-193 nm, and the release of the loaded cargo was between 60 and 80% in PBS after 6 hours. The particles were found through a study in mice to exhibit more benefit in terms of the reduction of inflammation than drug suspensions or hydrogels. Kang *et al.* made nanoparticles from naturally derived chitosan in 2016.<sup>128</sup> The particles were 150 nm in diameter, and were not loaded with a drug cargo, but instead were conjugated with kartogenin, a small molecule that has been proposed to promote the repair of damaged cartilage.

Nanoparticles remained localized in the joint for up to 24 days post injection, and when OA was surgically induced in rats, the treatment with the nanoparticles led to a statistically lower score on the Osteoarthritis Research Society International (OARSI) scale, which grades histopathology of OA and reflects depth of the lesions and extent of OA over the joint surface. It was hypothesized that the nanoparticles led to a more efficient differentiation of chondrocytes, and therefore had a protective effect against OA degradation.

In another example of solid lipid nanoparticles for IA use, Jain *et al.* studied a nanoparticle formulation created from a mixture of Pluronic F68, stearic acid, citric acid and lecithin in 2014.<sup>129</sup> The nanoparticles had a diameter of about 400 nm, and compared to the work provided by Thakkar, had a higher drug loading at 15.6%. Diacerein, an anthraquinone that inhibits IL-1B, was encapsulated. A rapid release of the loaded cargo was noted, with 40% being released after just 4 hours *in vitro*. Despite the rapid release of drug, it was noted that when tested *in vivo* the particles were able to come into close contact with the articular cartilage, though their diffusion into the cartilage was not noted. This led researchers to conclude that the system could be promising for the use of cartilage targeted therapies, such as tissue specific disease modifying agents.

Synthetic polymers have also been used for the synthesis of nanoparticles for IA delivery. Morgen *et al.* in 2013 showed that when using polycaprolactone-*block*-poly(ethylene oxide) (PEG), coated with positively charged dextran derivatives as external shells, they could prepare nanoparticles that were cationic, and were then able to crosslink with the negative charges on HA.<sup>130</sup> These nanoparticles had diameters between 100 and 150 nm, but had a longer retention time in the joint of six days, which was believed to be a result of the interactions with HA. Poh *et al.* formulated nanoparticles from another synthetic polymer source: PEGylated poly(*N*-isopropylacrylamide) (pNIPAM).<sup>131</sup> The nanoparticles were prepared with disulfide crosslinks to ensure degradability, and were designed to deliver anti-inflammatory peptides directly into chondrocytes. These nanoparticles had diameter of 237 nm, and a higher drug loading of around 35%.

Challenges with the nanoparticle delivery systems for IA use remain. While the systems are well tolerated, the resident joint time of nanoparticles remains low. Nanoparticles that are injected are subject to clearance from the joint over 2 days to around 2 weeks. Despite this shortcoming, nanoparticles continue to hold promise for the delivery of drugs to cartilage, and for their potential to diffuse through the tissues of the joint, such as cartilage or the synovium.

### 1.9.3 Microparticles

Whereas the rapid clearance of nanoparticles from the joint is often attributed to their small size, microparticles are larger and can potentially be retained longer, making them useful for IA delivery. Microparticles are commonly defined as being larger than 1 micron in diameter, and can have diameters of up to 100  $\mu\text{m}$ . The microparticle platform has been used in a wide array of applications, such as painting or imaging. Within their use in drug delivery, a number of different diseases have been investigated for potential treatment with microparticle drug delivery systems. For example, a number of microparticles have been considered for treatment of cancer,<sup>132</sup> and more recently their use for the treatment of type II diabetes has been studied.<sup>133</sup> Microparticles for drug delivery formulations have been commercialized, with a number of FDA approved systems on the market today; Ozurdex is one example, that utilizes a microparticle

formulation to deliver dexamethasone through an intravitreal injection into the eye.<sup>83</sup> A number of different studies have been performed to assess the feasibility of microparticles for IA drug delivery.

Though there are seemingly fewer examples than compared to nanoparticles, microparticles can also be prepared from natural polymer sources. Chitosan is a natural polymer that has been widely used in the preparation of microparticles for IA use. In 2012, Chen *et al.* used chitosan to develop a microparticle system for IA drug delivery.<sup>134</sup> The study looked at the encapsulation of brucine, a drug that is not as commonly seen in studies for OA, but is known for its analgesic and anti-inflammatory properties.<sup>135</sup> The particles were determined to have a diameter of 2.45  $\mu\text{m}$ , and released between 70 and 80 percent of the loaded cargo after 60 hours. They were found to be well tolerated by the synovium in a rabbit model, but the joint retention time was low.

Chitosan was also used as the polymer in a 2014 study by Kang *et al.*<sup>128</sup> Researchers followed the same preparation methods as they did when creating nanoparticles, but aimed for a larger sized particle. The particles were 1.8  $\mu\text{m}$  in diameter, and although they were well tolerated, the microparticles exhibited a faster release than the nanoparticles, and no significant difference was noted in joint retention between micro-sized and nano-sized particles over 24 days.

Inorganic polyphosphate was used to make microparticles for the delivery of zoledronic acid, a bisphosphonate, in a study by Müller *et al.* from 2018.<sup>136</sup> Zoledronic acid is commonly used to treat bone disorders, and it was determined that it may have a protective effect on articular cartilage as well, making it a promising agent for OA treatment.<sup>137</sup> Interestingly, the particles were smaller than what is typically described as microparticles, having a diameter of only 60 nm, and were described as having a meso-crystal structure that formed overall structures of up to 500 nm in size.

A number of different synthetic polymers have been used to develop microparticles for IA delivery. Synthetic polymers can be useful because they can be highly tuned, thereby changing their properties and their potential for use in drug delivery systems. The most extensively used synthetic polymer in the preparation of microparticles for IA treatment

is poly(lactic-*co*-glycolic acid) (PLGA). PLGA is commonly used due to the fact that it is well tolerated *in vivo*, biodegradable, has variable erosion times, tunable mechanical properties and is approved for use in multiple medical and dental applications by the United States Food and Drug Administration (FDA).<sup>138</sup>

PLGA microparticles are already approved by the FDA for IA delivery to treat OA. In particular, Flexion Therapeutics' FX006 is marketed under the brand name Zilretta. These particles are about 45  $\mu\text{m}$  in diameter, are loaded with the corticosteroid triamcinolone acetonide, and exhibit a prolonged release of the loaded therapeutic when tested in a rat model.<sup>139</sup> The particles were well tolerated in preclinical studies, and in a recent Phase II trial it was determined that the particles were able to provide persistent pain relief for up to 12 weeks when compared to a placebo injection.

Other researchers have also used PLGA microparticles to encapsulate a variety of drugs, and investigated their efficacy for IA administration. In 2013 for instance, Ko *et al.* encapsulated sulphoraphane, a natural organosulfur compound, in particles that were 15  $\mu\text{m}$  in diameter. The system exhibited a prolonged release; only 6% of the loaded cargo was released after 30 days *in vitro*. In rats that had OA induced by a surgical method, the microparticles delayed the progression of OA. Gomez-Gaete *et al.* prepared PLGA microparticles in 2017, encapsulating Rhein, an anti-inflammatory.<sup>140</sup> The size of the prepared microparticles differed in this study, with the particles measured to be about 4  $\mu\text{m}$  in diameter. Interestingly, the release properties of these particles were vastly different than the aforementioned system. A rapid release of the loaded molecule Rhein was observed, with 45% of the loaded cargo released over 24 hours *in vitro*. The particles were once again well tolerated, and remained localized in the joint even 1 month after injection, but were without drug at this time. In 2018, Maudens *et al.* incorporated dexamethasone in PLGA microparticles.<sup>141</sup> The particles were 10-15  $\mu\text{m}$  in diameter and were able to incorporate nanocrystalline domains of the drug within the particles in order to prolong the release of the drug over 3 months.

Another aspect of PLGA that makes it attractive for use in microparticles is the ability to blend the polymer with other polymers to alter the properties of the drug delivery system.

Indeed, multiple examples of blending PLGA with other polymers to prepare microparticles for IA use exist. One example was a study by Goto *et al.* in 2017 in which PLGA was blended with gelatin to develop microparticles.<sup>142</sup> Fluvastatin was encapsulated within the microparticles which were about 25  $\mu\text{m}$  in diameter, and the particles released only 27.5% of the loaded cargo after 7 days *in vitro*. It was determined *in vivo* using a rabbit model that the delivery of a statin could have potential beneficial effects on OA, as it was found to inhibit the degradation of cartilage after surgical induction of OA.

One specific class of synthetic polymers that has garnered increasing interest in recent research is poly(ester amide)s (PEAs). Characterized by the presence of both ester and amide bonds, and often containing amino acids, PEAs have highly tunable structures and properties. PEAs containing various amino acids, as well as different spacers between the ester and amide bonds, have been extensively studied. Furthermore, PEAs have shown excellent compatibility with cells when used as scaffolds for tissue engineering.<sup>143, 144</sup>

The tunability of PEAs make them especially promising for IA drug delivery systems. In 2016, Janssen *et al.* studied the development of microparticles from PEAs that were responsive to stimuli.<sup>145</sup> The particles were made from a PEA that was comprised of three random blocks, and had the NSAID celecoxib loaded within them. The particles had a wide range in diameters from 10-100  $\mu\text{m}$ . *In vitro* drug release was promising, with an initial burst noticed, but at 80 days in release medium only 50% of the loaded cargo had been released. *In vivo* it was seen in a rat model that the particles did degrade over 12 weeks, but no side effects were noted from the degradation of the particles. Furthermore, it was shown that the polymer particles were able to respond to external stimuli—serine proteases in this case, to increase the rate of release of loaded cargo.

Microparticles are very promising for IA drug delivery, as evidenced by their FDA approval and clinical use. Despite this, challenges still persist with their use. Concerns with microparticles include the potential for the particle degradation products (depending on their compositions) to induce adverse inflammatory reactions in the joint.<sup>146, 147</sup> In

addition, there is a potential for the particles themselves to cause irritation in the joint if their mechanical properties are not compatible with joint tissues.<sup>148</sup>

### 1.9.4 Hydrogels

Hydrogels are another highly tunable class of drug delivery systems that are promising for IA delivery. The polymers used to make hydrogels can be derived from natural sources, such as HA or collagen, or synthetically prepared polymers, such as PEG.<sup>149</sup> Not only can different polymer structures be used to develop hydrogels, but the crosslinking mechanisms can be varied as well. Physical crosslinks can be induced through changes in temperature, pressure, light, pH, salt concentration, or electric field. The junctions that form in a physically crosslinked system are more transient and can range from chain entanglement to ionic or hydrophobic interactions. Chemically crosslinked hydrogels are another class of hydrogels that have more permanent junctions. Linkages here can come from the addition of different molecules to induce chemical changes, such as covalent bonds. Hydrogels designed for IA use have employed physical crosslinks, covalent crosslinks, or a combination of both. Examples of hydrogels prepared for IA use have followed a wide range of preparation methods as well. A representation of both chemically and physically crosslinked hydrogel networks is depicted in Figure 1.8.

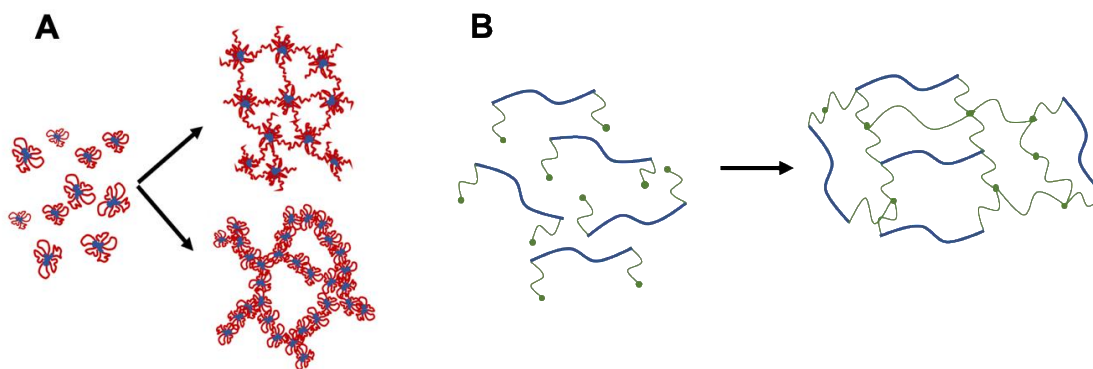


**Figure 0.8: Hydrogel networks with varying gelation mechanisms.** (A) Shows physical crosslinking with two proposed mechanisms: bridging of hydrophilic chains (top left), and micelle agglomeration (bottom left). (B) Shows a covalently crosslinked

network before and after gelation is induced. Polymer chains seen in blue have covalently crosslinkable groups on their backbone (green).

Many of the early examples of hydrogels designed for IA use involved naturally derived polymers. In 2002, Barbucci *et al.* described a hydrogel prepared from HA that was designed to release HA to the joint for chondrocyte protection. In a rabbit model, the researchers elucidated that the hydrogel had a longer resident joint time than injections of HA alone, which resulted in improved chondrocyte density and appearance.<sup>150</sup> Furthermore, hydrogels made from gelatin were studied by Saito *et al.* in 2009. Other hydrogels that were prepared from natural sources include those prepared from alginate<sup>151</sup> and chitosan,<sup>152</sup> two materials that were deemed to be similar to HA, and could act as a viscosupplementation method. While most natural polymers used for IA hydrogels were for viscosupplementation, more recently, synthetic hydrogels have been derived to deliver encapsulated therapeutics. PEG is an important synthetic polymer that has favorable properties *in vitro* and *in vivo*, leading to its use in many different hydrogel systems.

Physically crosslinked hydrogels can be prepared by a variety of methods, such as varying the temperature, or combining polyelectrolytes with multivalent ions of opposite charge.<sup>153</sup> Thermally induced crosslinking mechanisms are especially common for hydrogels that are designed for IA use, due to the ease of injection of a free-flowing liquid, followed by a rapid transition to a hydrogel upon reaching physiological temperature.

Early examples of thermo-responsive, physically crosslinked hydrogels were studied in 2012 by Petit *et al.* In their work, two different thermo-responsive poly( $\epsilon$ -caprolactone-*co*-lactide) (PCLA)-*block*-PEG-*block*-PCLA triblock copolymers (Figure 1.9) were prepared - one that was capped with a hydroxyl end group, and one that was capped with a hexanoyl end group. They were then mixed at differing ratios to form hydrogels.<sup>154</sup> The researchers determined the crosslinking to occur from an entropically driven increase in the polymer-polymer interactions at higher temperature, resulting from dehydration of the PEG and polyester copolymers, and leading to aggregation. The gelation process was

reversible upon a return to lower temperatures. The study found that the rheological properties, as well as degradation, were easy to modulate, and led to another study involving the IA administration of a hydrogel made from the PCLA-PEG-PCLA copolymer, but with an acetyl end cap.<sup>155</sup> The rheological properties of this gel were studied and it was found that the storage modulus ( $G'$ ) was  $\sim 200$  Pa. In 2014 Petit *et al.* studied these PCLA-PEG-PCLA hydrogels, loaded with celecoxib, both *in vitro* and *in vivo*. *In vitro* drug release studies of celecoxib showed that about 40% of the loaded cargo was released after 75 days.<sup>156</sup> *In vivo*, celecoxib was measurable in the synovial fluid after 30 days, although levels were below  $1 \mu\text{g/mL}$  after 5 days.<sup>157</sup>

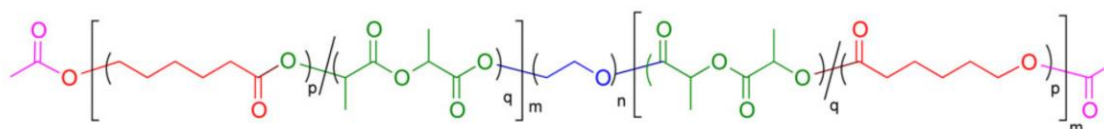


**Figure 0.9: PCLA-PEG-PCLA structure.**

In 2018 Prince *et al.* worked on a similar hydrogel, made from PCLA-PEG-PCLA copolymers with acetyl end caps but using different PEG lengths ranging from 1500-3000 g/mol, and attempted to load different drugs into the hydrogel networks. The effects of drug loading on the compressive moduli and rheological properties were studied.<sup>158</sup> As with other thermo-responsive gels, gelation occurred rapidly at  $37^\circ\text{C}$ , and was reversible. However, the incorporation of drugs into these hydrogels had significant effects on their physical properties. For instance, the addition of methotrexate to the gels increased the viscous modulus,  $G''$ , of the gel by nearly 500 Pa, while the loading of celecoxib raised it by only roughly 200 Pa. The incorporation of drug decreased the  $G'$  of the gels for all drugs tested, showing that it is important to examine the effects of drug loading on gelation.

The incorporation of kartogenin into a thermo-responsive hydrogel was studied in 2019 by Wang *et al.*<sup>159</sup> In their study, a hydrogel was prepared from a PLGA-PEG-PLGA triblock copolymer, and kartogenin was incorporated after the gel had formed. The small molecule did appear to release from the gel at a rapid rate, with a distinct burst release noted between 0 and 2 days; almost 25% of the loaded cargo was released in this time.

The release of kartogenin was measurable for up to 20 days, at which point 80% of the loaded cargo had been released. To determine the efficacy of the gel, researchers performed gene analysis post-injection in a rabbit. Kartogenin thermogels exhibited an enhanced expression of hyaline-cartilage specific genes COL-2 and AGC, and inhibited the expression of matrix metalloproteinase (MMP-13), indicating a positive effect on OA progression.

Non-covalent hydrogels have also been developed from natural polymers. The mixture of high molecular weight HA and Pluronic F127 (Figure 1.10) was studied in 2017 by Jung *et al.*<sup>160</sup> It was hypothesized in this work that the inclusion of the HA would lead to a stronger hydrogel that was capable of a prolonged joint time and release of loaded NSAIDs. The gelation of the hydrogel was measured through cloud point measurements, and the authors observed that at about 37 °C, the system gelled. It was noted that this was only seen in the mixture of Pluronic 127 and HA, but not with either polymer alone. The viscosity of the material was measured over different temperatures, and it was seen that the gel had a viscous modulus of around 700 MPa at 37 °C. *In vitro* drug release was studied using piroxicam (PX) as a loaded drug. The system did show a prolonged release, but it was less prolonged than other hydrogel systems had reported. About 50% of the loaded cargo had been released after 250 hours, which was longer than other pluronic based hydrogels that had been tested, but lower than the amount of time that would be desired for an IA injection. The *in vivo* pharmacokinetics showed that the PX loaded hydrogel had a significantly longer half-life, and a higher bioavailability than current clinically available PX injections, though no comparison to other hydrogels was performed.

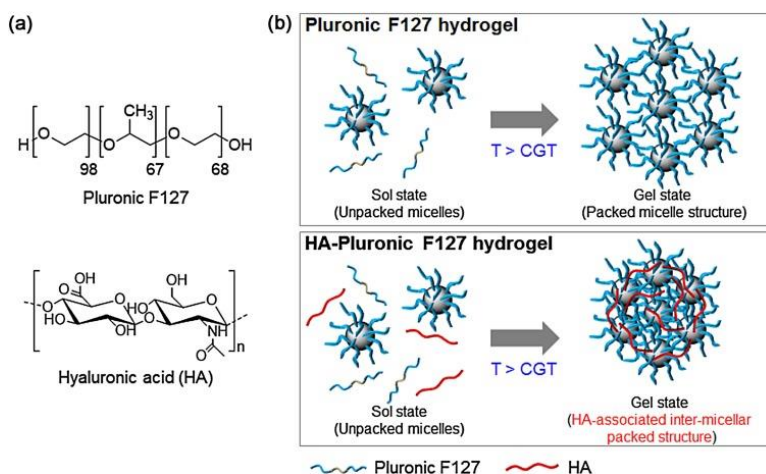


**Figure 0.10: The mixture of Pluronic F127 and Hyaluronic acid to form a hydrogel.** Reproduced with permission from reference 157. Copyright 2017, Elsevier.

Li *et al.* examined a different hydrogel synthesized from Pluronic F127 (PF) in 2018.<sup>161</sup> In addition to PF, this gel was made with GAGs, and bone morphogenetic proteins, and was designed to mimic the extracellular matrix of cartilage cells. Rheological characterization of the gels showed a distinct transition into the gel state around 25 °C, and  $G'$  and  $G''$  values close to 10 kPa and 1 kPa, respectively. *In vitro* release studies were performed using bovine serum albumin (BSA) as a model drug. It was noted by the researchers that the release of BSA from the PF/GAG gel exhibited a slower burst than other Pluronic based gels. It was hypothesized that the presence of GAGs allowed for the slowed release of the BSA protein, due to the affinity between the two molecules. A variety of different gels with Pluronic 127 and GAGs were tested for their effects on cell viability, and none of them showed significant toxicity. Furthermore, hydrogels made from PF/GAG resulted in better recovery of cartilage damage when injected into the joints of rats, as compared to Pluronic gels without GAGs.

Not all recent examples of non-covalent hydrogels intended for IA use are thermally responsive systems. In 2018 Joshi *et al.* performed a study using triglycerol monostearate (TG-18) to create a self-assembling hydrogel, that was capable of encapsulating the steroid triamcinolone acetonide (TA).<sup>162</sup> Here, the hydrogel components were dissolved in dimethyl sulfoxide (DMSO) at 55-60 °C. Upon cooling of the solution, the TG-18 self-assembled into a hydrogel with fibrous structures that had interdigitated bilayers and

extended micelles. The researchers showed that it was possible to load up to 40 w/w% of TA into the hydrogel. Rheological and mechanical properties were not assessed as part of this study, but the release of TA in response to an enzymatic stimuli of MMP inhibitors was measured. The gel in PBS showed a prolonged release, with less than 35% of the loaded cargo being released over 30 days. The gels were determined to be stimuli responsive, increasing their release when fresh enzyme was added to the gel. MTT assays, as well as LIVE/DEAD assays, were used to study the cytocompatibility *in vitro*; metabolic activity did not drop lower than 65% across all time points for the cells treated with the TG-18 hydrogel and LIVE/DEAD staining did not show any significant changes in the viability of the cells. *In vivo* work was performed, and it was found that mice treated with the TG-18 hydrogel and had lower clinical scores related to OA progression than animals treated with gel having no drug, or no gel at all. The tests also demonstrated that the system was able to respond to flares *in vitro*; inflammatory flares were modeled through the addition of esterase to the release media, causing spikes in release.

In order to create strong, robust hydrogels that can withstand the mechanical forces in the joint after IA injection, covalent crosslinking has been studied. Gels that use covalent crosslinking mechanisms tend to have increased stiffness and strength relative to non-covalent gels, and also have the ability to encapsulate drug within their network. In addition, they may have the added benefit of a slower degradation time, and therefore a slower release time in the joint.

In 2019, Prince *et al.* studied a modification of the above described non-covalently linked PCLA-PEG-PCLA hydrogels.<sup>158</sup> The gels were synthesized using the previously reported synthetic method, but methacrylate groups were added as endcaps, which could be chemically crosslinked using potassium persulfate (KPS) and tetramethylethylenediamine (TEMED) as a catalyst/initiator system.<sup>163</sup> The covalent crosslinking of the hydrogel had profound effects on the gelation, which was rapidly induced by the addition of KPS/TEMED and increasing the temperature to 37 °C. The  $G'$  of the hydrogel was 7.7 kPa  $\pm$  1.2 after 60 minutes, while the compressive modulus was 19 kPa. Both of these values were large increases compared to the previously measured  $G'$  and compressive moduli of the non-covalently crosslinked gels that were prepared from similar

copolymers with acetyl end-caps. The release of celecoxib from these hydrogels was measured *in vitro* and *in vivo*. After 30 days, only 20% of the loaded cargo had been released from the hydrogel *in vitro*. In a horse model, celecoxib was detectable for up to 60 days, and was at a therapeutic level (above 1  $\mu\text{g}/\text{mL}$ ) for 30 days. Despite the increased mechanical integrity of the covalently-linked hydrogel, animals tolerated the system well, with no adverse reactions noted in the study.

Similar to their use in non-covalently crosslinked systems, natural polymers have been used in chemically crosslinked systems as well. One such example was studied by Lu *et al.* in 2019.<sup>164</sup> Here, a hydrogel was composed of HA, fucoidan and gelatin, and was crosslinked chemically using the natural fruit extract genipin. All hydrogels that were prepared using genipin as a crosslinking agent showed relatively high compressive moduli, above 7 kPa, with the HA containing hydrogel having the highest modulus of 11.4 kPa. Gelation, as measured by rheometry, was found to occur after about 20 minutes. No cytotoxicity was observed when chondrocytes were treated with the hydrogel, and the release of a loaded growth factor occurred over 15 days.

In some instances, work has been performed to study the effects of injecting hydrogels to serve as a therapy, rather than encapsulating a drug. In 2017, von Lospichl *et al.* studied the rheological properties of a degradable dendritic polyglycerol sulfate (DPGS) hydrogel (Figure 1.11), that was designed to mimic the viscoelastic and mechanical properties of HA when used in an IA injection.<sup>165</sup> The covalent network of DPGS was hypothesized to have similar properties to HA, but with the added benefit of a covalent crosslinking mechanism, allowing for longer joint retention time. The  $G'$  values of the DPGS hydrogel were found to be very similar to those of commercially available HA injections, and it was elucidated that at certain concentrations DPGS could be used as an alternative to HA for viscosupplementation.

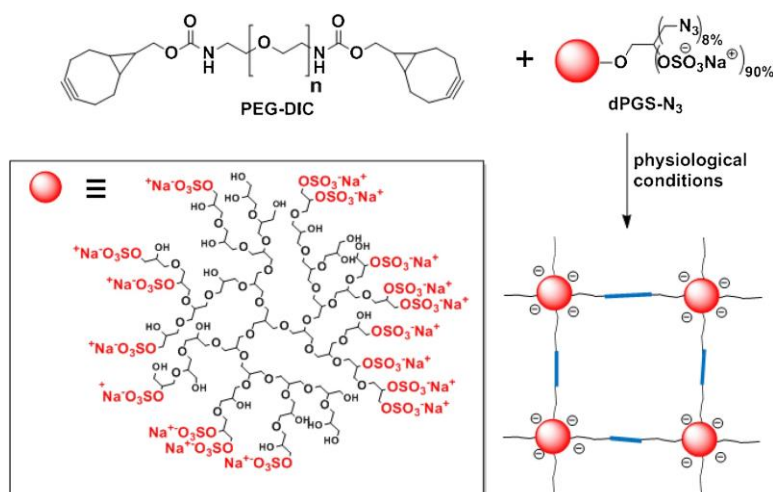


**Figure 0.11: Chemical structure of DPGS and hydrogel formation.** Reproduced with permission from reference 162. Copyright 2017, Elsevier.

The work that has been performed on IA hydrogels has moved treatment ahead, but the challenge of prolonging the release from hydrogels still remains. It is well documented that even when drugs are loaded within a hydrogel, they are subject to diffusion of the drug, which can lower the efficacy of an IA hydrogel, even if it has a long joint residence time. The desire to overcome the rapid diffusion of drug from hydrogels, and increase the release time of drug after IA injection has led to new hydrogels that combine technologies, or utilize new mechanisms to slow drug release.

In 2017, Stalder *et al.* researched the incorporation of liposomes within a hydrogel matrix.<sup>166</sup> Here, a dextran was used to make the hydrogel, and relied on in situ gelation post injection. The study examined the effect of different linkages of the liposomes to the hydrogel, and compared covalently bound liposomes to ones that were simply physically entrapped. It was found through dynamic mechanical loading that by covalently linking liposomes to the hydrogel, the release rate of the loaded cargo was lowered by 50%, and after 200 cycles of loading, only 5% of the loaded dye had been released. Despite the differences in linkages to the liposomes, all the hydrogels showed the same modulus of 1 kPa.

Furthermore, the ability to enhance the mechanical integrity of hydrogels through different linkage strategies has been studied. Here, the goal is to develop hydrogels that

are strong enough to withstand mechanical forces, and therefore will not release drug as quickly. Zhang *et al.* studied a dual physically crosslinked gel that employed both hydrophobic associations as well as ionic interactions.<sup>167</sup> The tensile strengths of these materials were measured and found to be between 150 and 300 kPa, making them some of the strongest hydrogel materials that have been developed for biomedical applications to date. However, the formulations were always in a gel state, and the development of injectable versions would require further research.

The challenge to effectively deliver medications directly to the area of injury for OA treatment remains. While hydrogel drug delivery systems have become excellent avenues for the administration and delivery of drugs, the challenges of resident joint time, rapid diffusion of drugs from the gel networks, and bioavailability of the drug still persist. The use of covalent linkages has led to stronger hydrogel networks, that are capable of having the long resident joint time required, but in many cases a rapid release of drug was still noted, thereby lowering the likelihood of any loaded drug molecule imparting the target biological effects prior to clearance.

## 1.10 Project overview

To date, a number of different disease modifying agents for OA have been proposed, yet there is still no clinically available disease modifying agent. Previous work in the Beier lab implicated PPAR $\delta$  as a potential therapeutic target for a disease modifying agent in OA. However, due to the likelihood of negative systemic side effects that could develop from the result of oral or subcutaneous delivery, a suitable drug delivery system would need to be prepared so that GSK3787 could be encapsulated, and released directly into the joint over a time period of months. A number of IA drug delivery systems with the goal of hydrophobic drug delivery have been studied to date, but no perfect system exists. IA drug delivery systems are still limited by their poor mechanical integrity, leading to a rapid breakdown in the joint, as well as burst release of drug after injection. Particles are a commonly used for IA delivery due to their injectability and relatively favorable release properties. Many other groups have reported on particle platforms made from synthetic polyesters, such as PLGA, or PLA. Here, we propose the use of PEAs,<sup>145, 168-170</sup> which are

attractive because of their tunable properties<sup>171</sup> and the fact that they are well tolerated by cells.<sup>172</sup>

The development of a platform delivery system is hallmarked by the ability to alter the types, or amounts of medications that can be delivered using it, while only making minor alterations to the formulation of the drug delivery system. Here, we experiment first on the development of drug delivery systems designed to encapsulate and deliver the NSAID celecoxib. This drug was chosen due to its common use in OA treatment, as well as continued desires for increased celecoxib use in horses. It has been shown to be effective for the treatment of the disease in animals, despite well documented side effects, so a local delivery system could be beneficial. In addition, it is inexpensive and readily available, allowing for extensive experimentation and characterization using techniques that require large amounts of material. An initial delivery system developed for celecoxib should be applicable to GSK3787.

Hydrogels have been commonly used as well for IA delivery, and remain an attractive option for IA use as they can often be formulated as injectable liquids. Furthermore, hydrogels have no history of causing mechanical irritation within the joint post-administration. Prolonging the release of drug from the hydrogel matrix after it has been injected remains a goal for the development of new hydrogel formulations.

Overall, the goal of this thesis work is to develop new platform drug delivery systems that can encapsulate GSK3787, as well as other medications, and provide a prolonged release after injection into the joint.

### 1.10.1 Hypothesis

Poly(ester amide)s can be used to develop an intra-articular drug delivery system capable of encapsulating and releasing GSK3787 and celecoxib in a controlled manner. Particles prepared with poly(ester amide) will exhibit no cellular toxicity, and no measurable host response when injected into animal models.

### 1.10.2 Specific Aims

**Objective 1:** To compare two different PEAs for the preparation of particle-based delivery systems for celecoxib and to evaluate the systems based on physicochemical characteristics, toxicity on cells, and host response *in vivo*.

**Objective 2:** To use the results from objective 1, to develop and study PEA particles loaded with the potential OA therapeutic GSK3787.

**Objective 3:** To develop a PEA particle-loaded thermo-responsive and covalently crosslinked hydrogels to encapsulate and deliver GSK3787, and to evaluate the effect of particle incorporation on the physicochemical properties of the hydrogels.

## 1.11 References

1. Sharid, B.; Kopec, J.; Bansback, N.; Rahman, M. M.; Flanagan, W. M.; Wong, H., Projecting the direct cost burden of osteoarthritis in Canada using a microsimulation model. *Osteoarthr. Cartil.* **2015**, *23*, 1654-1663.
2. Suri, P.; Morgenroth, D. C.; Hunter, D. J., Epidemiology of osteoarthritis and associated comorbidities. *PM. R.* **2012**, *4*, S10-S19.
3. Zhang, Y.; Jordan, J. M., Epidemiology of osteoarthritis. *Clin. Geriatr. Med.* **2010**, *26*, 355-369.
4. Zhao, X.; Shah, D.; Gandhi, K.; Wei, W.; Dwibedi, N.; Webster, L.; Sambamoorthi, U., Clinical, humanistic, and economic burden of osteoarthritis among noninstitutionalized adults in the United States. *Osteoarthr. Cartil.* **2019**, *27*, 1618-1626.
5. Vrdoljak, D.; Selimovic, M.; Marin, A.; Utrobicic, A.; Tugwell, P.; Puljak, L.; Puljak, L., Celecoxib for osteoarthritis. In *Cochrane Database Syst. Rev.* 2012; 5,1-8.
6. Glyn-Jones, S.; Palmer, A. J. R.; Agricola, R.; Price, A. J.; Vincent, T. L.; Weinans, H.; Carr, A. J., Osteoarthritis. *Lancet* **2015**, *386*, 376-387.
7. Ratneswaran, A.; LeBlanc, E. A.; Walser, E.; Welch, I.; Mort, J. S.; Borradaile, N.; Beier, F., Peroxisome proliferator-activated receptor delta promotes the progression of posttraumatic osteoarthritis in a mouse model. *Arthritis Rheumatol.* **2015**, *67*, 454-464.

8. Ratneswaran, A.; Sun, M. M.; Dupuis, H.; Sawyez, C.; Borradaile, N.; Beier, F., Nuclear receptors regulate lipid metabolism and oxidative stress markers in chondrocytes. *J. Mol. Med. (Berl)* **2017**, *95*, 431-444.
9. Ratneswaran, A.; LeBlanc, E. A.; Walser, E.; Welch, I.; Mort, J. S.; Borradaile, N.; Beier, F., Peroxisome Proliferator–Activated Receptor Promotes the Progression of Posttraumatic Osteoarthritis in a Mouse Model. *Arthritis Rheumatol.* **2015**, *67*, 454-464.
10. Lee, C. H.; Olson, P.; Hevener, A.; Mehl, I.; Chong, L. W.; Olefsky, J. M.; Gonzalez, F. J.; Ham, J.; Kang, H.; Peters, J. M.; Evans, R. M., PPAR $\delta$  regulates glucose metabolism and insulin sensitivity. *Proc. Natl. Acad. Sci. U. S. A.* **2006**, *103*, 3444-3449.
11. Mirza, A. Z.; Althagafi, II; Shamshad, H., Role of PPAR receptor in different diseases and their ligands: Physiological importance and clinical implications. *Eur. J. Med. Chem.* **2019**, *166*, 502-513.
12. Loeser, R. F.; Goldring, S. R.; Scanzello, C. R.; Goldring, M. B., Osteoarthritis: a disease of the joint as an organ. *Arthritis Rheum.* **2012**, *64*, 1697-1707.
13. Glyn-Jones, S.; Palmer, A. J. R.; Agricola, R.; Price, A. J.; Vincent, T. L.; Weinans, H.; Carr, A. J., Osteoarthritis. *The Lancet* **2015**, *386*, 376-387.
14. Liu-Bryan, R.; Terkeltaub, R., Emerging regulators of the inflammatory process in osteoarthritis. *Nat. Rev. Rheumatol.* **2015**, *11*, 35-44.
15. Guilak, F., Biomechanical factors in osteoarthritis. *Best Pract Res. Clin. Rheumatol.* **2011**, *25*, 815-823.
16. MacDonald, K. V.; Sanmartin, C.; Langlois, K.; Marshall, D. A., Symptom onset, diagnosis and management of osteoarthritis. *Health Reports* **2014**, *25*.
17. Bortoluzzi, A.; Furini, F.; Scire, C. A., Osteoarthritis and its management - Epidemiology, nutritional aspects and environmental factors. *Autoimmun. Rev.* **2018**, *17*, 1097-1104.
18. Wallace, I. J.; Worthington, S.; Felson, D. T.; Jurmain, R. D.; Wren, K. T.; Maijanen, H.; Woods, R. J.; Lieberman, D. E., Knee osteoarthritis has doubled in prevalence since the mid-20th century. *Proc. Natl. Acad. Sci. U S A* **2017**, *114*, 9332-9336.

19. Hunter, D. J., Osteoarthritis. *Best Pract. Res. Clin. Rheumatol.* **2011**, 25, 801-814.
20. Palazzo, C.; Nguyen, C.; Lefevre-Colau, M. M.; Rannou, F.; Poiraudou, S., Risk factors and burden of osteoarthritis. *Ann. Phys. Rehabil. Med.* **2016**, 59, 134-138.
21. Vincent, H. K.; Heywood, K.; Connelly, J.; Hurley, R. W., Obesity and weight loss in the treatment and prevention of osteoarthritis. *PM. R.* **2012**, 4, S59-S67.
22. Christensen, R.; Bartels, E. M.; Astrup, A.; Bliddal, H., Effect of weight reduction in obese patients diagnosed with knee osteoarthritis: a systematic review and meta-analysis. *Ann. Rheum. Dis.* **2007**, 66, 433-439.
23. Fernandez-Moreno, M.; Rego, I.; Carreira-Garcia, V.; Blanco, F. J., Genetics in Osteoarthritis. *Curr. Genomics* **2008**, 9, 542-547.
24. Kerkhof, H. J.; Lories, R. J.; Meulenbelt, I.; Jonsdottir, I.; Valdes, A. M.; Arp, P.; Ingvarsson, T.; Jhamai, M.; Jonsson, H.; Stolk, L.; Thorleifsson, G.; Zhai, G.; Zhang, F.; Zhu, Y.; van der Breggen, R.; Carr, A.; Doherty, M.; Doherty, S.; Felson, D. T.; Gonzalez, A.; Halldorsson, B. V.; Hart, D. J.; Hauksson, V. B.; Hofman, A.; Ioannidis, J. P.; Kloppenburg, M.; Lane, N. E.; Loughlin, J.; Luyten, F. P.; Nevitt, M. C.; Parimi, N.; Pols, H. A.; Rivadeneira, F.; Slagboom, E. P.; Stykarsdottir, U.; Tsezou, A.; van de Putte, T.; Zmuda, J.; Spector, T. D.; Stefansson, K.; Uitterlinden, A. G.; van Meurs, J. B., A genome-wide association study identifies an osteoarthritis susceptibility locus on chromosome 7q22. *Arthritis Rheum.* **2010**, 62, 499-510.
25. Buckwalter, J. A., Sports, Joint Injury, and Posttraumatic Osteoarthritis. *J. Orthop. & Sports Physical Therapy* **2003**, 33.
26. Fox, A.; Bedi, A.; Rodeo, S. A., The basic science of articular cartilage: structure, composition, and function. *Sports Health* **2009**, 1, 461-468.
27. Camarero-Espinosa, S.; Rothen-Rutishauser, B.; Foster, E. J.; Weder, C., Articular cartilage: from formation to tissue engineering. *Biomater. Sci.* **2016**, 4, 734-767.

28. Hunter, D. J.; Guermazi, A., Imaging techniques in osteoarthritis. *PM. R.* **2012**, 4, S68-S74.
29. Akkiraju, H.; Nohe, A., Role of Chondrocytes in Cartilage Formation, Progression of Osteoarthritis and Cartilage Regeneration. *J. Dev. Biol.* **2015**, 3, 177-192.
30. Cooke, M. E.; Lawless, B. M.; Jones, S. W.; Grover, L. M., Matrix degradation in osteoarthritis primes the superficial region of cartilage for mechanical damage. *Acta Biomater.* **2018**, 78, 320-328.
31. Madry, H.; van Dijk, C. N.; Mueller-Gerbl, M., The basic science of the subchondral bone. *Knee Surg. Sports Traumatol. Arthrosc.* **2010**, 18, 419-433.
32. Lyons, T. J.; McClure, S. F.; Stoddart, R. W.; McClure, J., The normal human chondro-osseous junctional region: evidence for contact of uncalcified cartilage with subchondral bone and marrow spaces. *BMC Musculoskelet. Disord.* **2006**, 52-58.
33. Kapoor, M.; Martel-Pelletier, J.; Lajeunesse, D.; Pelletier, J. P.; Fahmi, H., Role of proinflammatory cytokines in the pathophysiology of osteoarthritis. *Nat. Rev. Rheumatol.* **2011**, 7, 33-42.
34. Weinans, H.; Siebelt, M.; Agricola, R.; Botter, S. M.; Pijpers, T. M.; Waarsing, J. H., Pathophysiology of peri-articular bone changes in osteoarthritis. *Bone* **2012**, 51, 190-196.
35. Castaneda, S.; Roman-Blas, J. A.; Largo, R.; Herrero-Beaumont, G., Subchondral bone as a key target for osteoarthritis treatment. *Biochem. Pharmacol.* **2012**, 83, 315-323.
36. Smith, M. D., The Normal Synovium. *The Open Rheumatology Journal* **2011**, 5, 100-106.

37. Baker, K.; Grainger, A.; Niu, J.; Clancy, M.; Guermazi, A.; Crema, M.; Hughes, L.; Buckwalter, J.; Wooley, A.; Nevitt, M.; Felson, D. T., Relation of synovitis to knee pain using contrast-enhanced MRIs. *Ann. Rheum. Dis.* **2010**, 69, 1779-1783.
38. Hui, A. Y.; McCarty, W. J.; Masuda, K.; Firestein, G. S.; Sah, R. L., A systems biology approach to synovial joint lubrication in health, injury, and disease. *Wiley Interdiscip. Rev. Syst. Biol. Med.* **2012**, 4, 15-37.
39. Swann, D. A.; Silver, F. H.; Slayter, H. S.; Stafford, W.; Shore, E., The molecular structure and lubricating activity of lubricin isolated from bovine and human synovial fluids. *Biochemistry* **1985**, 225, 195-201.
40. Schumacher, B. L.; Block, J. A.; Schmid, T. M.; Aydelotte, M. B.; Kuettner, K. E., A Novel Proteoglycan Synthesized and Secreted by Chondrocytes of the Superficial Zone of Articular Cartilage. *Archives of Biochemistry and Biophysics* **1994**, 311, 144-152.
41. Schwarz, I. M.; Hills, B. A., Surface-active phospholipid as the lubricating component of lubricin  
. *British Journal of Rheumatology* **1998**, 37, 21-26.
42. Braun, H. J.; Gold, G. E., Diagnosis of osteoarthritis: imaging. *Bone* **2012**, 51, 278-288.
43. Peat, G.; Thomas, E.; Duncan, R.; Wood, L.; Hay, E.; Croft, P., Clinical classification criteria for knee osteoarthritis: performance in the general population and primary care. *Ann. Rheum. Dis.* **2006**, 65, 1363-1367.
44. Woods, B.; Manca, A.; Weatherly, H.; Saramago, P.; Sideris, E.; Giannopoulou, C.; Rice, S.; Corbett, M.; Vickers, A.; Bowes, M.; MacPherson, H.; Sculpher, M., Cost-effectiveness of adjunct non-pharmacological interventions for osteoarthritis of the knee. *PLoS One* **2017**, 12, 1-12.

45. Regnaud, J. P.; Lefevre-Colau, M. M.; Trinquart, L.; Nguyen, C.; Boutron, I.; Brosseau, L.; Ravaud, P., High-intensity versus low-intensity physical activity or exercise in people with hip or knee osteoarthritis. *Cochrane Database Syst Rev* **2015**, CD010203.
46. Semanik, P. A.; Chang, R. W.; Dunlop, D. D., Aerobic activity in prevention and symptom control of osteoarthritis. *PM. R.* **2012**, 4, S37-S44.
47. Tenforde, A. S.; Shull, P. B.; Fredericson, M., Neuromuscular prehabilitation to prevent osteoarthritis after a traumatic joint injury. *PM. R.* **2012**, 4, S141-S144.48.
48. Vincent, K. R.; Vincent, H. K., Resistance exercise for knee osteoarthritis. *PM. R.* **2012**, 4, S45-S52.
49. Brakke, R.; Singh, J.; Sullivan, W., Physical therapy in persons with osteoarthritis. *PM. R.* **2012**, 4, S53-S58.
50. Segal, N. A., Bracing and orthoses: a review of efficacy and mechanical effects for tibiofemoral osteoarthritis. *PM. R.* **2012**, 4, S89-S96.
51. De Luigi, A. J., Complementary and alternative medicine in osteoarthritis. *PM. R.* **2012**, 4, S122-S133.
52. Leong, D. J.; Choudhury, M.; Hirsh, D. M.; Hardin, J. A.; Cobelli, N. J.; Sun, H. B., Nutraceuticals: potential for chondroprotection and molecular targeting of osteoarthritis. *Int. J. Mol. Sci.* **2013**, 14, 23063-23085.
53. Lopez, H. L., Nutritional interventions to prevent and treat osteoarthritis. Part II: focus on micronutrients and supportive nutraceuticals. *PM. R.* **2012**, 4, S155-S168.
54. Wang, A.; Leong, D. J.; Cardoso, L.; Sun, H. B., Nutraceuticals and osteoarthritis pain. *Pharmacol. Ther.* **2018**, 187, 167-179.
55. Lopez, H. L., Nutritional interventions to prevent and treat osteoarthritis. Part I: focus on fatty acids and macronutrients. *PM. R.* **2012**, 4, S145-154.

56. Messier, S. P.; Gutekunst, D. J.; Davis, C.; DeVita, P., Weight loss reduces knee-joint loads in overweight and obese older adults with knee osteoarthritis. *Arthritis Rheum.* **2005**, *52*, 2026-2032.
57. Messier, S. P.; Resnik, A. E.; Beavers, D. P.; Mihalko, S. L.; Miller, G. D.; Nicklas, B. J.; deVita, P.; Hunter, D. J.; Lyles, M. F.; Eckstein, F.; Guermazi, A.; Loeser, R. F., Intentional Weight Loss in Overweight and Obese Patients With Knee Osteoarthritis: Is More Better? *Arthritis Care Res.* **2018**, *70*, 1569-1575.
58. Koybasi, M.; Borman, P.; Kocaoglu, S.; Ceceli, E., The effect of additional therapeutic ultrasound in patients with primary hip osteoarthritis: a randomized placebo-controlled study. *Clin. Rheumatol.* **2010**, *29*, 1387-1394.
59. Hurley, M. V.; Walsh, N. E.; Mitchell, H. L.; Pimm, T. J.; Patel, A.; Williamson, E.; Jones, R. H.; Dieppe, P. A.; Reeves, B. C., Clinical effectiveness of a rehabilitation program integrating exercise, self-management, and active coping strategies for chronic knee pain: a cluster randomized trial. *Arthritis Rheum.* **2007**, *57*, 1211-1219.
60. Lespasio, M. J.; Sultan, A. A.; Piuizzi, N. S.; Khlopas, A.; Husni, M. E.; Muschler, G. F.; Mont, M. A., Hip Osteoarthritis: A Primer. *Perm. J.* **2018**, *22*, 17-84.
61. Krumholz, H.; Ross, J.; Presler, A.; Egilman, D., What have we learnt from Vioxx? *BMJ* **2007**, *334*, 120-123.
62. Cheng, D. S.; Visco, C. J., Pharmaceutical therapy for osteoarthritis. *PM. R.* **2012**, *4*, S82-S88.
63. Mahmud, T.; Scott, D. L.; Bjarnason, I., A Unifying Hypothesis for the Mechanism of NSAID Related Gastrointestinal Toxicity. *Annals Rheum. Dis.* **1996**, *55*, 211-213.
64. Grosser, T.; Fries, S.; FitzGerald, G. A., Biological basis for the cardiovascular consequences of COX-2 inhibition: therapeutic challenges and opportunities. *J. Clin. Invest.* **2006**, *116*, 4-15.

65. Brown, J. P.; Boulay, L. J., Clinical experience with duloxetine in the management of chronic musculoskeletal pain. A focus on osteoarthritis of the knee. *Ther Adv Musculoskelet. Dis.* **2013**, 5, 291-304.
66. Haroutiunian, S.; Drennan, D. A.; Lipman, A. G., Topical NSAID Therapy for Musculoskeletal Pain. *Pain Medicine* **2010**, 11, 535-549.
67. Mason, L.; Moore, R. A.; Derry, S.; Edwards, J. E.; McQuay, H. J., Systematic review of topical capsaicin for the treatment of chronic pain. *BMJ* **2004**, 328,991.
68. Gossec, L.; Dougados, M., Intra-articular treatments in osteoarthritis: from the symptomatic to the structure modifying. *Ann. Rheum. Dis.* **2004**, 63, 478-482.
69. Douglas, R. J., Corticosteroid injection into the osteoarthritic knee: drug selection, dose, and injection frequency. *Int. J. Clin. Pract.* **2012**, 66, 699-704.
70. Habib, G. S., Systemic effects of intra-articular corticosteroids. *Clin. Rheumatol.* **2009**, 28, 749-756.
71. Habib, G. S.; Saliba, W.; Nashashibi, M., Local effects of intra-articular corticosteroids. *Clin. Rheumatol.* **2010**, 29, 347-356.
72. Evans, C. H.; Kraus, V. B.; Setton, L. A., Progress in intra-articular therapy. *Nature Reviews Rheumatology* **2013**, 10, 11-22.
73. Bellamy, N.; Campbell, J.; Robinson, V.; Gee, T.; Bourne, R.; Wells, G., Intraarticular corticosteroid for treatment of osteoarthritis of the knee. *Cochrane Database Syst. Rev.* **2006**, CD005328.
74. Goodrich, L. R.; Nixon, A. J., Medical treatment of osteoarthritis in the horse - a review. *Vet. J.* **2006**, 171, 51-69.
75. Bellamy, N.; Campbell, J.; Robinson, V.; Gee, T.; Bourne, R.; Wells, G., Viscosupplementation for the treatment of osteoarthritis of the knee. *Cochrane Database Syst Rev* **2005**, CD005321.

76. Grayson, C. W.; Decker, R. C., Total joint arthroplasty for persons with osteoarthritis. *PM. R.* **2012**, 4, S97-S103.
77. Losina, E.; Paltiel, A. D.; Weinstein, A. M.; Yelin, E.; Hunter, D. J.; Chen, S. P.; Klara, K.; Suter, L. G.; Solomon, D. H.; Burbine, S. A.; Walensky, R. P.; Katz, J. N., Lifetime medical costs of knee osteoarthritis management in the United States: impact of extending indications for total knee arthroplasty. *Arthritis Care Res.* **2015**, 67, 203-215.
78. Sharif, B.; Kopec, J.; Bansback, N.; Rahman, M. M.; Flanagan, W. M.; Wong, H.; Fines, P.; Anis, A., Projecting the direct cost burden of osteoarthritis in Canada using a microsimulation model. *Osteoarth. Cartilage* **2015**, 23, 1654-1663.
79. Kenney, N. A.; Farmer, K. W., Minimally invasive versus conventional joint arthroplasty. *PM. R.* **2012**, 4, S134-S140.
80. Hunter, D. J.; McDougall, J. J.; Keefe, F. J., The Symptoms of Osteoarthritis and the Genesis of Pain. *Rheumatic Disease Clinics of North America* **2008**, 34, 623-643.
81. Stevens, R.; Hanson, P.; Wei, N.; Allen, R.; Guedes, K.; Burges, R.; Campbell, J., (382) Safety and Tolerability of CNTX-4975 in Subjects with Chronic, Moderate to Severe Knee Pain Associated With Osteoarthritis (OA): A Pilot Study. *The Journal of Pain* **2017**, 18, 122-129.
82. Kelly, S.; Chapman, R. J.; Woodhams, S.; Sagar, D. R.; Turner, J.; Burston, J. J.; Bullock, C.; Paton, K.; Huang, J.; Wong, A.; McWilliams, D. F.; Okine, B. N.; Barrett, D. A.; Hathway, G. J.; Walsh, D. A.; Chapman, V., Increased function of pronociceptive TRPV1 at the level of the joint in a rat model of osteoarthritis pain. *Ann. Rheum. Dis.* **2015**, 74, 252-259.
83. Maudens, P.; Jordan, O.; Allemann, E., Recent advances in intra-articular drug delivery systems for osteoarthritis therapy. *Drug Discov. Today* **2018**, 0, 1-15.
84. Brown, W.; Leff, R. L.; Griffin, A.; Hossack, S.; Aubray, R.; Walker, P.; Chiche, D. A., Safety, Pharmacokinetics, and Pharmacodynamics Study in Healthy

Subjects of Oral NEO6860, a Modality Selective Transient Receptor Potential Vanilloid Subtype 1. *Antagonist. J. Pain* **2017**, 18, 726-738.

85. Quiding, H.; Jonzon, B.; Svensson, O.; Webster, L.; Reimfelt, A.; Karin, A.; Karlsten, R.; Segerdahl, M., TRPV1 antagonistic analgesic effect: a randomized study of AZD1386 in pain after third molar extraction. *Pain* **2013**, 154, 808-812.

86. Schuelert, N.; McDougall, J. J., Involvement of Nav 1.8 sodium ion channels in the transduction of mechanical pain in a rodent model of osteoarthritis. *Arthritis Res. Ther.* **2012**, 14, 2-9.

87. Hochberg, M. C., Serious joint-related adverse events in randomized controlled trials of anti-nerve growth factor monoclonal antibodies. *Osteoarth. Cartilage* **2015**, 23, S18-S21.

88. Maloney, J.; Kivitz, A.; Schnitzer, T. J.; Dakin, P.; Di Martino, S.; Gao, H.; Stehman-Breen, C.; Geba, G., Fasinumab in the treatment of hip and knee osteoarthritic pain: efficacy and safety in a 36-week randomized, double-blind placebo-controlled clinical trial. *Osteoarth. and Cartilage* **2017**, 25, S56-S57.

89. Schnitzer, T. J.; Ekman, E. F.; Spierings, E. L.; Greenberg, H. S.; Smith, M. D.; Brown, M. T.; West, C. R.; Verburg, K. M., Efficacy and safety of tanezumab monotherapy or combined with non-steroidal anti-inflammatory drugs in the treatment of knee or hip osteoarthritis pain. *Ann. Rheum. Dis.* **2015**, 74, 1202-1211.

90. Malfait, A. M.; Miller, R. J., Emerging Targets for the Management of Osteoarthritis Pain. *Curr. Osteoporos. Rep.* **2016**, 14, 260-268.

91. Alcaraz, M. J.; Guillen, M. I.; Ferrandiz, M. L., Emerging therapeutic agents in osteoarthritis. *Biochem. Pharmacol.* **2019**, 165, 4-16.

92. Sophocleous, A.; Borjesson, A. E.; Salter, D. M.; Ralston, S. H., The type 2 cannabinoid receptor regulates susceptibility to osteoarthritis in mice. *Osteoarth. Cartilage* **2015**, 23, 1586-1594.

93. Philpott, H. T.; O'Brien, M.; McDougall, J. J., Attenuation of early phase inflammation by cannabidiol prevents pain and nerve damage in rat osteoarthritis. *Pain* **2017**, 158, 2442-2451.
94. Hammell, D. C.; Zhang, L. P.; Ma, F.; Abshire, S. M.; McIlwrath, S. L.; Stinchcomb, A. L.; Westlund, K. N., Transdermal cannabidiol reduces inflammation and pain-related behaviours in a rat model of arthritis. *Eur. J Pain* **2016**, 20, 936-948.
95. Takano, S.; Uchida, K.; Miyagi, M.; Inoue, G.; Fujimaki, H.; Aikawa, J.; Iwase, D.; Minatani, A.; Iwabuchi, K.; Takaso, M., Nerve Growth Factor Regulation by TNF-alpha and IL-1beta in Synovial Macrophages and Fibroblasts in Osteoarthritic Mice. *J Immunol. Res.* **2016**, 5706359.
96. Fernandes, J. C.; Martel-Pelletier, J.; Pelletier, J. P., The role of cytokines in osteoarthritis pathophysiology. *Biorheology* **2002**, 39, 237-246.
97. Chevalier, X., Upregulation of enzymatic activity by interleukin-1 in osteoarthritis. *Biomed and Pharmacother.* **1997**, 51, 58-62.
98. Scoville, C.; Dickson, J., Open-label use of Anakinra (Kineret) in the treatment of patients with osteoarthritis. *Indian Journal of Rheumatology* **2017**, 12.
99. Lacy, S. E.; Wu, C.; Ambrosi, D. J.; Hsieh, C. M.; Bose, S.; Miller, R.; Conlon, D. M.; Tarcsa, E.; Chari, R.; Ghayur, T.; Kamath, R. V., Generation and characterization of ABT-981, a dual variable domain immunoglobulin (DVD-Ig(TM)) molecule that specifically and potently neutralizes both IL-1alpha and IL-1beta. *MAbs.* **2015**, 7, 605-619.
100. Maksymowych, W. P.; Russell, A. S.; Chiu, P.; Yan, A.; Jones, N.; Clare, T.; Lambert, R. G., Targeting tumour necrosis factor alleviates signs and symptoms of inflammatory osteoarthritis of the knee. *Arthritis Res. Ther.* **2012**, 14 (R206).
101. Grothe, K.; Flechsenhar, K.; Paehler, T.; Ritzeler, O.; Beninga, J.; Saas, J.; Herrmann, M.; Rudolphi, K., IkappaB kinase inhibition as a potential treatment of

osteoarthritis - results of a clinical proof-of-concept study. *Osteoarth. Cartilage* **2017**, *25*, 46-52.

102. Pradal, J.; Zuluaga, M. F.; Maudens, P.; Waldburger, J. M.; Seemayer, C. A.; Doelker, E.; Gabay, C.; Jordan, O.; Allemann, E., Intra-articular bioactivity of a p38 MAPK inhibitor and development of an extended-release system. *Eur. J. Pharm. Biopharm.* **2015**, *93*, 110-117.

103. Shearer, B. G.; Steger, D. J.; Way, J. M.; Stanley, T. B.; Lobe, D. C.; Grillot, D. A.; Iannone, M. A.; Lazar, M. A.; Willson, T. M.; Billin, A. N., Identification and Characterization of a Selective Peroxisome Proliferator-Activated Receptor  $\beta/\delta$  (NR1C2) Antagonist. *Mol. Endocrinol.* **2008**, *22*, 523-529.

104. Palkar, P.; Borland, M. G.; Naruhn, S.; Ferry, C. H.; Lee, C.; Sk, U. H.; Sharma, A. K.; Amin, S.; Murray, I. A.; Anderson, C. R.; Perdew, G. H.; Gonzalez, F. J.; Muller, R.; Peters, J. M., Cellular and Pharmacological Selectivity of the Peroxisome Proliferator-Activated Receptor-  $\beta/\delta$  Antagonist GSK3787. *Mol. Pharmacol.* **2010**, *78*, 419-430.

105. Schmuth, M.; Haqq, C. M.; Cairns, W. J.; Holder, J. C.; Dorsam, S.; Chang, S.; Lau, P.; Fowler, A. J.; Chuang, G.; Moser, A. H.; Brown, B. E.; Mao-Qiang, M.; Uchida, Y.; Schoonjans, K.; Auwerx, J.; Chambon, P.; Willson, T. M.; Elias, P. M.; Feingold, K. R., Peroxisome proliferator-activated receptor (PPAR)- $\beta/\delta$  stimulates differentiation and lipid accumulation in keratinocytes. *J. Invest. Dermatol.* **2004**, *122*, 971-983.

106. Billin, A. N., PPAR- $\beta/\delta$  agonists for type 2 diabetes and dyslipidemia: a adopted orphan still looking for a home. *Expert Opin. Invest. Drugs* **2008**, *17*, 1465-1471.

107. Sprecher, D. L.; Massein, C.; Pearce, G.; Billin, A. N.; Perlstein, I.; Willson, T. M.; Hassall, D. G.; Ancellin, N.; Patterson, S. D.; Lobe, D. C.; Johnson, T. G., Triglyceride: High-density lipoprotein cholesterol effects in healthy subjects administered a peroxisome proliferator activated receptor delta agonist. *Thromb. Vasc. Biol.* **2007**, *27*, 359-365.

108. Sauerberg, P.; Olsen, G. S.; Jeppesen, L.; Mogensen, J. P.; Pettersson, I.; Jeppesen, C. B.; Daugaard, J. R.; Galsgaard, E. D.; Ynddal, L.; Fleckner, J.; Panajotova, V.; Polivka, Z.; Pihera, P.; Havranek, M.; Wulff, E. M., Identification and Synthesis of a Novel Selective Partial PPAR $\delta$  Agonist with Full Efficacy on Lipid Metabolism in Vitro and in Vivo. *J. Med. Chem.* **2007**, 50, 1495-1503.
109. Riserus, U.; Sprecher, D.; Johnson, T.; Olson, E.; Hirschberg, S.; Liu, A.; Fang, Z.; Hegde, P.; Richards, D.; Sarov-Blat, L.; Strum, J. C.; Basu, S.; Cheeseman, J.; Fielding, B. A.; Humphreys, S. M.; Danoff, T.; Moore, N. R.; Murgatroyd, P.; O'Rahilly, S.; Sutton, P.; Willson, T.; Hassall, D.; Frayn, K. N.; Karpe, F., Activation of Peroxisome Proliferator-Activated Receptor(PPAR) $\delta$  Promotes Reversal of Multiple Metabolic Abnormalities, Reduces Oxidative Stress, and Increases Fatty Acid Oxidation in Moderately Obese Men. *Diabetes* **2008**, 57, 332-339.
110. Kalinin, S.; Richardson, J. C.; Feinstein, D. L., A PPARdelta agonist reduces amyloid burden and brain inflammation in a transgenic mouse model of Alzheimer's disease. *Curr. Alzheimer Res.* **2009**, 6, 431-437.
111. Abdel-Rahman, E. A.; Bhattacharya, S.; Buabeid, M.; Majrashi, M.; Bloemer, J.; Tao, Y. X.; Dhanasekaran, M.; Escobar, M.; Amin, R.; Suppiramaniam, V., PPAR- $\delta$  Activation Ameliorates Diabetes-Induced Cognitive Dysfunction by Modulating Integrin-linked Kinase and AMPA Receptor Function. *J. Am. Coll. Nutr.* **2019**, 38, 693-702.
112. Larsen, C.; Østergaard, J.; Larsen, S. W.; Jensen, H.; Jacobsen, S.; Lindegaard, C.; Andersen, P. H., Intra-articular depot formulation principles: Role in the management of postoperative pain and arthritic disorders. *J. Pharm. Sci.* **2008**, 97, 4622-4654.
113. Edwards, S. H., Intra-articular drug delivery: the challenge to extend drug residence time within the joint. *Vet J.* **2011**, 190, 15-21.
114. Gerwin, N.; Hops, C.; Lucke, A., Intraarticular drug delivery in osteoarthritis. *Adv. Drug Deliv. Rev.* **2006**, 58, 226-242.

115. Popot, M. A.; Bonnaire, Y.; Guechotp, J.; Toutain, L., Hyaluronan in horses: physiological production rate, plasma and synovial fluid concentrations in control conditions and following sodium hyaluronate administration. *Equine Vet J* **2004**, 36, 234-237.
116. Knight, A. D.; Levick, J. R., Morphometry of the ultrastructure of the blood-joint barrier in the rabbit knee. *Quarterly Journal of Experimental Physiology* **1984**, 69, 271-288.
117. Malone, M. A.; Kaushik, N.; Waheed, A., Intra-articular steroids: How soon and how often after the first injection? *SM. J. Community Med.* **2016**, 2, 1014.
118. Stephens, M. B.; Beutler, A. I.; O'Connor, F. G., Musculoskeletal injections: A review of the evidence. *Am. Family Phys.* **2008**, 78, 970-976.
119. Cheng, J.; Abdi, S., Complications of joint, tendon, and muscle injections. *Tech. Reg. Anesth. Pain Manag.* **2007**, 11, 141-147.
120. Maudens, P.; Jordan, O.; Allemann, E., Recent advances in intra-articular drug delivery systems for osteoarthritis therapy. *Drug Discov. Today* **2018**, 23, 1761-1775.
121. Dong, J.; Jiang, D.; Wang, Z.; Wu, G.; Miao, L.; Huang, L., Intra-articular delivery of liposomal celecoxib-hyaluronate combination for the treatment of osteoarthritis in rabbit model. *Int J Pharm* **2013**, 441, 285-290.
122. Bangham, A. D.; Standish, M. M.; Watkins, J. C., Diffusion of Univalent Ions across the Lamellae of Swollen Phospholipids. *J. Mol Bio* **1965**, 13, 238-252.
123. Edwards, S. H.; Cake, M. A.; Spoelstra, G.; Read, R. A., Biodistribution and clearance of intra-articular liposomes in a large animal model using a radiographic marker. *J. Liposome Res.* **2007**, 17, 249-261.
124. Mota, A. H.; Direito, R.; Carrasco, M. P.; Rijo, P.; Ascensao, L.; Viana, A. S.; Rocha, J.; Eduardo-Figueira, M.; Rodrigues, M. J.; Custodio, L.; Kuplennik, N.; Sosnik, A.; Almeida, A. J.; Gaspar, M. M.; Reis, C. P., Combination of hyaluronic acid

and PLGA particles as hybrid systems for viscosupplementation in osteoarthritis. *Int. J. Pharm.* **2019**, 559, 13-22.

125. Cho, K.; Wang, X.; Nie, S.; Chen, Z. G.; Shin, D. M., Therapeutic nanoparticles for drug delivery in cancer. *Clin. Cancer Res.* **2008**, 14, 1310-1316.

126. Ibrahim, M. M.; Abd-Elgawad, A. E.; Soliman, O. A.; Jablonski, M. M., Nanoparticle-based topical ophthalmic formulations for sustained celecoxib release. *J. Pharm. Sci.* **2013**, 102, 1036-1053.

127. Ryan, S. M.; McMorrow, J.; Umerska, A.; Patel, H. B.; Kornerup, K. N.; Tajber, L.; Murphy, E. P.; Perretti, M.; Corrigan, O. I.; Brayden, D. J., An intra-articular salmon calcitonin-based nanocomplex reduces experimental inflammatory arthritis. *J. Control. Release* **2013**, 167, 120-129.

128. Kang, M. L.; Ko, J. Y.; Kim, J. E.; Im, G. I., Intra-articular delivery of kartogenin-conjugated chitosan nano/microparticles for cartilage regeneration. *Biomaterials* **2014**, 35, 9984-9994.

129. Jain, A.; Mishra, S. K.; Vuddanda, P. R.; Singh, S. K.; Singh, R.; Singh, S., Targeting of diacerein loaded lipid nanoparticles to intra-articular cartilage using chondroitin sulfate as homing carrier for treatment of osteoarthritis in rats. *Nanomedicine* **2014**, 10, 1031-1040.

130. Morgen, M.; Tung, D.; Boras, B.; Miller, W.; Malfait, A. M.; Tortorella, M., Nanoparticles for improved local retention after intra-articular injection into the knee joint. *Pharm. Res.* **2013**, 30, 257-268.

131. Poh, S.; Lin, J. B.; Panitch, A., Release of anti-inflammatory peptides from thermosensitive nanoparticles with degradable cross-links suppresses pro-inflammatory cytokine production. *Biomacromolecules* **2015**, 16, 1191-1200.

132. Gong, J.; Jaiswal, R.; Dalla, P.; Luk, F.; Bebawy, M., Microparticles in cancer: A review of recent developments and the potential for clinical application. *Semin. Cell Dev. Biol.* **2015**, 40, 35-40.

133. Wong, C. Y.; Al-Salami, H.; Dass, C. R., Microparticles, microcapsules and microspheres: A review of recent developments and prospects for oral delivery of insulin. *Int. J. Pharm.* **2018**, 537, 223-244.
134. Chen, Z. P.; Liu, W.; Liu, D.; Xiao, Y. Y.; Chen, H. X.; Chen, J.; Li, W.; Cai, H.; Li, W.; Cai, B. C.; Pan, J., Development of brucine-loaded microsphere/thermally responsive hydrogel combination system for intra-articular administration. *J. Control Release* **2012**, 162, 628-635.
135. Yin, W.; Wang, T.-S.; Yin, F.-Z.; Cai, B.-C., Analgesic and anti-inflammatory properties of brucine and brucine N-oxide extracted from seeds of *Strychnos nux-vomica*. *Journal of Ethnopharmacology* **2003**, 88, 205-214.
136. Muller, W. E. G.; Neufurth, M.; Wang, S.; Ackermann, M.; Munoz-Espi, R.; Feng, Q.; Lu, Q.; Schroder, H. C.; Wang, X., Amorphous, Smart, and Bioinspired Polyphosphate Nano/Microparticles: A Biomaterial for Regeneration and Repair of Osteo-Articular Impairments In-Situ. *Int. J. Mol. Sci.* **2018**, 19, 1-12.
137. She, G.; Zhou, Z.; Zha, Z.; Wang, F.; Pan, X., Protective effect of zoledronic acid on articular cartilage and subchondral bone of rabbits with experimental knee osteoarthritis. *Exp. Ther. Med.* **2017**, 14, 4901-4909.
138. Makadia, H. K.; Siegel, S. J., Poly Lactic-co-Glycolic Acid (PLGA) as Biodegradable Controlled Drug Delivery Carrier. *Polymers (Basel)* **2011**, 3, 1377-1397.
139. Kumar, A.; Bendele, A. M.; Blanks, R. C.; Bodick, N., Sustained efficacy of a single intra-articular dose of FX006 in a rat model of repeated localized knee arthritis. *Osteoarth. Cartilage* **2015**, 23, 151-160.
140. Gomez-Gaete, C.; Retamal, M.; Chavez, C.; Bustos, P.; Godoy, R.; Torres-Vergara, P., Development, characterization and in vitro evaluation of biodegradable rhein-loaded microparticles for treatment of osteoarthritis. *Eur. J. Pharm. Sci.* **2017**, 96, 390-397.

141. Pradal, J.; Maudens, P.; Gabay, C.; Seemayer, C. A.; Jordan, O.; Allemann, E., Effect of particle size on the biodistribution of nano- and microparticles following intra-articular injection in mice. *Int. J. Pharm.* **2016**, 498, 119-129.
142. Goto, N.; Okazaki, K.; Akasaki, Y.; Ishihara, K.; Murakami, K.; Koyano, K.; Ayukawa, Y.; Yasunami, N.; Masuzaki, T.; Nakashima, Y., Single intra-articular injection of fluvastatin-PLGA microspheres reduces cartilage degradation in rabbits with experimental osteoarthritis. *J Orthop. Res.* **2017**, 35, 2465-2475.
143. Karimi, P.; Rizkalla, A. S.; Mequanint, K., Versatile Biodegradable Poly(ester amide)s Derived from  $\alpha$ -Amino Acids for Vascular Tissue Engineering. *Materials* **2010**, 3, 2346-2368.
144. Knight, D. K.; Gillies, E. R.; Mequanint, K., Biomimetic L-aspartic acid-derived functional poly(ester amide)s for vascular tissue engineering. *Acta Biomater.* **2014**, 10, 3484-3496.
145. Janssen, M.; Timur, U. T.; Woike, N.; Welting, T. J.; Draaisma, G.; Gijbels, M.; van Rhijn, L. W.; Mihov, G.; Thies, J.; Emans, P. J., Celecoxib-loaded PEA microspheres as an auto regulatory drug-delivery system after intra-articular injection. *J. Controlled Release* **2016**, 244, 30-40.
146. Martin, C.; Winet, H.; Bao, J. Y., Acidity near eroding polylactide-polyglycolide in vitro and in vivo in rabbit tibial bone chambers. *Biomaterials* **1996**, 17, 2373-2380.
147. Suganuma, J.; Alexander, H., Biological response of intramedullary bone to poly-L-lactic acid. *J. Appl. Biomater.* **1993**, 4, 13-27.
148. Sukarto, A.; Amsden, B. G., Low melting point amphiphilic microspheres for delivery of bone morphogenetic protein-6 and transforming growth factor-beta3 in a hydrogel matrix. *J. Controlled Release* **2012**, 158, 53-62.
149. Ahmed, E. M., Hydrogel: Preparation, characterization, and applications: A review. *J Adv Res* **2015**, 6, 105-21.

150. Barbuccia, R.; Lamponia, S.; Borzacchiello, L.; Ambrosio, L.; Finic, P.; Torricelli, D.; Giardinoc, R., Hyaluronic acid hydrogel in the treatment of osteoarthritis. *Biomaterials* **2002**, *23*, 4503-4513.
151. Stevens, M. M.; Qanadilo, H. F.; Langer, R.; Prasad Shastri, V., A rapid-curing alginate gel system: utility in periosteum-derived cartilage tissue engineering. *Biomaterials* **2004**, *25*, 887-894.
152. Hao, T.; Wen, N.; Cao, J. K.; Wang, H. B.; Lu, S. H.; Liu, T.; Lin, Q. X.; Duan, C. M.; Wang, C. Y., The support of matrix accumulation and the promotion of sheep articular cartilage defects repair in vivo by chitosan hydrogels. *Osteoarth. Cartilage* **2010**, *18*, 257-65.
153. Trombino, S.; Servidio, C.; Curcio, F.; Cassano, R., Strategies for Hyaluronic Acid-Based Hydrogel Design in Drug Delivery. *Pharmaceutics* **2019**, *11*, 1-17.
154. Petit, A.; Muller, B.; Bruin, P.; Meyboom, R.; Piest, M.; Kroon-Batenburg, L. M.; de Leede, L. G.; Hennink, W. E.; Vermonden, T., Modulating rheological and degradation properties of temperature-responsive gelling systems composed of blends of PCLA-PEG-PCLA triblock copolymers and their fully hexanoyl-capped derivatives. *Acta Biomater.* **2012**, *8*, 4260-4267.
155. Petit, A.; Muller, B.; Meijboom, R.; Bruin, P.; van de Manakker, F.; Versluijs-Helder, M.; de Leede, L. G.; Doornbos, A.; Landin, M.; Hennink, W. E.; Vermonden, T., Effect of polymer composition on rheological and degradation properties of temperature-responsive gelling systems composed of acyl-capped PCLA-PEG-PCLA. *Biomacromolecules* **2013**, *14*, 3172-3182.
156. Petit, A.; Sandker, M.; Muller, B.; Meyboom, R.; van Midwoud, P.; Bruin, P.; Redout, E. M.; Versluijs-Helder, M.; van der Lest, C. H.; Buwalda, S. J.; de Leede, L. G.; Vermonden, T.; Kok, R. J.; Weinans, H.; Hennink, W. E., Release behavior and intra-articular biocompatibility of celecoxib-loaded acetyl-capped PCLA-PEG-PCLA thermogels. *Biomaterials* **2014**, *35*, 7919-7928.

157. Petit, A.; Redout, E. M.; van de Lest, C. H.; de Grauw, J. C.; Muller, B.; Meyboom, R.; van Midwoud, P.; Vermonden, T.; Hennink, W. E.; Rene van Weeren, P., Sustained intra-articular release of celecoxib from in situ forming gels made of acetyl-capped PCLA-PEG-PCLA triblock copolymers in horses. *Biomaterials* **2015**, 53, 426-436.
158. Prince, D. A.; Villamagna, I. J.; Hopkins, C. C.; de Bruyn, J. R.; Gillies, E. R., Effect of drug loading on the properties of temperature-responsive polyester–poly(ethylene glycol)–polyester hydrogels. *Polymer International* **2019**, 68, 1074-1083.
159. Wang, S.-J.; Qin, J.-Z.; Zhang, T.-E.; Xia, C., Intra-articular Injection of Kartogenin-Incorporated Thermogel Enhancing Osteoarthritis Treatment. *Frontiers in Chemistry* **2019**, 7, 1-5.
160. Jung, Y. S.; Park, W.; Park, H.; Lee, D. K.; Na, K., Thermo-sensitive injectable hydrogel based on the physical mixing of hyaluronic acid and Pluronic F-127 for sustained NSAID delivery. *Carbohydr. Polym.* **2017**, 156, 403-408.
161. Li, Y.; Cao, J.; Han, S.; Liang, Y.; Zhang, T.; Zhao, H.; Wang, L.; Sun, Y., ECM based injectable thermo-sensitive hydrogel on the recovery of injured cartilage induced by osteoarthritis. *Artif. Cells Nanomed. Biotechnol.* **2018**, 46, 152-160.
162. Joshi, N.; Yan, J.; Levy, S.; Bhagchandani, S.; Slaughter, K. V.; Sherman, N. E.; Amirault, J.; Wang, Y.; Riegel, L.; He, X.; Rui, T. S.; Valic, M.; Vemula, P. K.; Miranda, O. R.; Levy, O.; Gravalles, E. M.; Aliprantis, A. O.; Ermann, J.; Karp, J. M., Towards an arthritis flare-responsive drug delivery system. *Nat. Commun.* **2018**, 9, 1275.
163. Prince, D. A.; Villamagna, I. J.; Borecki, A.; Beier, F.; de Bruyn, J. R.; Hurtig, M.; Gillies, E. R., Thermoresponsive and Covalently Cross-Linkable Hydrogels for Intra-Articular Drug Delivery. *ACS Applied Bio Materials* **2019**, 2, 3498-3507.
164. Lu, H. T.; Chang, W. T.; Tsai, M. L.; Chen, C. H.; Chen, W. Y.; Mi, F. L., Development of Injectable Fucoidan and Biological Macromolecules Hybrid Hydrogels for Intra-Articular Delivery of Platelet-Rich Plasma. *Mar. Drugs* **2019**, 17.

165. von Lospichl, B.; Hemmati-Sadeghi, S.; Dey, P.; Dehne, T.; Haag, R.; Sittinger, M.; Ringe, J.; Gradzielski, M., Injectable hydrogels for treatment of osteoarthritis - A rheological study. *Colloids Surf. B Biointerfaces* **2017**, 159, 477-483.
166. Stalder, E.; Zumbuehl, A., Liposome-Containing Mechanoresponsive Hydrogels. *Macromolecular Materials and Engineering* **2017**, 302, 1-10.
167. Zhang, Y.; Hu, C.; Xiang, X.; Diao, Y.; Li, B.; Shi, L.; Ran, R., Self-healable, tough and highly stretchable hydrophobic association/ionic dual physically cross-linked hydrogels. *RSC Advances* **2017**, 7, 12063-12073.
168. Guo, K.; Chu, C. C., Biodegradation of unsaturated poly(ester-amide)s and their hydrogels. *Biomaterials* **2007**, 28, 3284-3294.
169. Guo, K.; Chu, C. C., Biodegradable and injectable paclitaxel-loaded poly(ester amide)s microspheres: fabrication and characterization. *J. Biomed. Mater. Res. B. Appl. Biomater.* **2009**, 89, 491-500.
170. Vera, M.; Puiggali, J.; Coudane, J., Microspheres from new biodegradable poly(ester amide)s with different ratios of L- and D-alanine for controlled drug delivery. *J. Microencapsul.* **2006**, 23, 686-697.
171. Soleimani, A.; Drappel, S.; Carlini, R.; Goredema, A.; Gillies, E. R., Structure–Property Relationships for a Series of Poly(ester amide)s Containing Amino Acids. *Ind. Eng. Chem. Res.* **2014**, 53, 1452-1460.
172. Knight, D. K.; Gillies, E. R.; Mequanint, K., Strategies in functional poly(ester amide) syntheses to study human coronary artery smooth muscle cell interactions. *Biomacromolecules* **2011**, 12, 2475-2487.

## Chapter 2

### 2 Poly(ester amide) particles for controlled delivery of celecoxib

Villamagna, I. J.; Gordon, T. N.; Hurtig, M. B.; Beier, F.; Gillies, E. R., Poly(ester amide) particles for controlled delivery of celecoxib. *J. Biomed. Mater. Res. A* **2019**, 1245-1243

*As originally published in Journal of Biomedical Materials Research Part A. Reprinted with Permission, copyright Wiley and Sons 2019.*

#### 2.1 Introduction

Osteoarthritis (OA) is a leading cause of mobility impairment and disability among adults worldwide.<sup>1</sup> The disease is prevalent in older generations, but the number and prevalence continues to rise in younger populations as well.<sup>2</sup> Although there are a number of potential treatments under development, there are few clinically approved therapies. Physical therapy and lifestyle changes are often first steps in treatment,<sup>3</sup> followed by the use of non-steroidal anti-inflammatory drugs (NSAIDs) to treat mild-to-moderate musculoskeletal pain.<sup>4</sup> However, systemically administered NSAIDs suffer from poor distribution to joints and significant side effects including gastrointestinal problems and cardiovascular risks. For example, celecoxib (CXB) is an NSAID that was approved for use in OA treatment in the late 1990s.<sup>5</sup> It is a potent cyclooxygenase-2 inhibitor that blocks the production of prostaglandins and attenuates the inflammatory and pain responses that are associated with OA. However, its side effects have become apparent recently, and arise in part due to the high plasma concentrations required to provide relief from OA symptoms.<sup>5,6</sup> The intra-articular injection of the drug using a delivery system can potentially lead to a higher delivered dose while minimizing the side effects to off-target tissues by reducing systemic drug levels.<sup>7</sup>

Several different classes of drug delivery systems have been studied for intra-articular use including hydrogels,<sup>8</sup> nanoparticles,<sup>9, 10</sup> and crystalline drug formations.<sup>11</sup> Although each of these systems has different structures and properties, they are all designed to release the drug over prolonged periods after injection into the joint without adverse reactions of the joint tissue to the delivery platform. Polymer particles are promising drug delivery systems due to their tunable properties, ease of preparation, and potential for prolonged drug release.<sup>12</sup> A wide variety of different polymers can be used, and the size and degradation rates of the particles can be controlled.<sup>13, 14</sup> Poly(ester amide)s (PEAs) are degradable polymers containing both ester and amide linkages in their backbones.<sup>15, 16</sup> Their thermal and mechanical properties as well as their degradation rates can be readily tuned through the incorporation of different monomers such as amino acids, diols, and dicarboxylic acids.<sup>17, 18</sup> PEAs have shown favorable properties as potential drug delivery systems when formulated as micelles<sup>19</sup> or microparticles.<sup>20-22</sup> They have also been shown to support the growth of cells<sup>23-25</sup> and to exhibit good biocompatibility when studied *in vivo*.<sup>26, 27</sup> Thus far, there are very few examples involving the use of PEAs for intra-articular drug delivery. In one study, PEA particles were shown to release CXB in response to inflammation,<sup>21</sup> while in another study they were demonstrated to release triamcinolone.<sup>22</sup> In each case, the particles were shown to exhibit sustained drug release and retention in rat joints with good host response. However, there are many different structures of PEAs with different properties that remain uninvestigated to date.

We describe here the comparative study of particles composed of two different PEAs – one composed of phenylalanine, 1,4-butanediol, and sebacic acid (PBSe) and the other composed of phenylalanine, 1,8-octanediol, and sebacic acid (POSe). This simple change in the diol component leads to different properties for the two polymers. The thermal and mechanical properties of the polymers with and without CXB were studied. The drug release rates and *in vitro* toxicity studies of the particles were evaluated. In addition, host response to the PEA particles was evaluated in a large animal (ovine) model.

## 2.2 Materials and Methods

### 2.2.1 General materials and procedures

PBSe and POSe were synthesized and characterized as previously reported.<sup>24</sup> Poly(vinyl alcohol) (PVA) and the 3-(4,5-dimethylthiazol-2-yl)-2,5-diphenyl tetrazolium bromide (MTT) were purchased from Millipore-Sigma (Oakville, ON). CXB was obtained from Ontario Chemicals Inc. (Guelph, ON). Dynamic light scattering was performed with a Zetasizer NanoZS from Malvern Instruments at 24.5 °C. The Z-average diameter and polydispersity index (PDI) for each type of particle were measured for three different batches. Differential scanning calorimetry (DSC) was performed on a Q2000 from TA instruments (New Castle, DE). The heating/cooling rate was 10 °C/min from 0 to +180 °C, and the data were obtained from the second heating cycle. Statistical analyses were performed by one way ANOVA (Microsoft Excel, 2016) with alpha set at 0.05, followed by a Bonferroni post-hoc analysis, when applicable.

### 2.2.2 Tensile testing

Polymer samples, either pure or mixed with 30 wt% CXB (mixing was performed by co-dissolution of drug and polymer in CH<sub>2</sub>Cl<sub>2</sub> followed by solvent evaporation), were prepared by melt pressing the polymer at 200 °C, and then cutting the resulting sheet into rectangular bars with dimensions of 25 mm × 10 mm × 1 mm (accurately measured with calipers). Tensile testing was performed on a CellScale Univert (Guelph, ON), in phosphate buffered saline (PBS) at 37 °C using a 10 N load cell. Samples were pulled at a rate of 2.5 mm/min for 240 seconds. Testing was performed on three separate samples of hydrogel (at minimum) for each system.

### 2.2.3 Contact angle measurements

Solutions were prepared by dissolving either pure polymer or polymer with 30 wt% CXB in CH<sub>2</sub>Cl<sub>2</sub> and then filtering the solution through a 0.2 µm filter. The solution was then added dropwise onto a silicon wafer until it was completely covered. The wafer was then

spun at 1000 rpm for 1 min. The static water contact angles of the resulting films were then measured using 10  $\mu\text{L}$  drops of deionized water with a Kruss DSA100 Drop Shape Analyzer (Hamburg, Germany). The drop was measured after 10 s of being on the surface. Three measurements were taken for each of the samples.

#### 2.2.4 Preparation of particles

Particles were prepared using an oil-in-water emulsion evaporation technique. The dispersed phase of the emulsion was prepared by dissolving 400 mg of polymer in 200 mL of  $\text{CH}_2\text{Cl}_2$ . For CXB-loaded particles, 175 mg of CXB was also added to the  $\text{CH}_2\text{Cl}_2$  phase. The continuous aqueous phase was prepared by dissolving 5 g of PVA in 1 L of deionized water. The emulsion was made by slowly pouring the dispersed phase into the continuous phase, while stirring using a Waring Commercial immersion blender, set to low ( $\sim 9000$  rpm). The emulsion was mixed at 9000 rpm for an additional 2 min, then transferred to a 1 L beaker, and the organic solvent was evaporated under constant stirring overnight. Particles were collected the next day by centrifugation at 2800 g for 10 min and were then lyophilized. The dried samples were stored at 4  $^\circ\text{C}$  until use.

#### 2.2.5 Scanning electron microscopy (SEM)

SEM was performed in the University of Western Ontario's Nanofabrication Facility using a LEO 1530 instrument, operating at 2.0 kV and a working distance of 6 mm. Samples were mounted on stubs covered in carbon tape and coated with osmium using a SPI Supplies, OC-60A plasma coater. Particles in three different images and three representative sections ( $\sim 30 \times 30 \mu\text{m}$ ) per image were measured to calculate the average diameters  $\pm$  standard deviation.

#### 2.2.6 Determination of drug loading and encapsulation efficiency

10 mg of dried particles were dissolved in 1 mL of deuterated dimethyl sulfoxide and  $^1\text{H}$  NMR spectra were obtained at 400 MHz on a Bruker 400 NMR Spectrometer (Bruker

Instruments, Milton, ON). Integration values of peaks for PEA, PVA and CXB were used to calculate the percentage of each, as seen in Appendix A, Figure A.7. Calculation was performed by first integrating the peaks at 2.8-3.0, corresponding to the four benzylic protons on the phenylalanine units of the PEA. These peaks were set to 4.0, corresponding to one repeat unit of PBSe (molar mass of repeat unit = 550.7 g/mol). The peak at 7.55 ppm was integrated corresponding to four protons on CXB. (molar mass of CXB = 381.4 g/mol). The peak at 3.85 ppm corresponding to PVA was integrated, and corresponds to 0.83 protons per repeat unit of PVA (note that the integration is not 1.0 as the PVA is partially acetylated) (molar mass of PVA repeat unit = 44.1 g/mol). Drug loading (DL) and encapsulation efficiency (EE) were then calculated according to equations (1) and (2).

$$\% \text{ Drug Loading} = \left( \frac{\text{Mass of drug encapsulated in particles}}{\text{Total mass of particles}} \right) \times 100 \quad (1)$$

$$\begin{aligned} \% \text{ Encapsulation Efficiency} \\ = \left( \frac{\text{Actual CXB:PEA mass ratio}}{\text{Theoretical max. CXB:PEA mass ratio}} \right) \times 100 \quad (2) \end{aligned}$$

### 2.2.7 *In vitro* release of CXB

300 mg of particles were suspended in 5 mL of pH 7.4 phosphate buffered saline (PBS) containing 2 wt% Tween 20. The suspension was dialyzed at 37 °C using a 10 kDa molecular weight cut-off dialysis membrane against 350 mL of PBS containing 2 wt% Tween 20. Aliquots (2 mL) of the dialysate were taken daily for 20 days, and then every 5 days for up to 60 days to measure the CXB released from the particles. The amount of released drug in the dialysate was quantified using UV-visible spectroscopy at a wavelength of 253 nm based on an extinction coefficient of coefficient of  $1.65 \times 10^4$  L·mol<sup>-1</sup>·cm<sup>-1</sup> for CXB in the same buffer system. All removed aliquots were replaced with PBS containing 2 wt% Tween 20. Furthermore, the dialysate was replaced completely when absorbance values were higher than 0.8. The experiment was performed on triplicate samples.

### 2.2.8 *In vitro* degradation of particles in PBS

The particles were incubated in PBS at 37 °C and were removed after 7, 14, 30 and 60 days. Once removed, the samples were washed once with deionized water then lyophilized and imaged by SEM as described above.

### 2.2.9 Cell culture

ATDC5 and C2C12 cells were thawed and cultured as previously described.<sup>28, 29</sup>

Reagents were purchased from Sigma Aldrich (Oakville, ON). ATDC5 cells were grown in culture medium containing 225 mL of Dulbecco's Modified Eagle's Medium (DMEM) and 225 mL F12 media with the addition of 10 mL of penicillin-streptomycin (1000 units/mL), 5 mL of L-Glutamine (200 mM) and 50 mL of Fetal Bovine Serum (FBS). C2C12 cells were grown in medium comprising 500 mL of DMEM supplemented with 10 mL of penicillin-streptomycin (1000 units/ mL), 5 mL of L-Glutamine (200 mM) and 50 mL of FBS. Cells were cultured at 37 °C in an incubator with 5% CO<sub>2</sub>. ATDC5 cells were induced to differentiate into chondrocytes with 1% Insulin-Transferrin-Selenium (ITS) in DMEM prior to experimentation

### 2.2.10 *In vitro* toxicity

Cells were seeded at a density of 5000 cells per well in a 96-well plate and incubated for 24 h prior to treatment. Varying concentrations of particles (0.025 -1.0 mg/mL) or free CXB (5-100 µg/mL) were suspended in cell culture media and added to the cells. Media alone was used as a negative control, and sodium dodecyl sulfate (SDS) was used as a positive control. After 48 h, the medium was aspirated and replaced with 100 µL of fresh medium containing 0.5 mg/mL of MTT reagent and allowed to react for 4 h in the incubator. After 4 h the plate was removed and the MTT reagent solution was aspirated. 50 µL of dimethyl sulfoxide was added to each well to solubilize the purple crystals. The plate was then placed in a plate reader (Tecan Infinite M1000 Pro) and the absorbance at 540 nm was measured to quantify the relative metabolic activities of the cells. Four biological replicates were performed, as well as six technical replicates per plate.

### 2.2.11 *In vivo* host response

All procedures were done in compliance with the guidelines of The Canadian Council on Animal Care guidelines (University of Guelph Protocol 3974). An ovine model was used to test the *in vivo* host response of the particles. Intra-articular injections of 50 mg of PBSe-CXB particles suspended in 1 mL of sterile saline were made into one knee (femoropatellar) joint of four sheep. Sheep were monitored daily for lameness, joint effusion, periarticular swelling, fever, and heart rate. Synovial fluid samples and plasma samples were collected under sedation at day 0, 8, and 15 days to measure leucocyte concentration using a solid state chip cytometer according to the manufacturer's instructions (Orflo Technologies, Ketchum, ID) and total protein content using a Goldberg refractometer.<sup>30</sup> Two animals were sacrificed on day 8 and two on day 15. After macroscopic assessments of the joint space, synovial membrane samples were harvested, fixed in 10% buffered formalin, and embedded in paraffin to create 5  $\mu$ M histological sections that were stained with a hematoxylin and eosin (H&E) stain.

## 2.3 Results

### 2.3.1 Particle preparation and characterization

The PEAs PBSe and POSe (Figure 2.1) were synthesized as previously reported and were characterized by <sup>1</sup>H NMR spectroscopy, size exclusion chromatography, and DSC (Figures A.1-A.4).<sup>24</sup> The batch of PBSe used in the current work had a number average molar mass ( $M_n$ ) of 30 kg/mol and dispersity ( $D$ ) of 2.0 while POSe had an  $M_n$  of 18 kg/mol and a  $D = 1.9$ . PBSe had a glass transition temperature ( $T_g$ ) of 34 °C, while POSe had a  $T_g$  of 14 °C and a melting temperatures ( $T_m$ ) of 106 and 150 °C. Using these PEAs, four different types of particles were prepared: non-drug-loaded PBSe (PBSe-NDL), non-drug-loaded POSe (POSe-NDL), CXB-loaded PBSe (PBSe-CXB) and CXB-loaded POSe (POSe-CXB). The average particle size was determined using the SEM and DLS (Figure 2.2, Table 2.1). Based on DLS, PBSe-NDL had a Z-average diameter of  $790 \pm 64$  nm, which was not statistically significantly different from PBSe-CXB with a Z-average diameter of  $836 \pm 51$  nm ( $p = 0.56$ ). In contrast, both POSe-NDL and POSe-CXB were

smaller with Z-average diameters of  $487 \pm 10$  nm and  $398 \pm 13$  nm, respectively, and were statistically significantly different from one another ( $p = 0.02$ ). SEM confirmed that the particles were all spherical. The diameters measured by SEM were generally larger than those obtained by DLS, but the trends were similar, with both POSe-based particles being statistically smaller than their PBSe counterparts ( $p = 0.03$ ). Based on SEM, neither PBSe or POSe exhibited a significant change in diameter when loaded with CXB ( $p = 0.09$ ). The drug loading was 23 wt% for PBSe particles, and 20% for POSe, with encapsulation efficiencies of 84 and 69%, respectively.

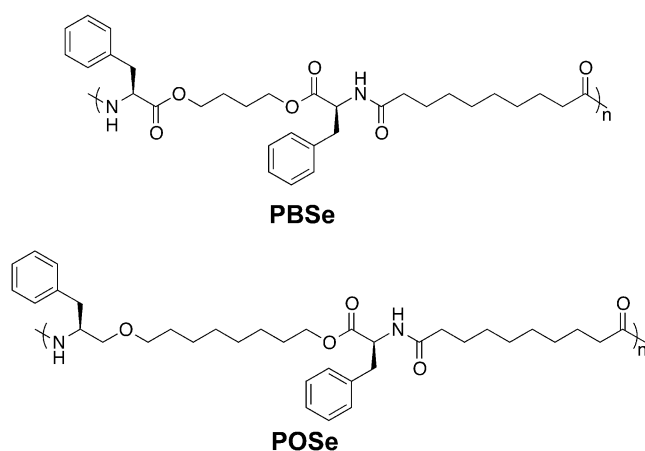


**Figure 2.1: Chemical structures of the polymers PBSe and POSe.**

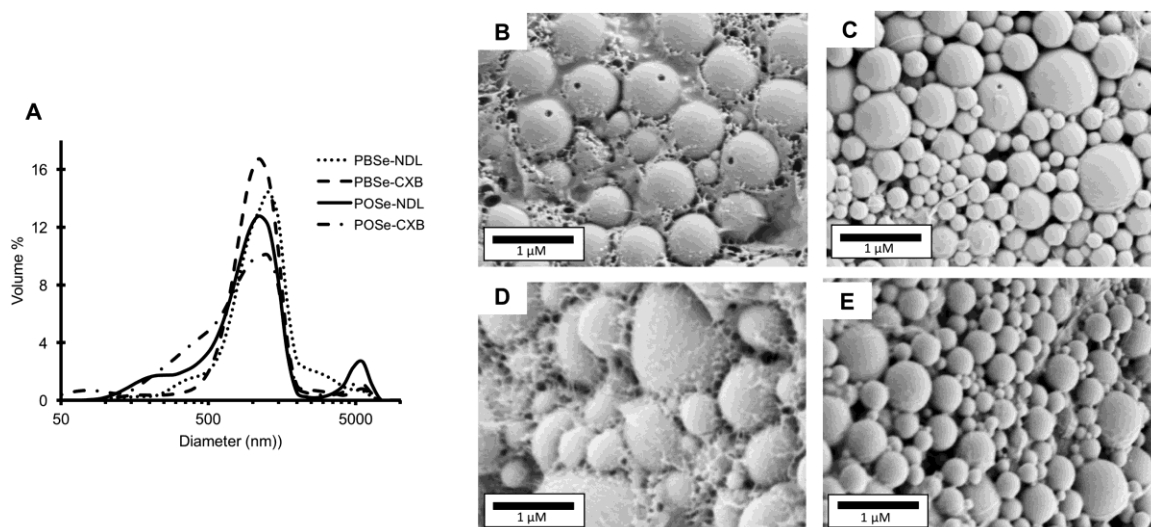


**Figure 2.2 Size and Morphology of Celecoxib particles.** A) DLS diameter distributions by volume % for CXB and non-drug-loaded particles made from either PBSe or POSe; B-E) SEM micrographs of prepared particles showing their spherical structures and size distributions: B) PBSe-NDL; C) PBSe-CXB; D) POSe-NDL; E) POSe-CXB. Material surrounding the particles in B and D is likely PVA.

**Table 2.1: Average diameters of the PEA-based particles obtained by DLS and SEM and CXB loading and encapsulation efficiency measured by NMR spectroscopy.**

Errors correspond to the standard deviations on triplicate measurements of three different particle compositions.

<b>Particle Composition</b>	<b>Z-Average diameter (DLS) (nM)</b>	<b>Measured particle diameter (SEM) (nM)</b>	<b>CXB loading (wt%)</b>	<b>CXB encapsulation efficiency (%)</b>
<b>PBSe-NDL</b>	790 ± 64	870 ± 74	-	-
<b>PBSe-CXB</b>	836 ± 51	1040 ± 100	23 ± 1	84 ± 4
<b>POSe-NDL</b>	487 ± 10	867 ± 92	-	-
<b>POSe-CXB</b>	398 ± 13	637 ± 101	20 ± 4	69 ± 15

DSC was used to investigate the effects of 30 wt% CXB incorporation on the thermal properties of the bulk polymers (Appendix A, Figure A.5). For PBSe, incorporation of CXB resulted in glass transitions at 31 and 45 °C, while for POSe it resulted in disappearance of crystallinity and an increase in the  $T_g$  to 29 °C. DSC was also performed on the particles (Figure 2.3). PBSe-NDL had a  $T_g$  of 38 °C while POSe-NDL had a  $T_g$  of 30 °C. The addition of CXB to the particles resulted in a small increase in  $T_g$  for PBSe-CXB to 41 °C, but no change for POSe-CXB. No melting point for CXB was observed.

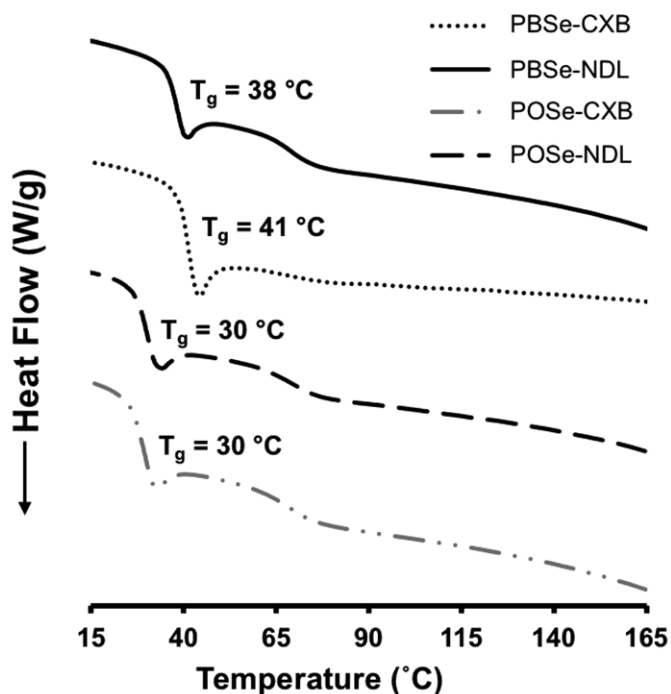


**Figure 2.3 DSC thermograms of drug-loaded and non-drug-loaded particles.** DSC traces showing that the  $T_g$  was increased through CXB incorporation only for PBSe. A subtle transition corresponding to PVA was observed at 60 – 70 °C but no melting temperature was observed for CXB.

Tensile testing of PBSe and POSe as well as their blends with and without 30 wt% CXB was performed in water at 37 °C. POSe had the highest Young's modulus of  $26 \pm 16$  MPa, while PBSe had a modulus of  $1.17 \pm 0.19$  MPa (Table 2.2). The addition of CXB to the polymers decreased the Young's moduli to  $0.43 \pm 0.15$  MPa and  $0.83 \pm 0.68$  MPa for POSe-CXB and PBSe-CXB, respectively. Contact angle measurements were performed to compare the hydrophobicities of the polymers and their blends with CXB in the form of thin films (Table 2.2). PBSe was more hydrophilic, having a contact angle of  $77.4 \pm 0.9$  °, compared to POSe having a contact angle of  $85.3 \pm 1.7$  °. The incorporation of CXB significantly increased the hydrophilicity in each case, lowering the contact angle to  $72.3 \pm 0.8$  ° for PBSe-CXB and  $79.2 \pm 0.1$  ° for POSe-CXB.

**Table 2.2: Young's moduli and ultimate tensile strengths of the polymers and their blends with CXB, as measured by tensile testing in water at 37 °C and contact angles of polymer films.** Errors on the measurements correspond to the standard deviations of triplicate samples.

<b>Polymer Composition</b>	<b>Young's modulus (MPa)</b>	<b>Ultimate Tensile Strength (MPa)</b>	<b>Contact angle (°)</b>
<b>PBSe-NDL</b>	1.17 ± 0.19	0.66 ± 0.3	77.4 ± 0.9
<b>PBSe-CXB</b>	0.83 ± 0.68	0.04 ± 0.01	72.3 ± 0.8
<b>POSe-NDL</b>	26 ± 16	5.6 ± 2.2	85.3 ± 1.7
<b>POSe-CXB</b>	0.43 ± 0.15	0.16 ± 0.04	79.2 ± 0.1

### 2.3.2 *In vitro* release of CXB and particle degradation

The release of CXB from PBSe-CXB and POSe-CXB particles was determined through dialysis and detection of the CXB in the dialysate. Both particle systems exhibited a slower release than free CXB, which was used as a control (Figure 2.4). PBSe-CXB had a slower release than POSe-CXB. At 40 days, 25% of the loaded CXB had been released from PBSe-CXB, while 70% had already been released from the POSe-CXB. The degradation of particles in pH 7.4 PBS at 37 °C over time was probed by SEM. PBSe-CXB particles showed a distinct surface degradation at all time points, with increased degradation over time (Figure 2.5A-C). However, particles were still visible at day 60. POSe-CXB underwent more rapid degradation, with the loss of most particles apparent by 7 and 14 days (Figure 2.5 D-E).

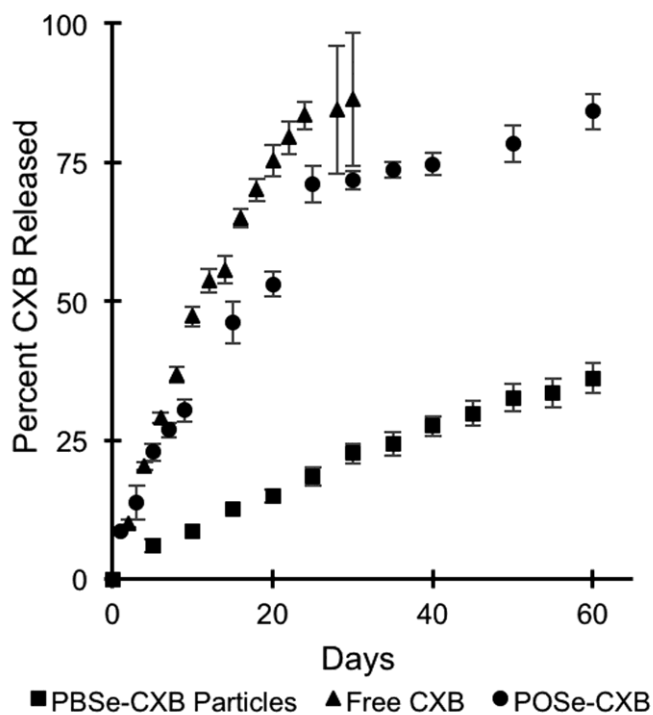


**Figure 2.4: CXB release from PBSe-CXB particles and POSe-CXB particles** performed in pH 7.4 PBS containing 2 wt% Tween 20 showing slower release of CXB from the PBSe-CXB particles. The release of insoluble free CXB through the dialysis membrane was also measured as a control to show that the release rate was not limited by the drug dissolution rate.

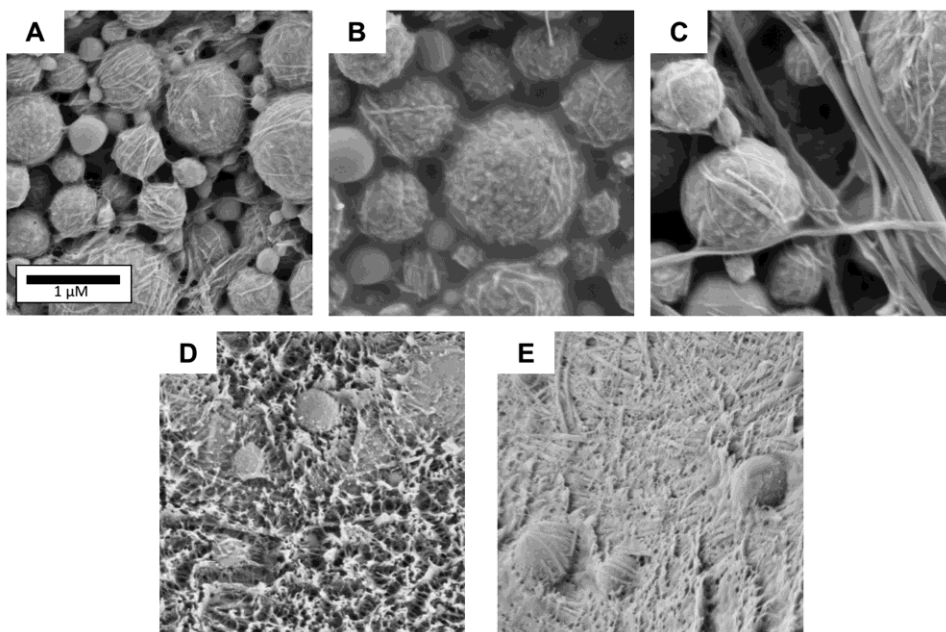


**Figure 2.5: Degradation of PEA particles in pH 7.4 PBS at 37 °C.** A-C) PBSe-CXB particles after A) 14, B) 30 and C) 60 days; D-E) POSe-CXB particles after D) 7 and E) 14 days. All images were obtained at the same magnification. While particles were still observed for PBSe-CXB at 60 days, most of the POSe-CXB particles were rapidly eroded.

### 2.3.3 *In vitro* and *in vivo* studies

Based on their CXB release and degradation properties, PBSe particles were evaluated using MTT assays in two different cell lines – mouse cartilage-like ATDC5 cells and mouse myoblasts C2C12. After 48 h of incubation with PBSe-NDL particles both cell lines retained high metabolic activity at all concentrations evaluated, up to 1 mg/mL (Figure 2.8), as measured by MTT activity. In contrast, PBSe-CXB particles exhibited concentration dependent decreases in metabolic activity for both cell lines, with a 50% reduction at ~0.1 mg/mL. Free CXB also exhibited concentration-dependent toxicity with a 50% reduction in metabolic activity of ATDC5 and C2C12 cells at ~20 μg/mL and 40 μg/mL, respectively (Figures 2.6-2.7).

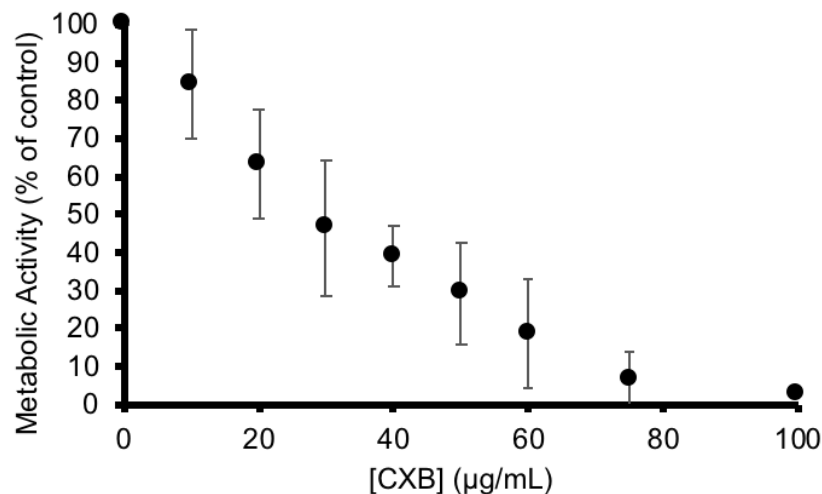


**Figure 2.6: Metabolic activity of ATDC5 cells as treated with increasing concentrations of CXB.** As measured by MTT assay. Metabolic activity reported as an average percentage of control cells (mean  $\pm$  SD), N=4.

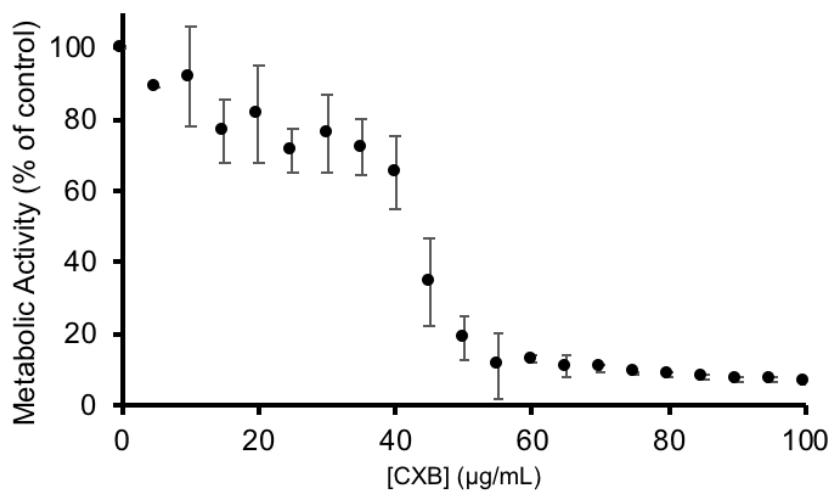


**Figure 2.7 Metabolic activity of C2C12 cells as treated with increasing concentrations of CXB.** As measured by MTT assay. Metabolic activity reported as an average percentage of control cells (mean  $\pm$  SD), N=4.

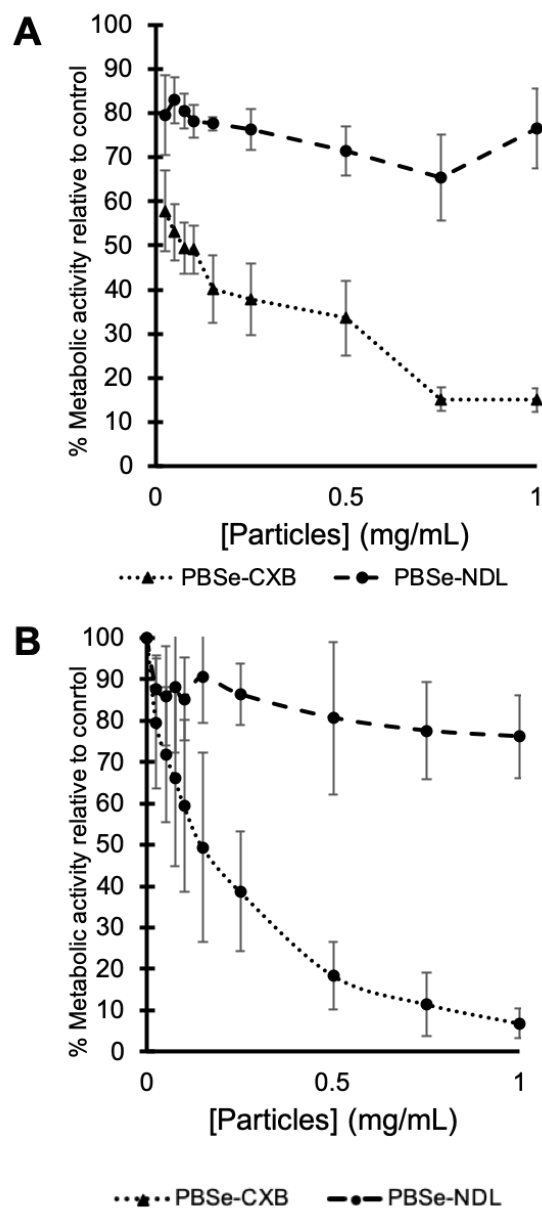


**Figure 2.8: Metabolic activity of cells treated with particles.** A) ATDC5 cells and B) C2C12 cells as measured by an MTT assay after a 48 h incubation with PBSe-CXB or PBSe-NDL particles. Reported as mean  $\pm$  SD. (N = 4).

After intra-articular injections of PBSe-CXB (50 mg particles in 1 mL of saline) in sheep, there was minimal effusion for 48 hours, but no lameness, fever, changes in eating habits, or changes in social interactions were observed. Synovial fluid analysis showed a small but significant increase in both white blood cells (WBC) and total protein concentrations

post injection (Figure 2.9). Histological analysis showed mild synovial intimal hyperplasia, with some increase in vascularity but no cellular infiltration. Specifically, the particles could be identified in the synovial lining and subintimal layer, but there was no presence of macrophages noted. (Figure 2.10).

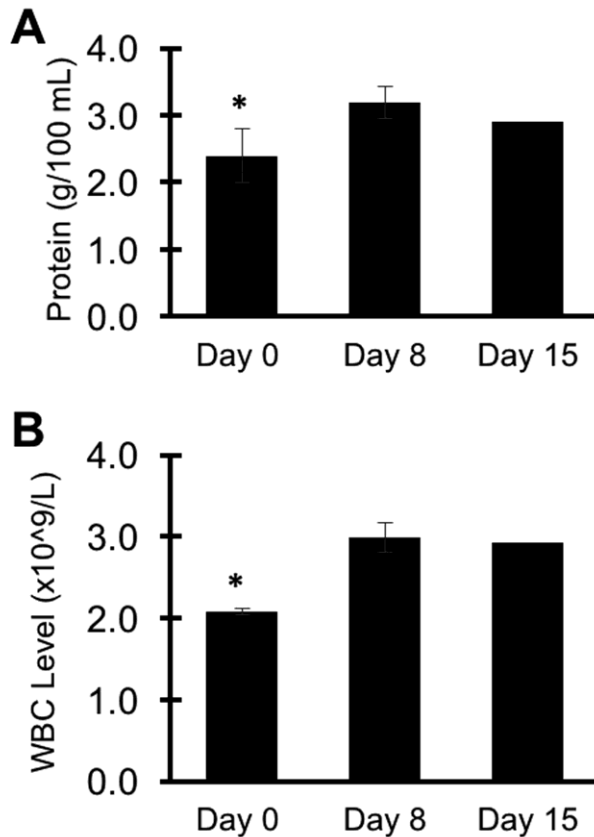


**Figure 2.9: Synovial fluid analysis of injected sheep joints.** A) Protein levels in synovial fluid at days 0, 8 and 15. \* Indicates a significant difference between day 0 and day 8. (ANOVA  $p = 0.04$ ) B) WBC levels at days 0, 8 and 15. \* Indicates a statistically significant difference between day 0 and day 8 (ANOVA  $p = 0.0001$ ).  $N = 4$  at days 0 and 8 and  $N = 2$  at day 15.



**Figure 2.10: Immunohistochemical analysis of the synovial membrane of an injected sheep 15 days post injection.** Hematoxylin and eosin staining was performed on sections of sheep synovium. Particles are visible within the membrane (indicated with red arrows).

## 2.4 Discussion

A wide variety of PEAs having different structures and properties have been previously reported.<sup>15, 16</sup> For the current work, PBSe and POSe were selected as they are easily synthesized, and have shown promising biological properties such as high cell compatibility in previous work.<sup>23, 24</sup> Furthermore, polymerizations that result in PBSe and POSe are easily scalable, allowing a large amount of bulk polymer to prepare particles from. In addition, despite the minor structural difference of containing butyl versus octyl chains in their backbones, they have been shown to exhibit different thermal and mechanical properties.<sup>31</sup> The  $T_g$  value of 34 °C for the bulk PBSe used in the current work was similar to those previously reported for this polymer (38 – 40 °C).<sup>24, 31</sup> POSe was semicrystalline in the bulk state with  $T_m$  values of 106 and 150 °C similar to those previously reported.<sup>24, 31</sup> However, the  $T_g$  of 14 °C measured for POSe was significantly lower than that previously reported (22 – 28 °C), which can likely be attributed to its lower molar mass ( $M_n$  of 18 kg/mol for current versus 30 – 78 kg/mol previously).

Prior to the preparation of particles, a large number of studies were performed, in which the variation of a number of parameters were tested for their effect on resultant particles. Surfactant amount, mixing methods, polymer concentration, and mixing methods were all varied, and their resultant effects on particles were examined by DLS and SEM.  $\text{CH}_2\text{Cl}_2$  was selected as the organic solvent for the emulsification-evaporation particle preparation because it is a good solvent for both PEA and CXB and is immiscible with water, as required for the process. In contrast to previously reported work on PEA particles, the use of  $\text{CH}_2\text{Cl}_2$  did not lead to particles of irregular shape.<sup>20</sup> This may result from different parameters such as solvent ratios, mixing time and evaporation time used in the current work.<sup>32</sup> We fixed the PEA concentration at 2 mg/mL because of solubility limitations. In addition, we fixed the water: $\text{CH}_2\text{Cl}_2$  at 5:1 mL based on previous work.<sup>20</sup> Different emulsification processes were explored and an immersion blender operating at 9000 rpm proved to be the best, whereas a magnetic stir bar led to large conglomerates of material in addition to spherical particles and sonication appeared to result in breakdown of particles. 5 wt% PVA in the water was the most appropriate concentration as lower concentrations led to insufficient particle stabilization and consequent agglomeration, whereas higher concentrations led to particles that were immersed in a large excess of PVA and were difficult to purify.

It has been suggested that particles of different sizes have different advantages and limitations in the context of intra-articular drug delivery. The size of synthesized particles was consistent with what is believed to be suitable for intra-articular delivery. With a diameter of 500-1000 nm, it is expected that particles will be small enough to not induce a significant immune response, but large enough to have a long residence time in the joint, and not be rapidly cleared.<sup>33</sup> The diameters measured by DLS were consistently smaller than those measured by SEM across all samples. While larger particles are often emphasized in DLS measurements due to their increased scattering of light relative to smaller particles, in this case it is likely that the larger particles settled during the measurement and were thus not completely captured in the size distribution. POSe particles were significantly smaller than the PBSe particles in both their CXB-loaded and non-loaded forms. However, a small fraction of larger (>1000 nm) particles was detected for POSe-NDL by both DLS and SEM. As supported by the contact angle

measurements, POSe is more hydrophobic, owing to the increased length of the diol component. This may make these particles more difficult to disperse, while at the same time favoring interactions with the PVA surfactant, which may lead to the stabilization of smaller particles. It was also notable that the incorporation of CXB produced particles with higher purity (less surrounding material) in the case of both POSe-CXB and PBSe-CXB. As previously reported, it was expected that the CXB could play the role of a surfactant, which could further stabilize the emulsion and allow for morphologically-optimized particles.<sup>34</sup>

High drug loading contents and acceptable encapsulation efficiencies were achieved for both the PBSe and POSe particles. High hydrophobicity of CXB results in its preferential partition into the organic phase, thereby resulting in its encapsulation rather than loss into the aqueous phase. The high drug content achievable also suggests high compatibility of CXB with the PEAs used here. It is notable that the drug content of our particles was much higher than the 5 wt% CXB reported by Janssen et. al in different PEA particles.<sup>21</sup> Higher drug content is desirable to minimize the dose of polymer required to administer a given quantity of drug. It was found that the drug loading percentage that was achieved in this study was the maximum amount that was able to be loaded without sacrificing particle integrity. A high amount of drug in particles was desired due to the desired prolonged release model that the particles were intended to be used for.

In comparing the thermal properties of the bulk polymers to those of the particles both with and without CXB, PBSe-NDL particles had a slightly higher  $T_g$  of 38 °C compared to 34 °C for the bulk polymer. A secondary  $T_g$  was observed at 60-70 °C for all of the particles, which likely corresponds to the PVA coating the particles and it is possible that some incorporation of PVA into the particles modestly increased the  $T_g$ . The incorporation of CXB into the PBSe particles increased the  $T_g$  by 3 °C, suggesting that interactions between CXB and PBSe decreased the mobility of the polymer. The incorporation of CXB into bulk PBSe resulted in a main  $T_g$  value of 31 and a small secondary  $T_g$  of 45 °C, suggesting the presence of small CXB-rich domains due to some degree of phase separation. This phase separation may have been induced by the melt pressing process, but it was deemed important to process the samples in the same way as

for the tensile testing samples in order to correlate their properties. While POSe in the bulk state was semicrystalline, no  $T_m$  was observed for POSe particles and instead a single  $T_g$  value of 30 °C was observed. This result highlights the importance of the processing conditions on the properties of the polymers. While the incorporation of CXB into the POSe particles did not affect their  $T_g$ , the incorporation of CXB into bulk POSe resulted in complete loss of crystallinity and a single  $T_g$  value of 29 °C, a result that is important for understanding the tensile properties of the samples. The thermal properties of bulk POSe-CXB were consequently very similar to POSe-CXB particles. No melting point for CXB was observed in the expected range (157-159 °C) for any of the particles, suggesting that CXB was mixed well with the PEAs.

The Young's moduli and ultimate tensile strengths of melt pressed polymers and their blends with CXB were explored. These tests were performed with the samples in a hydrated state at 37 °C to mimic physiological conditions, particularly because water is known to have a significant plasticizing effect on amorphous polymers.<sup>35</sup> Indeed, increasing the temperature to 37 °C immersed in water relative to ambient temperature in the dry state lowered the Young's modulus of PBSe from ~1 GPa to  $1.17 \pm 0.19$  MPa.<sup>31</sup> The addition of CXB resulted in a further decrease in modulus to  $0.83 \pm 0.68$  MPa. The decrease may correlate with the observed lowering of the main  $T_g$  for bulk PBSe-CXB relative to PBSe. Consistent with a decreased water contact angle upon CXB incorporation, it may also be attributed to CXB's ability to hydrogen bond to water, thereby enhancing interactions of the blends with water, further increasing the water plasticization effect. This brings the modulus into a range similar to articular cartilage,<sup>36</sup> which is desirable as the injection of high modulus materials into the joint may be expected to cause irritation. Similar trends were observed for the ultimate tensile strength, with immersion in water resulting in a ~30-fold decrease relative to the polymer in the dry state at ambient temperature and CXB inducing a further decrease.<sup>31</sup> POSe-NDL had a higher Young's modulus and higher tensile strength in water at 37 °C, which likely arises from its semi-crystallinity in the bulk, and would not likely be reflective of the properties of the particles, which were not semicrystalline. However, upon incorporation of CXB, POSe-CXB became completely amorphous, resulting in a decrease in the

Young's modulus to a value lower than that of PBSe-CXB. Plasticization by water may play an additional role in decreasing the modulus as a decrease in water contact angle was also observed for POSe upon CXB incorporation. The mechanical properties of the bulk POSe-CXB should reflect those of the POSe-CXB particles as they had very similar thermal properties. Overall, these results highlight the importance of small PEA structural variations as well as processing conditions in controlling the properties of the polymers under different conditions.

Due to CXB's very low solubility in water, 2 wt% of the surfactant Tween 20 was added to the dialysis release medium. A control experiment performed by the addition of unencapsulated solid CXB into a dialysis bag showed that CXB dissolution and diffusion through the dialysis bag was still quite slow with ~50% release after 10 days. However, it was faster than for CXB loaded into PEA particles, confirming that particle encapsulation was able to provide sustained release of drug due to rate-limiting release from the particles. PBSe-CXB in particular showed very slow release of drug, with only 36% released over 60 days. SEM images of the particles after 14, 30, and 60 days in PBS at 37 °C supported that the slow release can likely be attributed to slow degradation of the particles. The lack of burst release and ability of the PBSe particles to retain the drug over a prolonged time period are favorable properties for an intra-articular delivery system as it is desirable to maximize the time between required doses. On the other hand, POSe-CXB exhibited a release rate of CXB that approached that of the free drug and SEM images showed a rapid loss of particle structure even after 7-14 days. We attribute this behavior to the low  $T_g$  of POSe-CXB in water, which may result in particle fusion and reorganization, processes which are accompanied by the loss of CXB. It is also possible that the lower molar mass of POSe compared to PBSe resulted in more rapid polymer degradation.

PBSe particles were selected for biological studies due to their favorable CXB release and degradation properties. Cytotoxicity studies were performed on ATDC5 "chondrocyte-like" cells and C2C12 myoblast cells. The use of two different cell lines allows for the detection of cell line-dependent responses to the particles, and should provide an indication of how different tissues might react to the particles. C2C12 was

selected as it is a commonly used cell line for *in vitro* work. High metabolic activities were retained for the PBSe-NDL particles in both cell lines at concentrations up to 1 mg/mL. This was expected as previous studies have shown that PBSe was well tolerated by cells.<sup>23, 24</sup> On the other hand, concentration-dependent toxicity was observed for PBSe-CXB in both cell lines. This was expected as we observed significant toxicity of free CXB on both cell lines at 20 – 40 µg/mL and PBSe-CXB particles can release CXB during the assay. It is also in agreement with previous studies, where CXB has been showed to exhibit toxicity *in vitro*.<sup>37</sup> Interestingly, ATDC5 cells never reached 100% of the metabolic activity as compared to the control, even at low concentrations of PBSe-NDL or PBSe-CXB. An initial drop in the metabolic activity could be noted in all experiments, a phenomenon that was not seen in C2C12 cells, leading to the hypothesis that the presence of particles interacted with the cells and could be limiting transport into and out of the cell, thereby lowering the metabolic activity.

*In vivo* pilot studies were performed in an ovine model. This large animal model allowed for a robust histological examination, and serial synovial fluid analysis. Intra-articular injections were performed on 4 sheep, which was sufficient to provide an initial indication of host response to the PBSe-CXB particles. A dose of 50 mg/animal was selected in order to have the most possible CXB injected into the joint, while maintaining the injectability of the drug delivery system. As reported by Janssen et al. for different PEA particles, PBSe-CXB particles appeared to have been engulfed by synovial lining cells and local macrophages, resulting in particles within the synovial villi.<sup>21</sup> The mild increase in vascularity and intimal lining cells is consistent with the trauma of synovial fluid collection. The particles themselves appeared to be remarkably inert. White blood cell and protein concentrations in the synovial fluid post injection did increase significantly, but the increase was small and within the levels expected from arthrocentesis alone. Overall, our observations were similar to those reported previously following the injection of a CXB-containing hydrogel into horse joints.<sup>38</sup>

## 2.5 Conclusions

Particles composed of two different PEAs were prepared and characterized. It was found that small structural differences in the polymers led to significant changes in the particle properties including their  $T_g$  values and Young's moduli and also led to different CXB release rates. The slower release profile of the PBSe-CXB particles makes them more ideal for intra-articular drug delivery. PBSe-NDL particles were found to be well tolerated by both ATDC5 and C2C12 cells, while the presence of CXB in the PBSe-CXB particles induced concentration-dependent toxicity in both cells lines. Initial *in vivo* results in an ovine model showed that the PBSe particles migrated to the synovial membrane and surrounding tissue and were well tolerated at a dose of 50 mg/animal.

## 2.6 References

1. Gomez-Gaete, C.; Retamal, M.; Chavez, C.; Bustos, P.; Godoy, R.; Torres-Vergara, P., Development, characterization and *in vitro* evaluation of biodegradable rhein-loaded microparticles for treatment of osteoarthritis. *Eur. J. Pharm. Sci.* **2017**, *96*, 390-397.
2. Whittaker, J. L.; Woodhouse, L. J.; Nettel-Aguirre, A.; Emery, C. A., Outcomes associated with early post-traumatic osteoarthritis and other negative health consequences 3-10 years following knee joint injury in youth sport. *Osteoarthr. Cartil.* **2015**, *23*, 1122-1129.
3. Vincent, H. K.; Heywood, K.; Connelly, J.; Hurley, R. W., Obesity and weight loss in the treatment and prevention of osteoarthritis. *PM. R.* **2012**, *4*, S59-S67.
4. Cheng, D. S.; Visco, C. J., Pharmaceutical therapy for osteoarthritis. *PM. R.* **2012**, *4*, S82-S88.
5. Vrdoljak, D.; Selimovic, M.; Marin, A.; Utrobicic, A.; Tugwell, P.; Puljak, L.; Puljak, L., Celecoxib for osteoarthritis. In *Cochrane Database Syst. Rev.*, 2012; Vol. 5,1-8.
6. Simon, L. S.; Weaver, A. L.; Graham, D. Y.; Kivitz, A. J.; Lipsky, P. E.; Hubbard, R. C.; Isakson, P. C.; Verburg, K. M.; Yu, S. S.; Zhao, W. W.; Geis, G. S.,

Anti-inflammatory and Upper Gastrointestinal Effects of Celecoxib in Rheumatoid Arthritis: A Randomized Controlled Trial. *JAMA* **1999**, *282*, 1921-1928.

7. Maudens, P.; Jordan, O.; Allemann, E., Recent advances in intra-articular drug delivery systems for osteoarthritis therapy. *Drug Discov. Today* **2018**, *0*, 1-15.
8. He, Z.; Wang, B.; Hu, C.; Zhao, J., An overview of hydrogel-based intra-articular drug delivery for the treatment of osteoarthritis. *Colloids Surf. B Biointerfaces* **2017**, *154*, 33-39.
9. Kang, M. L.; Ko, J. Y.; Kim, J. E.; Im, G. I., Intra-articular delivery of kartogenin-conjugated chitosan nano/microparticles for cartilage regeneration. *Biomaterials* **2014**, *35*, 9984-9994.
10. Kim, S. R.; Ho, M. J.; Kim, S. H.; Cho, H. R.; Kim, H. S.; Choi, Y. S.; Choi, Y. W.; Kang, M. J., Increased localized delivery of piroxicam by cationic nanoparticles after intra-articular injection. *Drug Des., Dev. Ther.* **2016**, *10*, 3779-3787.
11. Rovati, L. C.; Girolami, F.; Persiani, S., Crystalline glucosamine sulfate in the management of knee osteoarthritis: efficacy, safety, and pharmacokinetic properties. *Ther. Adv. Musculoskelet. Dis.* **2012**, *4*, 167-180.
12. Freiberg, S.; Zhu, X. X., Polymer microspheres for controlled drug release. *Int. J. Pharm.* **2004**, *282*, 1-18.
13. Saralidze, K.; Koole, L. H.; Knetsch, M. L. W., Polymeric Microspheres for Medical Applications. *Materials (Basel)* **2010**, *3*, 3537-3564.
14. Tran, V. T.; Benoit, J. P.; Venier-Julienne, M. C., Why and how to prepare biodegradable, monodispersed, polymeric microparticles in the field of pharmacy? *Int. J. Pharm.* **2011**, *407*, 1-11.
15. Fonseca, A. C.; Gil, M. H.; Simões, P. N., Biodegradable poly(ester amide)s – A remarkable opportunity for the biomedical area: Review on the synthesis, characterization and applications. *Prog. Polym. Sci.* **2014**, *39*, 1291-1311.
16. Diaz, A.; Katsarava, R.; Puiggali, J., Synthesis, properties and applications of biodegradable polymers derived from diols and dicarboxylic acids: from polyesters to poly(ester amide)s. *Int. J. Mol. Sci.* **2014**, *15*, 7064-7069.
17. Pang, X.; Chu, C.-C., Synthesis, characterization and biodegradation of poly(ester amide)s based hydrogels. *Polymer* **2010**, *51*, 4200-4210.

18. Soleimani, A.; Moustafa, M. M. A. R.; Borecki, A.; Gillies, E. R., A comparison of covalent and noncovalent strategies for paclitaxel release using poly(ester amide) graft copolymer micelles. *Can. J. Chem.* **2015**, *93*, 399-405.
19. Zilinskas, G. J.; Soleimani, A.; Gillies, E. R., Poly(ester amide)-Poly(ethylene oxide) Graft Copolymers: Towards Micellar Drug Delivery Vehicles. *Int. J. Polym. Sci.* **2012**, *2012*, 1-11.
20. Guo, K.; Chu, C. C., Biodegradable and injectable paclitaxel-loaded poly(ester amide)s microspheres: fabrication and characterization. *J Biomed. Mater. Res. B Appl. Biomater.* **2009**, *89*, 491-500.
21. Janssen, M.; Timur, U. T.; Woike, N.; Welting, T. J.; Draaisma, G.; Gijbels, M.; van Rhijn, L. W.; Mihov, G.; Thies, J.; Emans, P. J., Celecoxib-loaded PEA microspheres as an auto regulatory drug-delivery system after intra-articular injection. *J. Controlled Release* **2016**, *244*, 30-40.
22. Rudnik-Jansen, I.; Colen, S.; Berard, J.; Plomp, S.; Que, I.; van Rijen, M.; Woike, N.; Egas, A.; van Osch, G.; van Maarseveen, E.; Messier, K.; Chan, A.; Thies, J.; Creemers, L., Prolonged inhibition of inflammation in osteoarthritis by triamcinolone acetone released from a polyester amide microsphere platform. *J. Controlled Release* **2017**, *253*, 64-72.
23. Knight, D. K.; Gillies, E. R.; Mequanint, K., Biomimetic L-aspartic acid-derived functional poly(ester amide)s for vascular tissue engineering. *Acta Biomater* **2014**, *10*, 3484-3496.
24. Knight, D. K.; Gillies, E. R.; Mequanint, K., Strategies in functional poly(ester amide) syntheses to study human coronary artery smooth muscle cell interactions. *Biomacromolecules* **2011**, *12*, 2475-2487.
25. Yamanouchi, D.; Wu, J.; Lazar, A. N.; Kent, K. C.; Chu, C. C.; Liu, B., Biodegradable arginine-based poly(ester-amide)s as non-viral gene delivery reagents. *Biomaterials* **2008**, *29*, 3269-3277.
26. Peters, T.; Kim, S. W.; Castro, V.; Stingl, K.; Strasser, T.; Bolz, S.; Schraermeyer, U.; Mihov, G.; Zong, M.; Andres-Guerrero, V.; Herrero Vanrell, R.; Dias, A. A.; Cameron, N. R.; Zrenner, E., Evaluation of polyesteramide (PEA) and

polyester (PLGA) microspheres as intravitreal drug delivery systems in albino rats.

*Biomaterials* **2017**, *124*, 157-168.

27. Lips, P. A.; van Luyn, M. J.; Chiellini, F.; Brouwer, L. A.; Velthoen, I. W.; Dijkstra, P. J.; Feijen, J., Biocompatibility and degradation of aliphatic segmented poly(ester amide)s: in vitro and in vivo evaluation. *J. Biomed. Mater. Res., Part A* **2006**, *76*, 699-710.

28. Yao, Y.; Wang, Y., ATDC5: an excellent in vitro model cell line for skeletal development. *J. Cell. Biochem.* **2013**, *114*, 1223-1229.

29. McMahan, D. K.; Anderson, P. A.; Nassar, R.; Bunting, J. B.; Saba, Z.; Oakeley, A. E.; Malouf, N. N., C2C12 cells: biophysical, biochemical, and immunocytochemical properties. *Am. J. Physiol.* **1994**, *266*, C1795-C1802.

30. Gika, H. G.; Theodoridou, A.; Michopoulos, F.; Theodoridis, G.; Diza, E.; Settas, L.; Nikolaidis, P.; Smith, C.; Wilson, I. D., Determination of two COX-2 inhibitors in serum and synovial fluid of patients with inflammatory arthritis by ultra performance liquid chromatography-inductively coupled plasma mass spectroscopy and quadrupole time-of-flight mass spectrometry. *J Pharm Biomed Anal* **2009**, *49*, 579-586.

31. Soleimani, A.; Drappel, S.; Carlini, R.; Goredema, A.; Gillies, E. R., Structure–Property Relationships for a Series of Poly(ester amide)s Containing Amino Acids. *Ind. Eng. Chem. Res.* **2014**, *53*, 1452-1460.

32. Nihnat, N.; Schugens, C.; Grandfils, C.; Jerome, R.; Teyssie, P., Polylactide Microparticles Prepared by Double Emulsion/Evaporation Technique. *Pharm Res.* **1994**, *11*, 1479-1484.

33. Edwards, S. H., Intra-articular drug delivery: the challenge to extend drug residence time within the joint. *Vet. J.* **2011**, *190*, 15-21.

34. Sekhon, B. S., Surfactants: Pharmaceutical and Medicinal Aspects. *J. Pharm. Technol. Res. Manag.* **2013**, *1*, 43-68.

35. Hancock, B. C.; Zografi, G., The Relationship Between the Glass Transition Temperature and the Water Content of Amorphous Pharmaceutical Solids. *Pharm Res.* **1994**, *11*, 471-477.

36. Camarero-Espinosa, S.; Rothen-Rutishauser, B.; Foster, E. J.; Weder, C., Articular cartilage: from formation to tissue engineering. *Biomater. Sci.* **2016**, *4*, 734-767.
37. Amrite, A. C.; Ayalasomayajula, S. P.; Cheruvu, N. P.; Kompella, U. B., Single periocular injection of celecoxib-PLGA microparticles inhibits diabetes-induced elevations in retinal PGE<sub>2</sub>, VEGF, and vascular leakage. *Invest Ophthalmol. Vis. Sci.* **2006**, *47*, 1149-1160.
38. Petit, A.; Redout, E. M.; van de Lest, C. H.; de Grauw, J. C.; Muller, B.; Meyboom, R.; van Midwoud, P.; Vermonden, T.; Hennink, W. E.; Rene van Weeren, P., Sustained intra-articular release of celecoxib from in situ forming gels made of acetyl-capped PCLA-PEG-PCLA triblock copolymers in horses. *Biomaterials* **2015**, *53*, 426-436.

## Chapter 3

### 3 Preparation and Characterization of Poly(ester amide) Particles Loaded with the PPAR $\delta$ Antagonist GSK3787

#### 3.1 Introduction

Osteoarthritis (OA) is the most common joint disorder worldwide, and is a leading cause of chronic pain and disability.<sup>1,2</sup> More than 242 million people worldwide suffer from OA, at a cost between 1 and 2.5% of gross domestic product in developed countries.<sup>3</sup> The disease is multi-faceted, affecting numerous tissues within the joint, including cartilage, bone and synovium. Exercise has been demonstrated to safely reduce pain and improve physical function in OA patients.<sup>4,5</sup> Nonsteroidal anti-inflammatory drugs (NSAIDs) can also be used, but can lead to cardiovascular<sup>6</sup> and gastrointestinal complications.<sup>7</sup> Next stage options include intra-articular injections of corticosteroids.<sup>8</sup> Unfortunately, none of the above treatments alter the progression of the disease.<sup>9</sup> Joint replacement therapy can be used for end stage disease, but is limited by risks of infection, the potential for implant failure, and altered biomechanics which can lead to degenerative changes in other parts of the body.<sup>10, 11</sup> Thus, improved treatments that are capable of slowing or halting OA progression are urgently needed.

In an effort to develop disease modifying treatments for OA, a greater emphasis has been placed on understanding of the molecular mechanisms involved in OA.<sup>12</sup> Recently, a number of targets have been identified. For example, inflammatory modulators such as interleukins,<sup>13</sup> or the NF- $\kappa$ B pathway<sup>14</sup> have been identified as potential targets. Ion channels, such as TRPV1<sup>15</sup> or voltage gated sodium channels, which are associated with pain, have also been investigated.<sup>16</sup> Recent research in our lab showed that activation of peroxisome proliferator activator receptor (PPAR)  $\delta$  resulted in the degradation of cartilage tissue in an explant culture model.<sup>17</sup> In addition, cartilage specific PPAR $\delta$  knockout mice were protected from post-traumatic OA (PTOA) following a destabilizing medial meniscus surgery. PPAR $\delta$  antagonists have been

previously developed. For example, GSK3787 was shown to have high selectivity for PPAR $\delta$  receptor.<sup>18</sup> However, PPAR $\delta$  has important roles throughout the body, particularly in glucose and lipid metabolism,<sup>19-21</sup> so the use of GSK3787 in a fashion that would lead to high drug levels systemically would likely not be feasible due to the high risk of side effects.

Localized delivery of drugs into the joints through intra-articular injection is recognized as a promising approach for the administration of OA therapeutics as it allows the drug to be delivered in the appropriate dose to the target tissue, while minimizing systemic exposure, and therefore potential side effects.<sup>22</sup> However, free drugs that are injected into the joint are subject to rapid clearance by lymphatic drainage within a matter of hours, thereby limiting their ability to achieve a therapeutic effect.<sup>23</sup> Drug delivery systems provide an opportunity to incorporate therapeutics into a material that can provide sustained release into the joint.<sup>24</sup> A number of drug delivery systems for intra-articular injection have been developed, including liposomes,<sup>25</sup> particles,<sup>26-28</sup> hydrogels,<sup>29-31</sup> and dendrimers.<sup>32</sup> Particles in particular have been shown to afford prolonged release in the joint over a period of months. For example, microparticles composed on poly(lactic-co-glycolic acid) (PLGA) encapsulating the corticosteroid triamcinolone were recently approved by the United States Food and Drug Administration.<sup>33</sup>

Poly(ester amide)s (PEAs) are an alternative class of biodegradable polymers to polyesters. They have tunable thermal and mechanical properties,<sup>34</sup> and often undergo surface erosion rather than bulk degradation, enabling controlled drug release and reduced concentrations of potentially inflammatory acidic species upon degradation.<sup>35, 36</sup> Furthermore, PEAs have been shown to be well tolerated in joints,<sup>27, 28</sup> and in other *in vitro*<sup>37, 38</sup> and *in vivo*<sup>39</sup> applications. For example, PEAs have been utilized as cell scaffolds for tissue regeneration purposes, and were found to support cell adhesion and proliferation.<sup>40, 41</sup> They have also been explored for their ability to encapsulate and release cell growth factors and bactericides.<sup>42, 43</sup> PEA particles loaded with celecoxib were shown to release the drug in response to inflammation and were well tolerated in a rat model.<sup>27</sup> They were also explored for the controlled release of triamcinolone.<sup>44</sup> We recently reported the preparation and study of celecoxib-loaded PEA particles and found

that minor changes in PEA chemical structure led to large differences in the release rate of the drug.<sup>28</sup> The particles were also well tolerated in an ovine model. However, as noted above, the delivery of NSAIDs or corticosteroids would not lead to disease-modifying effects, so it is of interest to develop delivery systems that will enable the study of potential disease-modifying therapies.

Here, we describe the incorporation of the PPAR $\delta$  antagonist GSK3787 to PEA particles. The particles were prepared through an emulsification-evaporation method and characterized by scanning electron microscopy (SEM), dynamic light scattering (DLS), atomic force microscopy (AFM), and thermal analyses. The release rate of GSK3787 *in vitro* was evaluated and the particles were tested for toxicity on primary immature murine articular cartilage (IMAC) cells. Confocal microscopy was performed to examine the interactions between the particles and cells. Tissue explant models were used to assess the injectability of the drug delivery system, as well as the passive diffusion of particles through tissue.

## 3.2 Materials and Methods

### 3.2.1 General materials and procedures

The PEA used in this work, referred to as PBSe, was composed of phenylalanine, butanediol, and sebacic acid, and was synthesized and characterized as previously reported.<sup>37</sup> For this study, the batch of polymer used had a number average molar mass ( $M_n$ ) of 30 kg/mol, and a dispersity ( $D$ ) of 1.9. Molar mass characteristics were determined by size exclusion chromatography (SEC) at a flow rate of 1 mL/min in DMF with 10 mM LiBr and 1% (v/v) NEt<sub>3</sub> at 85 °C using a Waters 515 HPLC pump and Waters Temperature Control Module II equipped with a Wyatt Optilab T-rEX refractometer and two Plgel 5  $\mu$ m mixed-D (300 mm  $\times$  7.5 mm) columns from Polymer Laboratories by Varian connected in series. The calibration was performed using poly(methyl methacrylate standards) (PMMA) standards. Poly(vinyl alcohol) (PVA) 4-88, 87-89% hydrolyzed and the 3-(4,5-dimethylthiazol-2-yl)-2,5-diphenyl tetrazolium bromide (MTT) reagent were purchased from Millipore-Sigma

(Oakville, ON). Concentrated (10x) phosphate buffer solution (PBS) was purchased from Sigma Aldrich, and was mixed with deionized (DI) water from a MilliQ system, to create 1x PBS, pH 7.4. GSK3787 was purchased from Ontario Chemicals (Guelph, ON). DLS was performed with a Zetasizer Nano ZS instrument from Malvern Instruments at 24.5 °C. The Z-average diameter and polydispersity index (PDI) for each type of particle were measured on three different batches of prepared particles. Differential scanning calorimetry (DSC) was performed on a Q2000 from TA instruments (New Castle, DE). The heating/cooling rate was 10 °C/min from 0 to +200 °C, and the data were obtained from the second heating cycle. Statistical analyses were performed by one way ANOVA (Microsoft Excel, 2016) with alpha set at 0.05, followed by a Bonferroni post-hoc analysis, when applicable.

### 3.2.2 GSK3787 loaded particle preparation (PBSe-GSK3787)

Particles loaded with the PPAR $\delta$  antagonist, denoted as **PBSe-GSK3787**, were prepared through an oil-in-water emulsification evaporation method. The dispersed phase of the emulsion was made by dissolving 400 mg of PBSe in 200 mL of a 50:50 mixture of CHCl<sub>3</sub> and CH<sub>2</sub>Cl<sub>2</sub>. 37.5 mg of GSK3787 was added to the dispersed phase simultaneously and was dissolved completely by stirring. The continuous phase was prepared by dissolving 5.0 g of PVA in 1.0 L of DI water, in a 5 L beaker. The emulsion was formed by slowly pouring the dispersed phase into the continuous phase, while mixing vigorously using a Waring Commercial immersion blender, set to low (~9000 rpm). The solution was continuously mixed at 9000 rpm for an additional 2 min. The resultant emulsion was immediately transferred to a 1 L beaker ensuring that the liquid filled the beaker entirely, before being covered with aluminum foil, perforated with five holes to slow the evaporation rate. The organic solvent was evaporated under constant stirring in a fume hood for 24 h. The emulsion was then transferred to 50 mL centrifuge tubes, which were spun at 2800 g for 10 min. Solid particles sedimented at the bottom of centrifuge tubes, and the aqueous layer was discarded. Particles in the tubes were resuspended in 50 mL of DI water, and were spun again for 10 min at 2800 g to wash the particles. After removing the aqueous layer, the particles were collected by resuspending the contents of each centrifuge tube in 5 mL of DI H<sub>2</sub>O. Fractions from different

centrifuge tubes were combined, and frozen overnight at -20 °C, before being lyophilized. The dried samples were kept refrigerated at 4 °C until use.

### 3.2.3 Non-drug-loaded particle preparation (PBSe-NDL)

Particles without drug were prepared by the same method as for **PBSe-GSK3787** except that no drug was added to the dispersed phase.

### 3.2.4 Dye-labeled particle preparation

When required for microscopic and stereoscopic examination, particles with dyes loaded into them were prepared by the same method as for **PBSe-GSK3787**, with the addition of either 5 mg of Nile red or 5 mg of IR-780 into the dispersed phase of the emulsion instead of GSK3787.

### 3.2.5 Scanning electron microscopy (SEM)

SEM was performed in the University of Western Ontario's Nanofabrication Facility using a Zeiss LEO 1530 instrument, operating at 2.0 kV and a working distance of 6 mm. Lyophilized samples of particles were mounted to stubs covered in carbon tape and coated with a 10 nm layer of Osmium, using an SPI Supplies, OC-60A plasma coater. Micrographs of the particles were taken, and images were produced to measure the size of particles. Particles in three different images and three representative sections ( $\sim 30 \times 30 \mu\text{m}$ ) per image were measured to calculate the average diameters  $\pm$  standard deviation.

### 3.2.6 Determination of drug loading and encapsulation efficiency

10 mg of **PBSe-GSK3787** particles were weighed gravimetrically using an analytical balance. The particles were then completely dissolved in 1 mL of dimethyl sulfoxide (DMSO). 20  $\mu\text{L}$  of the DMSO was taken and added to 980  $\mu\text{L}$  of the high performance liquid chromatography (HPLC) mobile phase, a 40:60 mixture of acetonitrile and DI water. Samples were filtered with 0.2  $\mu\text{M}$  membrane filters prior to injection. HPLC analysis was then performed using an instrument equipped with a Waters Separations

Module 2695, a Kinetex C18 5  $\mu\text{m}$  ( $4.6 \times 100$  mm) column connected to a C18 guard column, and a Photodiode Array (PDA) Detector (Waters 2998). The PDA detector was used to monitor GSK3787 absorbance at 238 nm. An isocratic eluent method with acetonitrile and DI water (40:60) was used. The retention time of GSK3787 was 2.5 minutes. The calibration curve was obtained by spiking the mobile phase with known concentrations of GSK3787, to form the following standard solutions: 100, 50, 25, 10, 5, and 1  $\mu\text{g/mL}$  GSK3787. All samples were filtered through 0.2  $\mu\text{m}$  membrane filters, and 100  $\mu\text{L}$  was injected using the instrument method described above. Three different particle preparations were used to evaluate drug loading and encapsulation efficiency, and each injection was performed in duplicate. Drug loading and encapsulation efficiency were calculated according to equations (1) and (2).

$$\% \text{ Drug Loading} = \left( \frac{\text{Mass of drug encapsulated in particles}}{\text{Total mass of particles}} \right) \times 100 \quad (1)$$

$$\begin{aligned} \% \text{ Encapsulation Efficiency} \\ = \left( \frac{\text{Actual GSK3787:PEA mass ratio}}{\text{Theoretical max. GSK3787:PEA mass ratio}} \right) \times 100 \quad (2) \end{aligned}$$

### 3.2.7 Atomic force microscopy of PBSe-GSK3787 and PBSe-NDL

Particles were resuspended in PBS, and deposited on glass coverslips, dropwise. After allowing liquid to evaporate at ambient temperature overnight, the samples were used for AFM imaging and mechanical testing. AFM measurements were carried out using a BioScope Catalyst AFM (Bruker) mounted on an inverted microscope (LSM 510, Zeiss). For indentation measurements, samples were immersed in water and heated to 37  $^{\circ}\text{C}$ , using the BioScope II Heater Stage and Veeco/LakeShore 331S Temperature Controller. Pyramidal silicon nitride MSCT cantilevers (Bruker) with a nominal spring constant of 0.1 N/m were used for contact mode imaging and indentation measurements. Determination of the spring constant of all cantilevers was carried out using the thermal noise method.<sup>45</sup> Images were recorded in air at a line rate of 1 Hz. For indentation measurements, the ‘point and shoot’ mode of the BioScope software was used. After hydration of the sample, an AFM image of a nanoparticle was acquired. A grid of  $10 \times 10$

points was placed on the nanoparticle surface, and a force indentation curve was recorded at each point at a force trigger of 5 nN. At each indentation position, the Young's modulus was determined by fitting a Hertz model (cone indenter) to the approach curve using AtomicJ.<sup>46</sup> 100 different points on each of eight individual **PBSe-GSK3787** particles and seven **PBSe-NDL** were used for measurements. Outliers from the data set were removed using a 1.5 x IQR statistical method. Moduli were recorded as the mean  $\pm$  standard deviation.

### 3.2.8 *In vitro* release of GSK3787

50 mg of **PBSe-GSK3787** particles were resuspended in 1 mL of pH 7.4 PBS containing 2 wt% of polysorbate 80 (sink solution) to facilitate the dissolution of the released drug. The particle suspension was then added into a float-a-lyzer dialysis cassette with a molecular weight cut-off of 10 kDa. Free (non-encapsulated) GSK3787 (50 mg/cassette) was also studied to ensure that the release of drug from the particles was not rate-limited by drug dissolution. Samples were placed in sealed containers with 3 mL of sink solution. All 3 mL of the sink solution was removed every 5 days for 30 days total and replaced with fresh solution. The concentration of drug in the sink solution was analyzed as using the HPLC method described above for the determination of the drug loading/encapsulation efficiency. Three replicates were studied for each of **PBSe-GSK3787** and free drug and every HPLC injection was performed in duplicate. Release was calculated as the cumulative percentage of drug in the sink solution as compared to the total drug in the sample, and is reported as the mean  $\pm$  standard deviation.

### 3.2.9 Primary chondrocyte harvest and culture

IMAC cells were harvested from 5 day old CD-1 mouse pups, as previously described.<sup>47</sup> Pups were sacrificed and fixated to dissection plates. Cartilage was removed from the femoral heads, femoral condyles, and tibial plateaus. The tissue was then subjected to 1 h (3 mg/mL) followed by 24 h (0.5 mg/ml) incubations in Collagenase D diluted in Dulbecco's Modified Eagles Medium supplemented with 2 mM L-glutamine, 50 U/mL penicillin, and 0.05 mg/mL streptomycin at 37 °C under 5% CO<sub>2</sub>. The tissue fragments

were then agitated, by pipetting, and were passed through a 50  $\mu$ M cell strainer. Cells were isolated by centrifugation for 10 min at 1300 g, allowing the formation of a pellet. The pellet was washed in PBS buffer 2 times, before being resuspended in fresh media. Cells were counted by combining 40  $\mu$ L of the cell suspension in media with 40  $\mu$ L of trypan blue, and pipetting up and down to mix. 10  $\mu$ L of the trypan blue/cell suspension was added to a cell counter plate, and was run on a Bio-Rad TC20 Automated cell counter. Cells were seeded in 96 well treatment plates at a density of 5000 cells/well, in 12 well plates at a density of  $3.0 \times 10^5$  cells/well, or in 24 well plates at a density of  $2.5 \times 10^5$  cells/well and were allowed to grow to confluency for 7 days, with the media being replaced every 48 h. Animal work was performed in compliance with the guidelines of The Canadian Council on Animal Care guidelines (University of Western Ontario Protocol 2019-035).

### 3.2.10 Cytotoxicity of GSK3787 to IMAC cells

GSK3787 was dissolved in DMSO at a concentration of 10 mg/mL, and was added to cell culture media to afford concentrations of 10, 20, 30, 40, 50, 60, 70, 80, 90 and 100  $\mu$ M. To each cell-containing well of a 96 well plate, 110  $\mu$ L of treatment media was added, and allowed to incubate with the cells for 48 h. Cells receiving media without drug served as negative controls, and cells receiving sodium dodecyl sulfate at a concentration of 1 mg/mL served as positive controls for cell death. The media was then aspirated and replaced with 110  $\mu$ L of media containing 0.5 mg/mL of MTT reagent, then the cells were incubated for 4 h. The MTT containing media was aspirated and 50  $\mu$ L of DMSO was added to each well to solubilize the resulting purple crystals. The plate was then placed in a plate reader (Tecan Infinite M1000 Pro) and the absorbance at 540 nm was measured to quantify the relative metabolic activities of the cells. Four biological replicates were performed, as well as six technical replicates per plate.

### 3.2.11 Cytotoxicity of PBSe-GSK3787 and PBSe-NDL to IMAC cells

**PBSe-GSK3787** particles were resuspended in cell culture media to afford concentrations of 5, 10, 25, 50, 100, 150, 250, 500, 750 and 1000  $\mu\text{g}/\text{mL}$ . **PBSe-NDL** particles were resuspended in media at the same concentrations. The suspensions were disinfected by placing them under the UV light of the cell culture hood for 1 h. The MTT assay was then performed as described above for GSK3787.

### 3.2.12 Brightfield imaging of IMAC cells treated with PBSe-GSK3787 particles

**PBSe-GSK3787** particles were resuspended in cell media at concentrations of 0, 25, 50, 100, 150, 250, 500, 750, and 1000  $\mu\text{g}/\text{mL}$ , and then sterilized under the UV light of the cell culture hood for 1 h. Then, 2 mL of suspension was added to the cell-containing wells of a 12 well plate and incubated for 48 h. Cells were imaged after 48 h of incubation with particles under bright field mode using a Biotek Cytation 5 microscope at 20x magnification.

### 3.2.13 IMAC staining and confocal microscopy

**PBSe-GSK3787-NR** were resuspended in culture media at a concentration of 100  $\mu\text{g}/\text{mL}$ , then sterilized under the UV light of the cell culture hood for 1 h. 1 mL of the particle containing media was added to each cell containing well, and then the cells were incubated for 48 h. The media was then aspirated, and the cells were washed 3 times with PBS before being fixed with a 4 wt% paraformaldehyde (PFA) solution for 10 min at room temperature. After washing with PBS, 1 wt% Triton X-100 was added and cells were incubated for 10 min at room temperature. Cells were washed with PBS again before adding a 1% bovine serum albumin (BSA) solution and incubating at room temperature for 30 min. AlexaFluor 488 Phalloidin stain (Sigma Aldrich, Oakville, ON) was added to PBS at a concentration of 10  $\mu\text{g}/\text{mL}$ , then 1 mL of the PBS containing AlexaFluor 488 was added to cells and incubated for 10 min at room temperature.

Coverslips were washed with PBS before being removed, and fixed to glass slides using Immunomount with DAPI (Fisher Scientific, Oakville, ON). Slides were stored in the dark until imaging. Confocal microscopy was performed using a Zeiss LSM 900 confocal microscope. A 3D rendering of confocal images was created using Oxford Instruments Imaris x64 software.

### 3.2.14 *Ex vivo* intra-articular injection of PBSe-GSK3787-IR

50 mg/mL suspensions of **PBSe-GSK3787-IR** were prepared, and 5  $\mu$ L was drawn up into 0.5 mL veterinary insulin syringes. Four healthy, male C57BL/6 mice of various ages were sacked under CO<sub>2</sub>. 5  $\mu$ L intra-articular injections of **PBSe-GSK3787-IR** were performed on the medial side of left hind limbs. After injection, the limbs were resected and cultured in tissue culture medium containing 500 mL of  $\alpha$ -minimum essential media (MEM), supplemented with 25 mg of ascorbic acid, 0.108 g/mL  $\beta$ -glycerophosphate, 1.0 mL BSA, 1.25 mL L-glutamine, and 10,000  $\mu$ g/mL pen-strep. Imaging was performed using a Leica M165C stereo microscope. Images were taken after 7d of limb culture to qualitatively assess the presence of particles in the joint, and any diffusion of the particles through surrounding tissue.

## 3.3 Results and Discussion

### 3.3.1 Preparation and characterization of PBSe particles.

The PEA used in this study, PBSe (Figure 3.1), was selected as we have previously demonstrated it to exhibit an acceptable host response in the joints of sheep.<sup>28</sup> It was prepared as previously reported, through the interfacial polycondensation of sebacyl chloride and the di-*p*-toluenesulfonic acid salt of the diamine-diester prepared from L-phenylalanine and 1,4-butanediol.<sup>37</sup> The resulting PBSe was characterized by <sup>1</sup>H NMR spectroscopy (Appendix B, Figure B.1) and SEC (Appendix B, Figure B.2). The batch of PBSe used in the current work had an  $M_n$  of 30 kg/mol and  $D$  of 2.0.

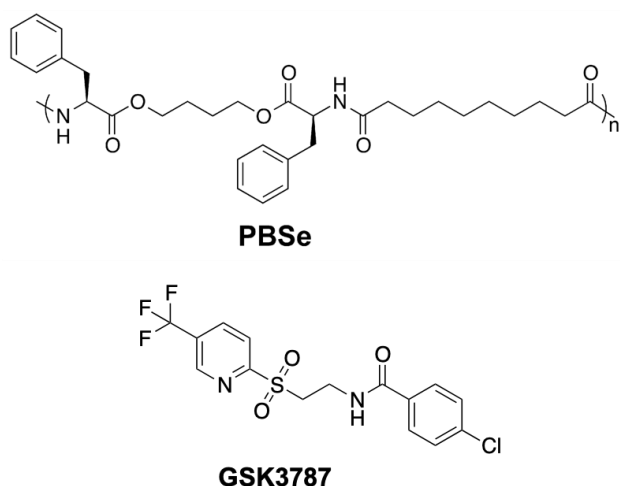


**Figure 3.1: Chemical structures of PBSe and GSK3787.**

Both GSK3787-loaded particles (**PBSe-GSK3787**) and non-drug-loaded (**PBSe-NDL**) control particles were prepared by an emulsification evaporation technique.<sup>48</sup> Initially, we investigated application of our previously developed conditions for the preparation of celecoxib-loaded PBSe particles, which involved 2 mg/mL of PBSe in  $\text{CH}_2\text{Cl}_2$ , 30 wt% of celecoxib relative to PBSe, 5 mg/mL of PVA in DI water, and a 5:1 ratio of the continuous to dispersed phase. At similar drug loadings of GSK3787, and even 10 – 15 wt% of GSK3787, particles formed, but were contaminated with non-particle debris (Appendix B, Figure B.3). It was suspected that the drug was disrupting the interface and/or might not exhibit high compatibility with the PEA. Upon lowering the amount of GSK3787 to 8.6 wt% relative to PEA, spherical particles were formed cleanly (Figure 3.2A). In addition, it was found that the formation of particles was tied to the evaporation rate of the organic phase of the emulsion, with a slower evaporation rate allowing for more consistent particle formation, with less debris. The evaporation rates of emulsions and their effect on resultant particles has been previously studied, and the results of these studies agree with the assertion that the slower rate of evaporation used herein, is more effective for particle preparation.<sup>49, 50</sup> To slow the evaporation rate, the dispersed phase was also changed from  $\text{CH}_2\text{Cl}_2$  to 1:1  $\text{CHCl}_3:\text{CH}_2\text{Cl}_2$ . The evaporation rates of these two organic solvents has been studied in the past, with  $\text{CHCl}_3$  having a slower evaporation rate.<sup>51</sup> Furthermore, the dissolution of PEA and drug were faster and more complete in the solvent mixture than in pure  $\text{CH}_2\text{Cl}_2$ . Overall, these results

indicated that particle preparation methods cannot necessarily be applied to different drugs but that adjusting of the preparation parameters can overcome this challenge. **PBSe-NDL** particles were prepared under the same conditions as **PBSe-GSK3787** particles.

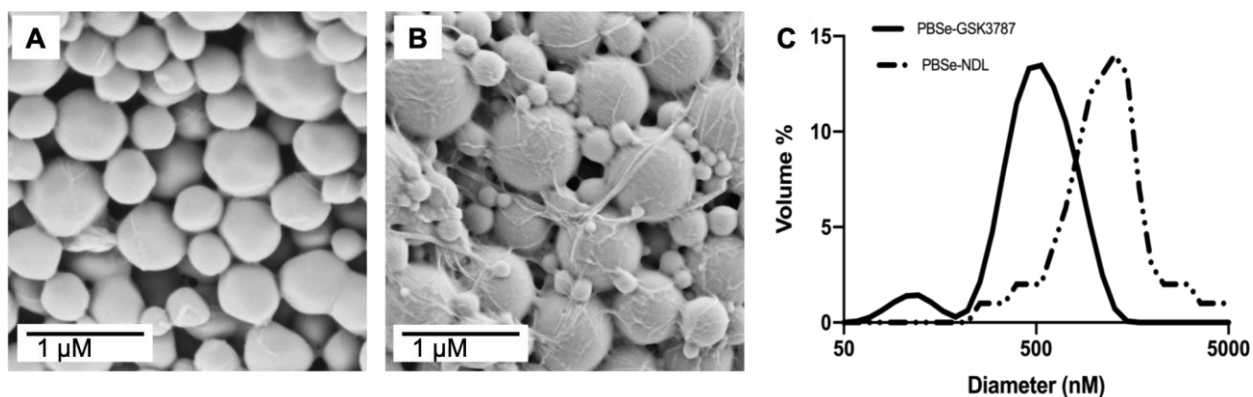


**Figure 3.2: Scanning electron micrographs of particles (A) PBSe-GSK3787 and (B) PBSe-NDL particles showing their spherical morphologies and diameters in the solid state; (C) DLS diameter distributions by volume % of PBSe-GSK3787 and PBSe-NDL particles showing the smaller diameters of the drug-loaded particles.**

Particles were first assessed for their morphology by SEM. The particles prepared using 8.6 wt% GSK3787 or with no drug had consistent spherical shapes, and no major surface defects were observed (Figure 3.2 A,B). **PBSe-NDL** particles had some debris as previously reported.<sup>28</sup> In previous work the debris was believed to PVA, as evidenced by the presence of a secondary  $T_g$  present in the DSC traces. Based on SEM analysis, **PBSe-GSK3787** particles had a diameter of  $580 \pm 290$  nm, while **PBSe-NDL** particles had a diameter of  $870 \pm 74$  nm (Table 3.1). The Z-average particle diameters measured by DLS were  $530 \pm 54$  nm for **PBSe-GSK3787** and  $790 \pm 64$  nm for **PBSe-NDL**. Thus, the diameters obtained for the two techniques were quite similar. **PBSe-GSK3787** particles were smaller than **PBSe-NDL** particles, but the dispersity of **PBSe-GSK3787** measured by SEM was much higher, and thus the difference in diameters between drug-loaded and non-drug-loaded particles was only statistically significant in the case of DLS. The

reduction in particle diameter might arise from the drug having a role at the solvent interface, as noted above.

**Table 3.1: Physiochemical characteristics of PBSe-GSK3787 and PBSe-NDL particles.**

<b>Particle Composition</b>	<b>Z-Average diameter (DLS) (nm)</b>	<b>Measured particle diameter (SEM) (nm)</b>	<b>GSK3787 loading (wt%)</b>	<b>GSK3787 encapsulation efficiency (%)</b>	<b>Young's Modulus (MPa)</b>	<b>Glass transition temperature (°C)</b>
<b>PBSe-NDL</b>	790 ± 64	870 ± 74	-	-	7.0 ± 1.4	34
<b>PBSe-GSK3787</b>	530 ± 54	580 ± 290	8.1 ± 0.4	94.0 ± 4.8	2.8 ± 1.0	35

Based on HPLC analysis (Appendix B, Figure B.4) of dissolved particles, the drug loading of **PBSe-GSK3787** particles was  $8.1 \pm 0.4$  wt% and the encapsulation efficiency was  $94 \pm 5\%$ . The high encapsulation efficiency can be attributed to the high hydrophobicity of GSK3787, which highly favours its partition into the dispersed phase, and thus encapsulation into the particles. As noted above, the drug loading of GSK3787 was lower than what was previously obtained with celecoxib, due to differences in the particle preparation procedure. However, this lower loading should not be a major issue. GSK3787 is known to bind to PPAR $\delta$  through covalent modification of cysteine 249 on the protein, which should lead to high potency.<sup>18</sup>

DSC was performed to assess the integration of drug within the particles. Both **PBSe-GSK3787** and **PBSe-NDL** showed similar glass transition temperatures of 35 °C and 34 °C, respectively. In addition, a sharp  $T_m$  was noted for the drug at 190 °C, and a broad  $T_m$  was observed for **PBSe-GSK3787** at about 187 °C. The presence of a melting transition in the particles suggests that crystalline domains of GSK3787 were present within the particles and that the drug and polymer were likely phase separated. The broad

transition can be attributed to domains of varying sizes. Previously, we observed homogeneous incorporation of celecoxib into PBSe particles, as evidenced by an increased  $T_g$  for the celecoxib-loaded particles, and no discernable  $T_m$ , despite the drug having a melting point at 158 °C.<sup>28</sup> These results may explain why it was possible to incorporate celecoxib at a much higher loading of >20 wt% compared with 8 wt% for GSK3787. Unlike in previous work, no secondary  $T_g$  was seen corresponding to excess PVA, which was hypothesized to be attributed to the increased evaporation time, resulting in more stable emulsions and PVA that was more effectively incorporated into particles.

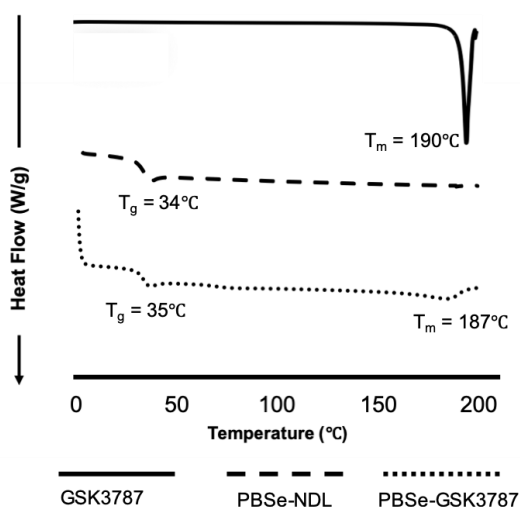


**Figure 3.3: Differential scanning calorimetry of GSK3787, PBSe-NDL, and PBSe-GSK3787.** DSC shows a  $T_m$  for the drug and for phase separated drug in the particles. Particles both with and without drug had very similar  $T_g$  values, again suggesting phase separation of the drug in the particles.

In previous work, we characterized the Young's modulus of bulk PEA and its blends with celecoxib by tensile testing in water at 37 °C.<sup>28</sup> However, the mechanical properties of the individual particles are important for their application in the joint, so in the current work AFM was used to measure the Young's moduli of individual particles by compression with the AFM tip at 37 °C in water and fitting of the data to the Hertz model (Figure 3.4).<sup>52</sup> **PBSe-GSK3787** particles had a Young's modulus of  $2.8 \pm 1.0$  MPa, significantly lower than the **PBSe-NDL** particles, which had a Young's modulus

measured at  $8.0 \pm 1.4$  MPa. A reduction in modulus was also observed previously when celecoxib was incorporated into bulk PBSe, and was attributed to increased plasticization of the polymer by water due to the capability of the drug to hydrogen bond to water.<sup>28</sup> This explanation may also apply to GSK3787 as it is also capable of hydrogen bonding. The compressive modulus of joint articular cartilage has been reported to range from 0.08 to 2 MPa, depending on the depth of tissue.<sup>53, 54</sup> Therefore, the **PBSe-GSK3787** particles have moduli that are similar to cartilage, which should minimize the potential for mechanical irritation to occur. If necessary, the modulus could be further reduced by varying the PEA structure.

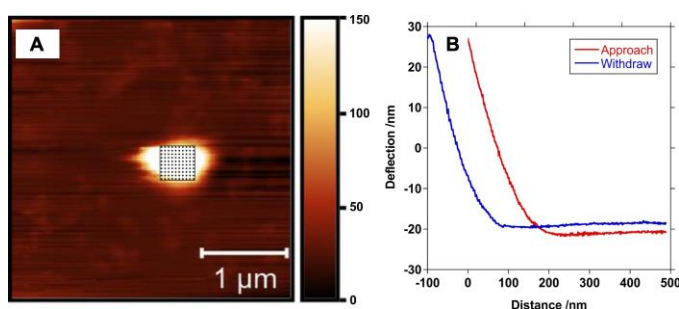


**Figure 3.4: AFM image of a PBSe-GSK3787 particle.** (A) showing the grid corresponding to the measurement of the modulus taken at 100 different points on a particle. (B) Representative approach and withdrawn curves that were used to calculate the modulus.

### 3.3.2 *In vitro* release of GSK3787

The release of GSK3787 was measured by placing a suspension of **PBSe-GSK3787** particles inside a dialysis cassette and then quantifying the concentration of drug in the dialysate over time by HPLC. The experiment was performed at 37 °C in PBS containing 2 wt% of polysorbate 80, to enhance the solubility of the drug in the release medium. The release medium was changed at each time point to ensure sink conditions. A suspension of free powdered GSK3787 placed in a dialysis bag was used as a control to ensure that the release was not rate-limited by simple dissolution of the drug. **PBSe-GSK3787** exhibited a slow release of drug, with only 11% of GSK3787 released after 30 days with no burst release observed. In contrast, 60% of the free GSK3787 was released into the

dialysate over the at the same time period showing that the drug release for **PBSe-GSK3787** was not limited by the dissolution rate of the drug (Figure 3.5). Previous results have suggested a surface erosion degradation mechanism for PBSe particles, and this mechanism may help explain the slow and apparent zero-order release of drug.<sup>28</sup> Representative HPLC traces are shown in Appendix B, figure B.4 and B.5, respectively.

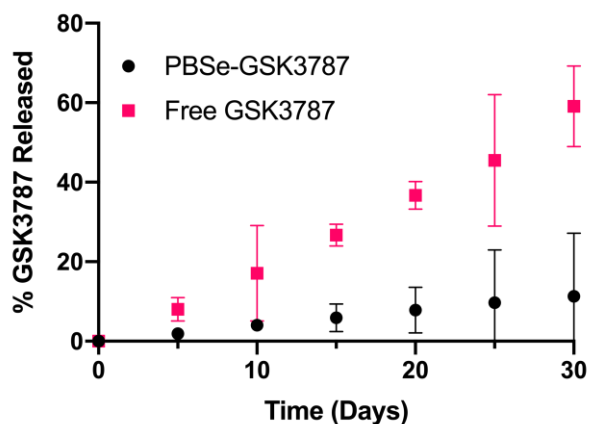


**Figure 3.5: Cumulative release of GSK3787 at 37 °C in PBS containing 2 wt% polysorbate 80.** Slower release of GSK3787 was observed from PBSe-GSK3787 particles compared to the free drug. Error bars correspond to the standard deviations on three separate particle populations in dialysis bags.

### 3.3.3 Cytotoxicity of GSK3787, PBSe-GSK3787, and PBSe-NDL on primary cell cultures

IMAC cells were used in this study as they are primary cells harvested directly from immature murine pups, allowing for a cell population that is as close to cartilage as possible. Specifically, when isolated and cultured properly, IMAC cells express a number of biomarkers that are found on chondrocytes *in vivo*, making them a good model for chondrocytes.<sup>55</sup> Free GSK3787 was first tested for cell toxicity by examining its effects on the metabolic activity using the MTT assay. No significant toxic effects were observed up to 100  $\mu$ M of drug, with metabolic activities remaining greater than 80% relative to control cells not exposed to drug (Figure 3.6A).

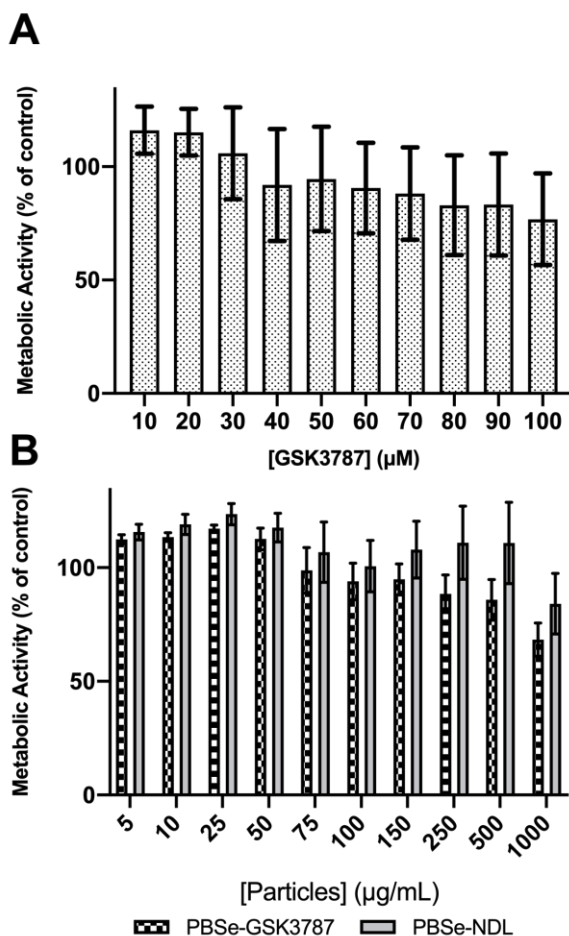


**Figure 3.6: Metabolic activity of IMAC cells, as measured by MTT assay.** 48 h after treatment with A) increasing concentrations of the PPAR $\delta$  inhibitor, GSK 3787 and B) **PBSe-GSK3787** and **PBSe-NDL** particles. No significant toxicity was observed for the free drug or for **PBSe-NDL**. However, a trend towards higher toxicity was observed for **PBSe-GSK3787** particles. Error bars correspond to standard deviations (N = 4).

The effects of **PBSe-GSK3787** and **PBSe-NDL** particles on IMAC cells were also evaluated using the MTT assay. There was a trend towards higher toxicity for the **PBSe-GSK3787** particles, but the metabolic activities remained above 68% of the control even at 1000  $\mu\text{g/mL}$ , the highest concentration tested (Figure 3.6B). It should be noted that at 8 wt% drug loading, 1000  $\mu\text{g/mL}$  corresponds to 80  $\mu\text{g/mL}$  ( $\sim 200 \mu\text{M}$ ) of drug. However, based on the drug release study, only a small fraction of drug should be released during

the 48 h incubation, so toxic concentrations of released drug would not be expected in the assay. Instead we proposed that any toxicity might arise from direct interactions between the particles and the cells. Thus, we also imaged live IMAC cells using brightfield microscopy after 48 h incubation of **PBSe-GSK3787** particles with cells. The 150  $\mu\text{g}/\text{mL}$  particle-treated cells were visible, and had healthy morphologies compared to control cells that were not treated with particles (Figure 3.7). At 1000  $\mu\text{g}/\text{mL}$ , the cells were remarkably covered with particles. It is possible that particle coverage on the cells limited the transport of nutrients or MTT reagent to cells, reducing their apparent metabolic activity.

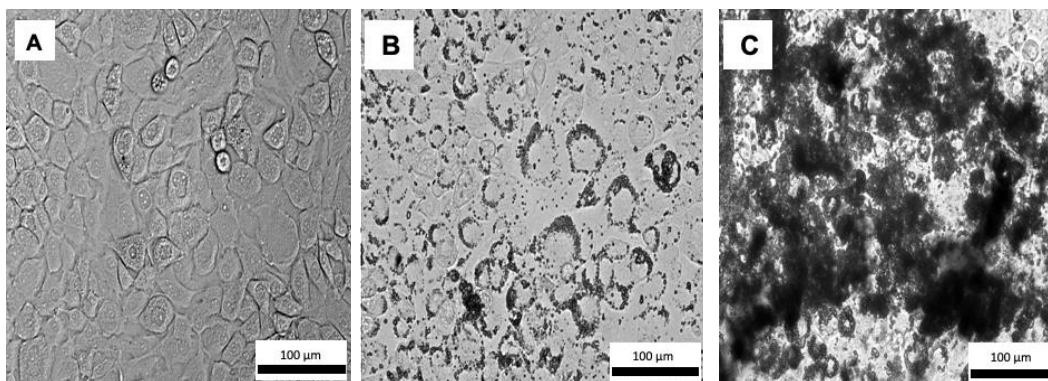


**Figure 3.7: Brightfield images of live IMAC cells.** Treated with A) no particles; B) 150  $\mu\text{g}/\text{mL}$  of **PBSe-GSK3787** particles; C) 1000  $\mu\text{g}/\text{mL}$  of **PBSe-GSK3787** particles. The particles agglomerated and adhered to the outsides of the cell membranes. Healthy cell morphologies were observed for cells treated with 150  $\mu\text{g}/\text{mL}$ , whereas the cells were almost completely coated with particles at 1000  $\mu\text{g}/\text{mL}$ .

**Confocal microscopy of IMAC cells treated with PBSe-GSK3787-NR.** Nile red-labeled **PBSe-GSK3787** particles (**PBSe-GSK3787-NR**) were prepared to enable visualization of the particles using fluorescence confocal microscopy. IMAC cells were incubated with 100  $\mu\text{g}/\text{mL}$  of **PBSe-GSK3787-NR** particles for 48 h, and then imaging was performed to assess how particles interacted with the cells and whether they were taken up by the cells. The cell cytoskeletons were also stained with AlexaFluor 488-Phalloidin (green) and the nuclei were stained with DAPI (Figure 3.8A). A 3D image rendering of the confocal images showed that the particles remained at the cell surface

(Figure 3.8B). The particles were somewhat agglomerated, and thus concentrated in certain regions rather than being uniformly distributed on the cell surfaces. It is likely that some particles that were initially on cells were washed away through the numerous washing steps that were associated with the staining of the cells.

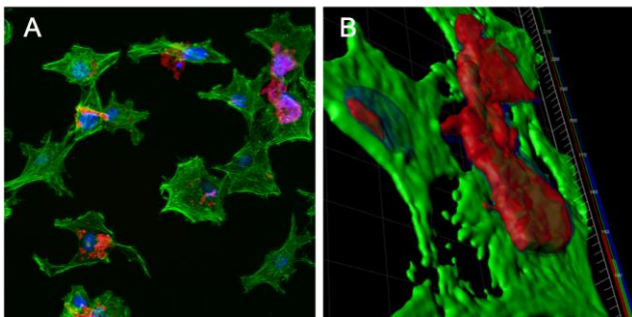


**Figure 3.8: Confocal microscopy images of IMAC cells.** Treated with 100  $\mu\text{g}/\text{mL}$  **PBSe-GSK3787-NR** particles (red) for 48 h, then stained with AlexaFluor 488 Phalloidin (green, cytoskeletons) and DAPI (blue, nuclei): A) 2D image showing agglomerates of particles on the cells; B) 3D rendering of cells showing particles localized at the cell surface and not taken up by the cells.

### 3.3.4 *Ex vivo* intra-articular injections

For intra-articular injections, the particles were labeled with the hydrophobic green dye IR780 (**PBSe-GSK3787-IR**) to provide contrast against tissues in brightfield imaging as well as fluorescence at 485 nm for fluorescence microscopy. Murine knee joints were obtained from C57BL/6 mice, and were injected with 5  $\mu\text{L}$  of a 100 mg/mL suspension of particles per joint into the intra-articular space. The joints were then resected and cultured in organ culture media for 7 d. The culture of joints has been determined previously to be a good model for the study of OA, because of its low expense, and ability of the tissue to maintain cytokine stimulation and osmotic pressure while in culture.<sup>56</sup> The joints were imaged to qualitatively assess the diffusion of particles away from the joint space and through the surrounding tissue. Using brightfield imaging, it was observed that distribution of particles had remained localized to the joint after 7 d, with

no distinct green dye seen outside of the joint space. Fluorescence microscopy at 7 d showed that while there was particle migration through both the joint and the limb, the bulk of the injected material remained within the joint space (Figure 3.9). Thus, the injection into joints *ex vivo* allowed for a better understanding of the distribution of particles post administration, and how they behave in the absence of mechanical loading.

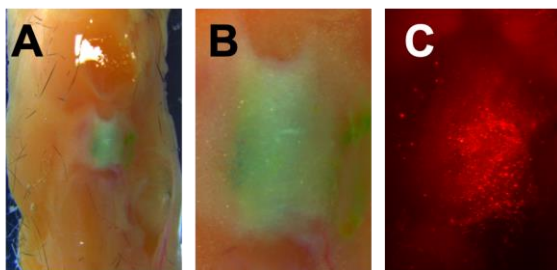


**Figure 3.9: Representative knee joint explant from a C57BL/6 mouse that was injected with 5  $\mu$ L of a 100 mg/mL suspension of PBSe-GSK3787-IR particles.** Upon resection of the limbs, images were taken with a stereoscope to determine injectability and localization of particles. Images taken 7 days post injection of (A) Knee joint at 7.3x magnification; (B) Knee joint at 1.6x magnification; (C) Particles as visualized in the joint under fluorescence microscopy, 1.6x magnification.

### 3.4 Conclusions

PBSe particles containing the PPAR $\delta$  antagonist, GSK3787, were successfully prepared by modifying our previously developed procedure. Specifically, it was important to lower the loading of drug from 30 wt% for celecoxib to 8.6 wt% for GSK3787 in order to achieve clean particle formation. This requirement may arise from GSK3787 acting at the interface, as supported by the formation of smaller particles in the presence of this drug, or due to incompatibility of the drug and PBSe, which was suggested by thermal analysis of the particles. Relative to particles without drug, the loading of GSK3787 into the particles lowered the Young's modulus, bringing it closer to the natural range of articular cartilage. The particles exhibited a slow release of GSK3787 *in vitro* with no burst release observed. GSK3787 exhibited low toxicity to IMAC cells as indicated by the MTT assay. The particles exhibited low toxicity, except at the highest concentrations

studied ( $> 500 \mu\text{g/mL}$ ) and this lowering of metabolic activity might be due to the high concentrations of particles localized on the cell surface, as indicated by bright field and fluorescence confocal microscopy. Knee joint explant cultures that were injected with particles showed that the particles remained localized in the joint, even after 7 days of injection. Therefore, this system encapsulates and releases a potent PPAR $\delta$  antagonist that cannot be delivered systemically, and serves as a promising vehicle for further investigated in intra-articular drug delivery for the treatment of OA.

### 3.5 References

1. Vina, E. R.; Kwok, C. K., Epidemiology of osteoarthritis: literature update. *Curr. Opin. Rheumatol.* **2018**, 30, 160-167.
2. Suri, P.; Morgenroth, D. C.; Hunter, D. J., Epidemiology of osteoarthritis and associated comorbidities. *PM. R.* **2012**, 4, S10-S19.
3. Neogi, T., The epidemiology and impact of pain in osteoarthritis. *Osteoarth. Cartilage* **2013**, 21, 1145-1153.
4. Hurley, M. V.; Walsh, N. E.; Mitchell, H. L.; Pimm, T. J.; Patel, A.; Williamson, E.; Jones, R. H.; Dieppe, P. A.; Reeves, B. C., Clinical effectiveness of a rehabilitation program integrating exercise, self-management, and active coping strategies for chronic knee pain: a cluster randomized trial. *Arthritis Rheum.* **2007**, 57, 1211-1219.
5. Brakke, R.; Singh, J.; Sullivan, W., Physical therapy in persons with osteoarthritis. *PM. R.* **2012**, 4, S53-S58.
6. Grosser, T.; Fries, S.; FitzGerald, G. A., Biological basis for the cardiovascular consequences of COX-2 inhibition: therapeutic challenges and opportunities. *J. Clin. Invest.* **2006**, 116, 4-15.

7. Mahmud, T.; Scott, D. L.; Bjarnason, I., A Unifying Hypothesis for the Mechanism of NSAID Related Gastrointestinal Toxicity. *Ann. Rheum. Dis.* **1996**, *55*, 211-213.
8. Douglas, R. J., Corticosteroid injection into the osteoarthritic knee: drug selection, dose, and injection frequency. *Int. J. Clin. Pract.* **2012**, *66*, 699-704.
9. Hunter, D. J., Osteoarthritis. *Best Pract. Res. Clin. Rheumatol.* **2011**, *25*, 801-814.
10. Grayson, C. W.; Decker, R. C., Total joint arthroplasty for persons with osteoarthritis. *PM. R.* **2012**, *4*, S97-S103.
11. Losina, E.; Paltiel, A. D.; Weinstein, A. M.; Yelin, E.; Hunter, D. J.; Chen, S. P.; Klara, K.; Suter, L. G.; Solomon, D. H.; Burbine, S. A.; Walensky, R. P.; Katz, J. N., Lifetime medical costs of knee osteoarthritis management in the United States: impact of extending indications for total knee arthroplasty. *Arthritis Care Res.* **2015**, *67*, 203-215.
12. Liu-Bryan, R.; Terkeltaub, R., Emerging regulators of the inflammatory process in osteoarthritis. *Nat. Rev. Rheumatol.* **2015**, *11*, 35-44.
13. Grothe, K.; Flechsenhar, K.; Paehler, T.; Ritzeler, O.; Beninga, J.; Saas, J.; Herrmann, M.; Rudolphi, K., IkappaB kinase inhibition as a potential treatment of osteoarthritis - results of a clinical proof-of-concept study. *Osteoarth. Cartilage* **2017**, *25*, 46-52.
14. Rigoglou, S.; Papavassiliou, A. G., The NF-kappaB signalling pathway in osteoarthritis. *Int. J. Biochem. Cell Biol.* **2013**, *45*, 2580-2584.
15. Kelly, S.; Chapman, R. J.; Woodhams, S.; Sagar, D. R.; Turner, J.; Burston, J. J.; Bullock, C.; Paton, K.; Huang, J.; Wong, A.; McWilliams, D. F.; Okine, B. N.; Barrett, D. A.; Hathway, G. J.; Walsh, D. A.; Chapman, V., Increased function of pronociceptive TRPV1 at the level of the joint in a rat model of osteoarthritis pain. *Ann. Rheum. Dis.* **2015**, *74*, 252-259.

16. Malfait, A. M.; Miller, R. J., Emerging Targets for the Management of Osteoarthritis Pain. *Curr. Osteoporos. Rep.* **2016**, 14, 260-268.
17. Ratneswaran, A.; LeBlanc, E. A.; Walser, E.; Welch, I.; Mort, J. S.; Borradaile, N.; Beier, F., Peroxisome proliferator-activated receptor delta promotes the progression of posttraumatic osteoarthritis in a mouse model. *Arthritis Rheumatol.* **2015**, 67, 454-464.
18. Shearer, B. G.; Wiethe, R. W.; Ashe, A.; Billin, A. N.; Way, J. M.; Stanley, T. B.; Wagner, C. D.; Xu, R. X.; Leesnitzer, L. M.; Merrihew, R. V.; Shearer, T. W.; Jeune, M. R.; Ulrich, J. C.; Willson, T. M., Identification and characterization of 4-chloro-N-(2-{[5-trifluoromethyl]-2-pyridyl}sulfonyl)ethyl)benzamide (GSK3787), a selective and irreversible peroxisome proliferator-activated receptor delta (PPARdelta) antagonist. *J. Med. Chem.* **2010**, 53, 1857-1861.
19. Lee, C. H.; Olson, P.; Hevener, A.; Mehl, I.; Chong, L. W.; Olefsky, J. M.; Gonzalez, F. J.; Ham, J.; Kang, H.; Peters, J. M.; Evans, R. M., PPARdelta regulates glucose metabolism and insulin sensitivity. *Proc. Natl. Acad. Sci.* **2006**, 103, 3444-3449.
20. Schmuth, M.; Haqq, C. M.; Cairns, W. J.; Holder, J. C.; Dorsam, S.; Chang, S.; Lau, P.; Fowler, A. J.; Chuang, G.; Moser, A. H.; Brown, B. E.; Mao-Qiang, M.; Uchida, Y.; Schoonjans, K.; Auwerx, J.; Chambon, P.; Willson, T. M.; Elias, P. M.; Feingold, K. R., Peroxisome proliferator-activated receptor (PPAR)-beta/delta stimulates differentiation and lipid accumulation in keratinocytes. *J. Invest. Dermatol.* **2004**, 122, 971-983.
21. Tan, N. S.; Icre, G.; Montagner, A.; Bordier-ten-Heggeler, B.; Wahli, W.; Michalik, L., The nuclear hormone receptor peroxisome proliferator-activated receptor beta/delta potentiates cell chemotactism, polarization, and migration. *Mol. Cell. Biol.* **2007**, 27, 7161-7175.
22. Chen, Y., Intra-Articular Drug Delivery Systems for Arthritis Treatment. *Rheumatol.: Curr. Res.* **2012**, 02.

23. Bajpayee, A. G.; Wong, C. R.; Bawendi, M. G.; Frank, E. H.; Grodzinsky, A. J., Avidin as a model for charge driven transport into cartilage and drug delivery for treating early stage post-traumatic osteoarthritis. *Biomaterials* **2014**, 35, 538-549.
24. Maudens, P.; Jordan, O.; Allemann, E., Recent advances in intra-articular drug delivery systems for osteoarthritis therapy. *Drug Discov. Today* **2018**,1-15.
25. Dong, J.; Jiang, D.; Wang, Z.; Wu, G.; Miao, L.; Huang, L., Intra-articular delivery of liposomal celecoxib-hyaluronate combination for the treatment of osteoarthritis in rabbit model. *Int. J. Pharm.* **2013**, 441, 285-90.
26. Chen, Z.; Liu, D.; Wang, J.; Wu, L.; Li, W.; Chen, J.; Cai, B. C.; Cheng, H., Development of nanoparticles-in-microparticles system for improved local retention after intra-articular injection. *Drug Deliv.* **2014**, 21, 342-50.
27. Janssen, M.; Timur, U. T.; Woike, N.; Welting, T. J.; Draaisma, G.; Gijbels, M.; van Rhijn, L. W.; Mihov, G.; Thies, J.; Emans, P. J., Celecoxib-loaded PEA microspheres as an auto regulatory drug-delivery system after intra-articular injection. *J. Controlled Release* **2016**, 30-40.
28. Villamagna, I. J.; Gordon, T. N.; Hurtig, M. B.; Beier, F.; Gillies, E. R., Poly(ester amide) particles for controlled delivery of celecoxib. *J Biomed Mater. Res. A* **2019**, 1235-1243.
29. Li, Y.; Cao, J.; Han, S.; Liang, Y.; Zhang, T.; Zhao, H.; Wang, L.; Sun, Y., ECM based injectable thermo-sensitive hydrogel on the recovery of injured cartilage induced by osteoarthritis. *Artif. Cells Nanomed. Biotechnol.* **2018**, 152-160.
30. Petit, A.; Sandker, M.; Muller, B.; Meyboom, R.; van Midwoud, P.; Bruin, P.; Redout, E. M.; Versluijs-Helder, M.; van der Lest, C. H.; Buwalda, S. J.; de Leede, L. G.; Vermonden, T.; Kok, R. J.; Weinans, H.; Hennink, W. E., Release behavior and intra-articular biocompatibility of celecoxib-loaded acetyl-capped PCLA-PEG-PCLA thermogels. *Biomaterials* **2014**, 35, 7919-7928.

31. Prince, D. A.; Villamagna, I. J.; Borecki, A.; Beier, F.; de Bruyn, J. R.; Hurtig, M.; Gillies, E. R., Thermoresponsive and Covalently Cross-Linkable Hydrogels for Intra-Articular Drug Delivery. *ACS Appl. Bio Mater.* **2019**, 2, 3498-3507.
32. Hu, Q.; Ding, B.; Yan, X.; Peng, L.; Duan, J.; Yang, S.; Cheng, L.; Chen, D., Polyethylene glycol modified PAMAM dendrimer delivery of kartogenin to induce chondrogenic differentiation of mesenchymal stem cells. *Nanomedicine* **2017**, 13, 2189-2198.
33. Kumar, A.; Bendele, A. M.; Blanks, R. C.; Bodick, N., Sustained efficacy of a single intra-articular dose of FX006 in a rat model of repeated localized knee arthritis. *Osteoarth. Cartilage* **2015**, 23, 151-60.
34. Soleimani, A.; Drappel, S.; Carlini, R.; Goredema, A.; Gillies, E. R., Structure–Property Relationships for a Series of Poly(ester amide)s Containing Amino Acids. *Ind. Eng. Chem. Res.* **2014**, 53, 1452-1460.
35. Place, E. S.; George, J. H.; Williams, C. K.; Stevens, M. M., Synthetic polymer scaffolds for tissue engineering. *Chem Soc. Rev.* **2009**, 38, 1139-51.
36. Fonseca, A. C.; Gil, M. H.; Simões, P. N., Biodegradable poly(ester amide)s – A remarkable opportunity for the biomedical area: Review on the synthesis, characterization and applications. *Prog. Polym. Sci.* **2014**, 39, 1291-1311.
37. Knight, D. K.; Gillies, E. R.; Mequanint, K., Strategies in functional poly(ester amide) syntheses to study human coronary artery smooth muscle cell interactions. *Biomacromolecules* **2011**, 12, 2475-87.
38. Karimi, P.; Rizkalla, A. S.; Mequanint, K., Versatile Biodegradable Poly(ester amide)s Derived from  $\alpha$ -Amino Acids for Vascular Tissue Engineering. *Materials* **2010**, 3, 2346-2368.
39. Tsitlanadze, G.; Machaidze, M.; Kviria, T.; Djavakhishvili, N.; Chu, C. C.; Katsarava, R., Biodegradation of amino-acid-based poly(ester amide)s: in vitro weight loss and preliminary in vivo studies. *J Biomater. Sci. Polym. Ed.* **2004**, 15, 1-24.

40. Knight, D. K.; Gillies, E. R.; Mequanint, K., Biomimetic L-aspartic acid-derived functional poly(ester amide)s for vascular tissue engineering. *Acta Biomater.* **2014**, *10*, 3484-3496.
41. Cao, K.; Flegg, D. S.; Lin, S.; Laguné-Labarthe, F.; Mequanint, K.; Gillies, E. R., Fabrication and In Situ Cross-Linking of Carboxylic-Acid-Functionalized Poly(Ester Amide) Scaffolds for Tissue Engineering. *ACS Appl. Polym. Mater.* **2019**, *1*, 2360-2369.
42. Murase, S. K.; del Valle, L. J.; Kobauri, S.; Katsarava, R.; Puiggali, J., Electrospun fibrous mats from a l-phenylalanine based poly(ester amide): Drug delivery and accelerated degradation by loading enzymes. *Polym. Degrad. Stabil.* **2015**, *119*, 275-287.
43. Said, S. S.; Pickering, J. G.; Mequanint, K., Controlled Delivery of Fibroblast Growth Factor-9 from Biodegradable Poly(ester amide) Fibers for Building Functional Neovasculature. *Pharm. Res.* **2014**, *31*, 3335-3347.
44. Rudnik-Jansen, I.; Colen, S.; Berard, J.; Plomp, S.; Que, I.; van Rijen, M.; Woike, N.; Egas, A.; van Osch, G.; van Maarseveen, E.; Messier, K.; Chan, A.; Thies, J.; Creemers, L., Prolonged inhibition of inflammation in osteoarthritis by triamcinolone acetonide released from a polyester amide microsphere platform. *J Controlled Release* **2017**, *253*, 64-72.
45. Mullin, N.; Hobbs, J. K., A non-contact, thermal noise based method for the calibration of lateral deflection sensitivity in atomic force microscopy. *Rev. Sci. Instrum.* **2014**, *85*, 113703.
46. Nagel, S. R.; Benedetti, L. R.; Bradley, D. K.; Hilsabeck, T. J.; Izumi, N.; Khan, S.; Kyrala, G. A.; Ma, T.; Pak, A., Comparison of implosion core metrics: A 10 ps dilation X-ray imager vs a 100 ps gated microchannel plate. *Rev. Sci. Instrum.* **2016**, *87*, 11E311.

47. Gosset, M.; Berenbaum, F.; Thirion, S.; Jacques, C., Primary culture and phenotyping of murine chondrocytes. *Nat. Protoc.* **2008**, 3, 1253-60.
48. Jelvehgari, M.; Montazam, S., Comparison of Microencapsulation by Emulsion-Solvent Extraction/ Evaporation Technique Using Derivatives Cellulose and Acrylate-Methacrylate Copolymer as Carriers. Jundishapur *J. Nat. Pharm. Prod.* **2012**, 7, 144-152.
49. Rosca, I. D.; Watari, F.; Uo, M., Microparticle formation and its mechanism in single and double emulsion solvent evaporation. *J. Controlled Release* **2004**, 99, 271-280.
50. Aranberri, I.; Beverley, K. J.; Binks, B. P.; Clint, J. H.; Fletcher, P. D. I., How Do Emulsions Evaporate. *Langmuir* **2002**, 18, 1-12.
51. Dilling, W., L. ; Tefertiller, N. B.; Kallos, G. J., Evaporation rates and reactivities of methylene chloride, chloroform, 1,1,1-trichloroethane, trichloroethylene, tetrachloroethylene, and other chlorinated compounds in dilute aqueous solutions. *Environ. Sci. Technol.* **1975**, 9.
52. Kontomaris, S.-V., The Hertz Model in AFM Nanoindentation Experiments: Applications in Biological Samples and Biomaterials. *Micro Nanosyst.* **2018**, 10, 11-22.
53. Athanasiou, K. A.; Rosenwasser, M. P.; Buckwalter, J. A.; Malinin, T. I.; Mow, V. C., Interspecies Comparisons of In Situ Intrinsic Mechanical Properties of Distal Femoral Cartilage. *J. Orthopaed. Res.* **1991**, 9, 330-340.
54. Schinagl, R. M.; Gurskis, D.; Chen, A. C.; Sah, R. L., Depth-Dependent Confined Compression Modulus of Full-Thickness Bovine Articular Cartilage. *J. Orthopaed. Res.* **1997**, 15.
55. Lamplot, J. D.; Liu, B.; Yin, L.; Zhang, W.; Wang, Z.; Luther, G.; Wagner, E.; Li, R.; Nan, G.; Shui, W.; Yan, Z.; Rames, R.; Deng, F.; Zhang, H.; Liao, Z.; Liu, W.; Zhang, J.; Zhang, Z.; Zhang, Q.; Ye, J.; Deng, Y.; Qiao, M.; Haydon, R. C.; Luu, H. H.; Angeles, J.; Shi, L. L.; He, T. C.; Ho, S. H., Reversibly Immortalized

Mouse Articular Chondrocytes Acquire Long-Term Proliferative Capability While Retaining Chondrogenic Phenotype. *Cell Transplant.* **2015**, 24, 1053-66.

56. Johnson, C. I.; Argyle, D. J.; Clements, D. N., In vitro models for the study of osteoarthritis. *Vet. J.* **2016**, 209, 40-49.

## Chapter 4

### 4 Thermo-responsive hybrid particle in hydrogel delivery system for intra-articular drug delivery

#### 4.1 Introduction

Osteoarthritis (OA) is a debilitating disease characterized by the degradation of articular joints.<sup>1</sup> The disease affects the entire joint, including the cartilage, synovium and surrounding bones, and is estimated to be present in 242 million people worldwide.<sup>1-3</sup> Incidence of the disease is rising rapidly; a 75% increase in years lived with disease was reported between 1993 and 2013 worldwide.<sup>3</sup> Current treatments focus on alleviating the symptoms of the disease, as no disease modifying agents currently exist for OA. Recently, significant research has focused on the discovery of potential disease-modifying drugs, and a number of compounds are being studied, which act by a variety of different mechanisms. Examples include CNTX-4975, which targets the capsaicin receptor (TRPV1) and acts to relieve pain associated with OA,<sup>4</sup> while doxycycline hyclate, a matrix metalloproteinase (MMP) inhibitor, acts to inhibit the enzymatic degradation of cartilage.<sup>5</sup> Our lab has identified PPAR $\delta$  receptors as potential targets,<sup>6, 7</sup> where treatment with antagonists such as GSK3787<sup>8</sup> could potentially lead to slowing or halting of OA progression.<sup>6-8</sup>

Localized delivery of therapeutics via intra-articular (IA) injection is recognized as a promising strategy to achieve the correct dose of drug in the joint, while reducing systemic side effects.<sup>9</sup> However, free drugs are subject to rapid clearance from the joint by the lymphatic system over 1-4 h.<sup>10</sup> Given that IA injections should not be given more than once every few months,<sup>11</sup> drugs delivered by IA may not reside in the joint for a sufficient time period to provide a therapeutic effect. To address this, drug delivery systems are needed, which are capable of prolonging the release of drugs in the joint following injection.

To date, multiple types of injectable IA delivery systems have been studied for OA treatment, including crystalline drug formations,<sup>12</sup> liposomes,<sup>13-15</sup> nanoparticles,<sup>16-19</sup> microparticles,<sup>16, 20</sup> and hydrogels.<sup>21, 22</sup> Particle-based delivery systems for IA injection have been extensively studied. For example, poly(lactic-*co*-glycolic acid) (PLGA) particles loaded with triamcinolone acetonide were recently approved by the United States Food and Drug Administration (FDA) for use as an OA treatment.<sup>23</sup> Poly(ester amide) (PEA) particles have also been investigated and were found exhibit good host response in the joints of sheep and rats.<sup>19, 24</sup> Despite progress with particles, sustained drug release over multiple months remains a challenge. For example, the aforementioned PLGA particles released triamcinolone acetonide at measurable levels for 6 weeks.<sup>23, 25</sup> Despite their slow release *in vitro*, we also found in preliminary experiments with PEA particles that drug release was not sustained within the joints of sheep, possibly due to mechanical or biochemical degradation of the particles in the joint or due to their trafficking to the synovial membrane.<sup>19</sup> (Villamagna, I.J. unpublished results)

Hydrogels are another class of promising materials for IA delivery. They typically have compression moduli less than that of cartilage, and have been shown to be well tolerated in the joint.<sup>26</sup> Furthermore, the macroscopic dimensions of hydrogels allow them to remain in the synovial space for a prolonged period post-injection, potentially leading to sustained release of drugs. Thermo-responsive hydrogels based on poly(caprolactone-*co*-lactide)(PCLA)-poly(ethylene glycol)(PEG)-PCLA have been investigated for IA delivery of the non-steroidal anti-inflammatory drug celecoxib (CXB).<sup>22, 27-29</sup> Drug-loaded formulations of these polymers exist as injectable liquids at and below room temperature, but gel spontaneously at 37 °C following injection. When the polymers were end-capped with acetyl groups, gelation was disrupted by drug loading and the resulting hydrogels released therapeutic levels of (CXB) over 10-15 days, with an initial burst release.<sup>21, 22</sup> The addition of methacrylate end caps to the polymer allowed for covalent crosslinking using a potassium persulfate (KPS)/tetramethylethylenediamine (TEMED) initiation system, resulting in improved mechanical properties of the hydrogels, reduced burst release, and sustained release of therapeutic celecoxib levels for more than 30 days in an equine model.<sup>21</sup> However, to reduce the required injection frequency, it is still

necessary to eliminate the burst release and prolong the time of therapeutic drug levels in the joint to ~3 months.

Here we explore a hybrid delivery system in which PEA particles are encapsulated into covalently crosslinked PCLA-PEG-PCLA hydrogels (Figure 1). We propose that the hydrogel should afford mechanical and biochemical protection of the particles in the joint and retain the particles in the joint space, ultimately leading to more sustained release. We focus on encapsulating the potential disease-modifying agent GSK3787.<sup>6,7</sup> The particle-in-gel hybrid system was compared against drug-loaded and non-drug-loaded gels to determine the effects of particle incorporation on hydrogel syneresis, degradation rate, drug release, mechanical and rheological properties, as well as *in vitro* cytotoxicity.

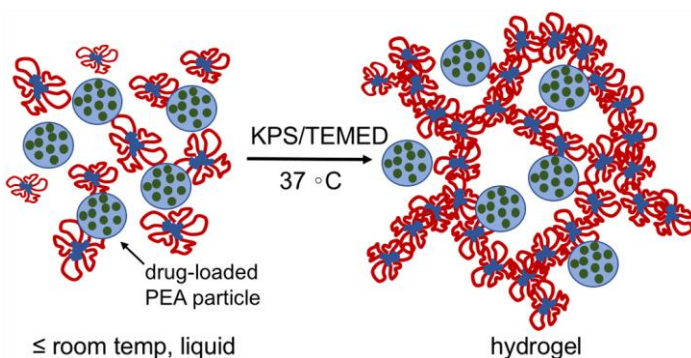


**Figure 4.1: Schematic illustrating the proposed particle in hydrogel hybrid drug delivery system**

## 4.1 Materials and Methods

### 4.1.1 General materials and procedures

The poly(ester amide) PBSe, composed of L-phenylalanine, 1,4-butanediol, and sebacic acid, was prepared and characterized according to previously reported procedures.<sup>30</sup> PBSe was used to prepare GSK3787-loaded particles (**PBSe-GSK3787**) as described in section 3.2.2, and the particles were characterized by dynamic light scattering and scanning electron microscopy as described in section 3.2.1. Methacrylate end-capped PCLA-PEG-PCLA was synthesized and characterized as previously reported.<sup>21</sup> KPS and

TEMED were obtained from Sigma Aldrich (Oakville, Canada). GSK3787 was purchased from Ontario Chemicals Inc. Acetonitrile was purchased from VWR Analytical (USA). Phosphate buffered saline (PBS) powder packs were purchased from Sigma Life Science and were used to prepare the pH 7.4 PBS solutions according to the manufacturer's instructions. Water used to prepare the buffer solutions was obtained from a Barnstead Easypure II system with a measured resistivity of 15 M $\Omega$  or greater. All other chemicals were used as received. Differential scanning calorimetry (DSC) was performed on a Q2000 from TA instruments (New Castle, DE). The heating/cooling rate was 10 °C/min from -80 to +200 °C, and the glass transition ( $T_g$ ) and melting point temperatures ( $T_m$ ) were obtained from the second heating cycle.

#### 4.1.2 Preparation of hydrogels

5.0 g (22 wt%) of molten polymer was added to 17.5 mL of PBS at 4 °C and then vortexed for 60 s. The mixture was then placed in a 37 °C oven for 1 h, and then returned to the fridge for 96 h to achieve complete dissolution. This base formulation was then used to prepare different hydrogel systems. **Control hydrogel** consisted only of the base formulation. **10 wt% particle-in-gel** was prepared by adding 1.0 g of **PBSe-GSK3787** particles to 9.0 mL of base formulation. **10 wt% GSK3787** was prepared by mixing 100 mg of GSK3787 with 900  $\mu$ L of formulation. Dispersion of the drug or particles in the formulations was achieved by vortexing vigorously over 30 min. Covalent crosslinking was initiated by adding 60  $\mu$ L of KPS solution (0.18 M) and 20  $\mu$ L of TEMED solution (1 M) per mL of polymer formulation to produce a final concentration of 10 mM KPS and 20 mM TEMED at 4 °C, then the temperature was increased to 37 °C.

#### 4.1.3 Scanning electron microscopy (SEM)

To prepare samples, 1 mL of hydrogel formulation, prepared as described above, was placed in a 3 mL vial and then gelled at 37 °C for 1 h. Samples were removed from the vials, affixed to stubs that had been covered in carbon tape, immediately submerged in liquid N<sub>2</sub> for 5 min, then lyophilized. They were then coated with 5 nm of osmium using a SCI Supplies, OC-60A plasma coater. SEM was performed at the Western

Nanofabrication Facility using a Leo 1530 instrument, operating at 2.0 kV and a working distance of 6 mm.

#### 4.1.4 Measurement of hydrogel syneresis

Water loss from prepared hydrogels was measured gravimetrically. 1.0 g of liquid hydrogel was placed in a pre-weighed 3 mL screw top vial, and then placed in a 37 °C oven, and allowed to gel. At specified time points, vials were removed, uncapped, and inverted for one min, allowing released water to flow from the vial. Vials were then weighed before being recapped and placed back in the oven. Measurements were performed on three different samples for each hydrogel system.

#### 4.1.5 Hydrogel degradation

Gravimetric analysis was performed on hydrogel samples that had been soaked in pH 7.4 PBS at 37 °C. 1.0 g of hydrogel was added to a 3 mL pre-weighed vial, and then the vial was placed in a 37 °C oven, and allowed to gel for 30 min. 2 mL of PBS was added to the vial and it was returned to the 37 °C oven. At specified time points, vials were inverted for 1 min, allowing the PBS to drain completely, and were re-weighed. 2 mL of PBS was then added to the vial again and it was placed back in the 37 °C oven until the next time point. The measurements were performed on three separate hydrogel samples of each hydrogel system.

#### 4.1.6 Measurement of Young's moduli under compression

Mechanical testing of hydrogel samples was performed using a CellScale Univert (Waterloo, ON, Canada), using a 10 N load cell. The different formulations were gelled in 3 mL syringes (internal diameter of 8.7 mm) at 37 °C for 1 h, yielding cylindrical samples of hydrogel in a 2:1 height:diameter ratio (1.0 mL of formulation). Samples were immersed in PBS at 37 °C and then loaded with uniaxial compression to a total strain of 30%, at a constant rate of 4%/s. Secant moduli, calculated as the slope between 5 and 20% strain, were determined. All systems were measured in triplicate.

#### 4.1.7 *In vitro* release of GSK3787 from hydrogels in PBS

The release of GSK3787 from **10 wt% GSK3787** and **10 wt% particle-in-gel** was measured in PBS at 37 °C. Hydrogels were prepared in 3 mL syringes (1.0 mL each) as described above for compression testing. The hydrogels were accurately weighed and then placed into vials with 3.0 mL of the release medium, which was PBS containing 2 wt% Tween 80. Vials were placed in a 37 °C incubator. At predetermined time points, the release medium was removed and replaced with fresh medium. The removed medium was filtered using a 0.2 µm PTFE membrane syringe filters and analyzed for drug using high performance liquid chromatography (HPLC). The HPLC instrument consisted of a Waters 2695 Separations Module, a Kinetex C18 5 µm (4.6 × 100 mm) column connected to a C18 guard column, and a Photodiode Array (PDA) Detector (Waters 2998). The PDA detector was used to monitor GSK3787 at 238 nm. An isocratic eluent method with acetonitrile and water (40:60) was used. The retention time of GSK3787 was 2.5 min (Figure S7). Standard solutions of 10, 5, 2, 1, 0.5, and 0.2 µg/mL were prepared by adding GSK3787 to PBS buffer. 100 µL of sample was injected. Release studies were performed in triplicate for each system and all samples were measured in duplicate by HPLC.

#### 4.1.8 Primary articular chondrocyte harvest and culture

Immature murine articular chondrocyte (IMAC) cells were harvested from C56BL/7 mouse pups as previously described.<sup>31</sup> Cells were plated at a density of  $3.0 \times 10^5$  cells in 96 well plates and then cultured in media composed of MEM, 10 mg/mL L-glutamine, 5 mg/mL pen/strep and high efficiency fetal bovine serum at a concentration of 5% (v/v) for one week prior to the treatment of cells for *in vitro* testing. Animal work was performed in compliance with the guidelines of The Canadian Council on Animal Care guidelines (University of Western Ontario Protocol 2019-035).

#### 4.1.9 Toxicity assays on IMAC cells

Treatment media was prepared by injecting 3 mL of liquid hydrogel formulation into 10 mL of pre-warmed cell culture media at 37 °C. Centrifuge tubes were sealed and placed

in an incubator for 14 days, with agitation of the tubes occurring every 48 h. After soaking, the media was sterilized by filtration through a 0.2  $\mu\text{m}$  PVDF syringe filter, and 110  $\mu\text{L}$  was added to each well for treatment. The three hydrogel preparations were soaked in cell media for 14 days before being filtered. Cells were cultured with the media for 48 h. 3-(4,5-dimethylthiazol-2-yl)-2,5-diphenyl tetrazolium bromide (MTT) reagent was dissolved in cell culture media at a concentration of 0.5 mg/mL and 110  $\mu\text{L}$  of the MTT media was added to each well, before being incubated for 4 h at 37  $^{\circ}\text{C}$ . The media was then aspirated, and 50  $\mu\text{L}$  of DMSO was added to each well to solubilize the purple crystals. The plate was then placed in a plate reader (Tecan Infinite M1000 Pro) and the absorbance at 540 nm was measured to quantify the relative metabolic activities of the cells. Four biological replicates were performed, as well as six technical replicates per plate.

#### 4.1.10 Statistical Analyses

When appropriate, one-way ANOVAs were performed using Microsoft Excel 2016, or GraphPad Prism 8.0. ANOVA was followed by a Bonferonni's post hoc test, when applicable. P values were set to 0.05.

## 4.2 Results and Discussion

### 4.2.1 Preparation of materials

The PEA polymer PBSe (Figure 4.2A) was prepared as previously reported,<sup>37</sup> and had a number average molar mass ( $M_n$ ) of 28 kg/mol and a dispersity ( $\mathcal{D}$ ) of 2.1 based on size exclusion chromatography (SEC) (Appendix C, Figures C.1-C.2). **PBSe-GSK3787** particles were prepared as described in chapter 3 of this thesis, with an alteration to the shear mixing rate, which was increased to 'high' (18,000 rpm) setting with a Waring Commercial Immersion Blender. They were measured to have a Z-average diameter of  $390 \pm 31$  nm, and a polydispersity index (PDI) of .375 based on dynamic light scattering (Appendix C, Figure C.3) and SEM confirmed their spherical morphology (Figure 4.2B). The loading of GSK3787 in **PBSe-GSK3787** particles was  $8.1 \pm 0.4$  wt%.

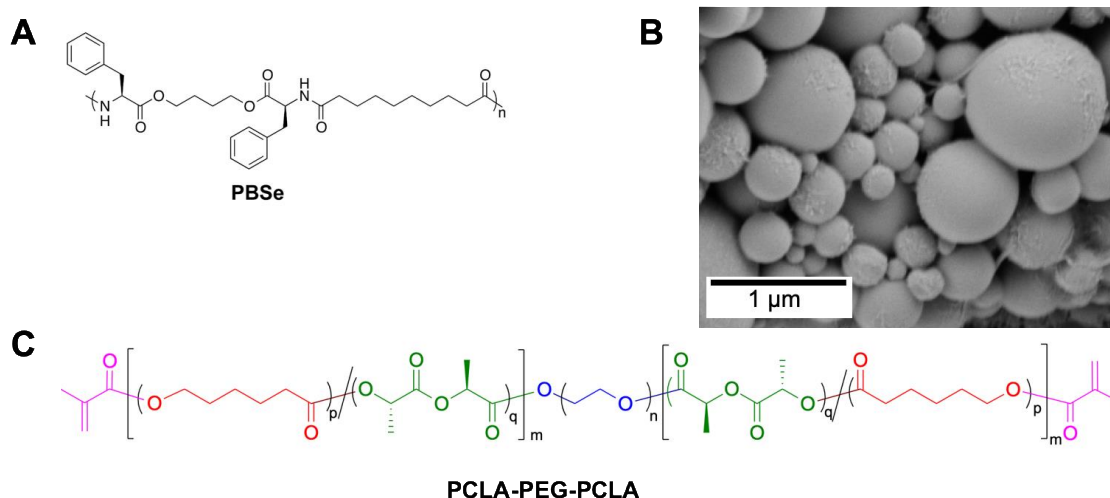


**Figure 4.2: Chemical structures and particle SEM.** A) Chemical structure of PBSe; B) Representative SEM image of **PBSe-GSK3787** particles; C) Chemical structure of PCLA-PEG-PCLA.

Methacrylate end-capped PCLA-PEG-PCLA was synthesized by the tin(II) 2-ethylhexanoate catalyzed ring-opening polymerization of L-lactide and  $\epsilon$ -caprolactone from 1500 g/mol PEG-diol, followed by reaction with methacrylic anhydride in the presence of  $\text{NEt}_3$  as previously reported.<sup>21</sup> The resulting polymer had an  $M_n$  of 3460 g/mol, PCLA/PEG mass ratio of 1.31, and a CL/LA ratio of 3.73 based on  $^1\text{H}$  nuclear magnetic resonance (NMR) spectroscopic analysis (Appendix C, Figure C.4) and an  $M_n$  of 5640 g/mol and a  $D$  of 2.13 based on SEC (Appendix C, Figure C.5).

#### 4.2.2 Preparation and characterization of hydrogels

Drug-free control, **GSK3787**-loaded, and **PBSe-GSK-3787** hydrogels were prepared (Table 4.1). The hydrogel formulations were prepared by first dissolving PCLA-PEG-PCLA at 4 °C and then adding drug or particles. Gelation was induced by the addition of KPS/TEMED, and increasing the temperature to 37 °C. Gelation was qualitatively complete after 30 min based on the vial flip test (Appendix C, Figure A18).

**Table 4.1: Hydrogel preparations and their physiochemical properties.**

<b>Hydrogel</b>	<b>Additive</b>	<b>Young's modulus (kPa)</b>
<b>Control hydrogel</b>	none	42.5 ± 0.3
<b>GSK3787 hydrogel</b>	10 wt% GSK3787	30.1 ± 2.5
<b>PBSe-GSK3787 hydrogel</b>	10 wt% PBSe-GSK3787 particles	16.3 ± 3.1

The hydrogels were characterized by SEM after being flash frozen in liquid nitrogen, and then lyophilized (Figure 4.3). Compared to the **control hydrogel**, the **GSK3787 hydrogel** had a different morphology, with plate-like structures throughout the material. Spherical particles were clearly visible in the **PBSe-GSK3787 hydrogel**. DSC was also performed to assess the incorporation of drug and particles into the hydrogel (Figure 4.4). The **control hydrogel** had a  $T_g$  of  $-47\text{ }^\circ\text{C}$ , which is attributed to the PEG. Multiple melting endotherms were present at 18 and  $20\text{ }^\circ\text{C}$ , which is attributed to crystalline caprolactone sequences. Direct incorporation of GSK3787 into the hydrogel caused a disappearance of the melting endotherms, suggesting it disrupted the crystallization of the caprolactone domains. A single  $T_g$  at  $-35\text{ }^\circ\text{C}$  was observed and no  $T_m$  for GSK3787 was observed, which is present for the pure drug at  $190\text{ }^\circ\text{C}$ , as shown in Chapter 3 (Figure 3.3). These results suggest a mixing of the drug and polymer domains, and are consistent with previous results for the incorporation of CXB was into the same hydrogel system.<sup>21</sup> In contrast, when **PBSe-GSK3787** particles were incorporated into the hydrogel, the  $T_g$  was  $-55\text{ }^\circ\text{C}$ , quite similar to that of the control hydrogel, and a single, broad melting

endotherm was observed at 18 °C. These results are consistent with the incorporation of the particles into the aqueous domains of the hydrogel, as shown in Figure 4.1, where they do not interfere with the assembly of the PCLA blocks.

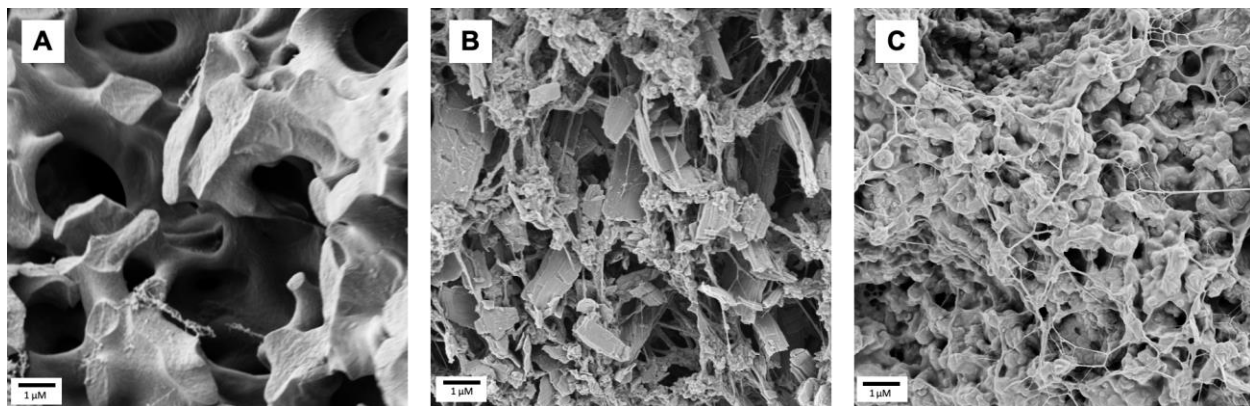


**Figure 4.3: SEM micrographs of: A) Control hydrogel; B) GSK3787 hydrogel; C) PBSe-GSK3787 particles in hydrogel.**

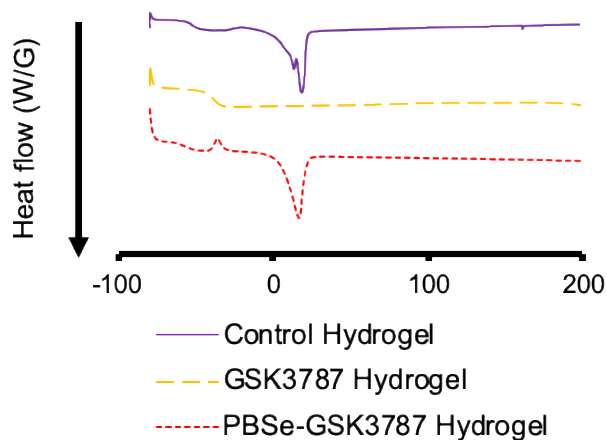


**Figure 4.4: DSC thermograms for control hydrogel, GSK3787 hydrogel, and PBSe-GSK3787 hydrogel.** Direct incorporation of GSK3787 disrupts packing of the caprolactone domains, resulting in disappearance of the melting endotherm, while the incorporation of PBSe-GSK3787 particles does not greatly affect the thermal properties relative to the control, likely due to their incorporation into the aqueous domains of the

hydrogel. A small exotherm at  $-35\text{ }^{\circ}\text{C}$  in the **PBSe-GSK3787 hydrogel** likely corresponds to cold crystallization.

The effects of drug and particle incorporation on the syneresis of the hydrogels were investigated. We previously reported up to  $\sim 40\text{ wt}\%$  water loss from non-covalent acetyl end-capped PCLA-PEG-PCLA hydrogels depending on the incorporated drug, due to collapse of the hydrogel network structure,<sup>32</sup> whereas less than  $10\text{ wt}\%$  water loss was observed for methacrylate capped PCLA-PEG-PCLA hydrogels that were covalently crosslinked using KPS/TEMED.<sup>29</sup> As shown in Figure 4.5, the water loss from the **control hydrogel**, **GSK3787 hydrogel**, and the **PBSe-GSK3787 hydrogel** were also all less than  $10\text{ wt}\%$ , showing that the incorporation of the particles or drug directly did not result in network collapse to a large extent. However, after 12 h, the extent of syneresis for the **GSK3787 hydrogel** was significantly higher than the **control hydrogel** suggesting that direct incorporation of drug has the largest effect on the network collapse.

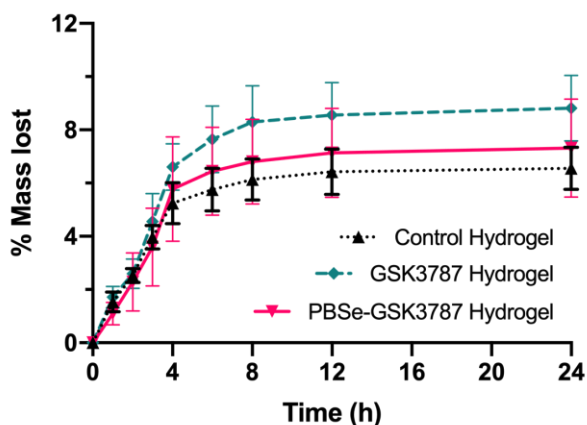


**Figure 4.5: Syneresis of hydrogel systems.** Measurement of the water loss from the hydrogels showing less than  $10\%$  syneresis for the control, drug-loaded, and particle-loaded hydrogels over 24 h. The Measurements were performed in triplicate and the error bars correspond to the standard deviations.

Degradation of the hydrogels was also probed based on their mass loss into PBS at  $37\text{ }^{\circ}\text{C}$  (Figure 4.6). The **control hydrogel** degraded very slowly, with only  $12\%$  mass loss over 60 days. The incorporation of drug or particles resulted in more rapid degradation. The

more rapid degradation of the **GSK3787 hydrogel** may result from disruption of the crystalline packing of the caprolactone domains, which was evidenced by the thermal analysis. Crystallinity is known to result in slower degradation of polycaprolactone.<sup>33</sup> Incorporation of the particles in **PBSe-GSK3787 hydrogel** resulted in even faster degradation. It is likely that the incorporation of particles into the gel hindered covalent crosslinking to some extent, making the resulting gel more susceptible to degradation. There was a statistically significant difference between the mass remaining for the **PBSe-GSK3787 hydrogel** compared to control hydrogel at 60 d.

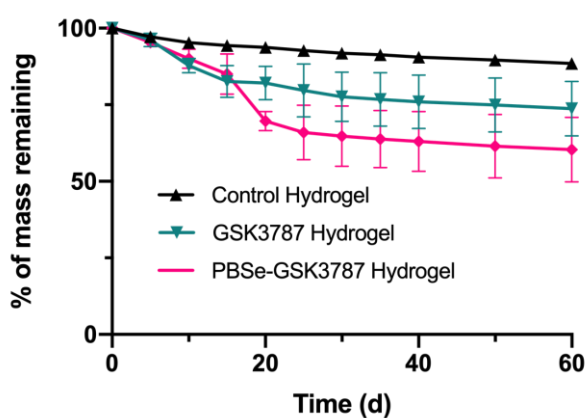


**Figure 4.6: Percent mass remaining over time for hydrogel systems at 37 °C, in PBS.**

Incorporation of GSK3787 or PBSe-GSK3787 particles resulted in more rapid degradation of the gels. All measurements were performed in triplicates, and the error bars correspond to the standard deviations. Error bars on the control hydrogel are too small to be visible.

The Young's moduli of the hydrogels were measured under unconfined compression in PBS at 37 °C to mimic physiological conditions (Figure 4.7). The control gel had the highest modulus of  $42.5 \pm 0.3$  KPa. This value is about 2-fold higher than that previously reported for a similar hydrogel and can likely be attributed to small differences in the polymer composition between the two studies. Incorporation of GSK3787 resulted in a reduction in the modulus to  $30.1 \pm 2.5$  KPa while the incorporation of PBSe-GSK3787 particles further lowered the modulus to  $16.3 \pm 3.1$  KPa. These results correlate with the observed degradation results, suggesting that the disruption of hydrophobic block

packing or disruption of network formation reduce the hydrogel stiffness. Particle in hydrogel systems have been previously reported, but their moduli under compression have not been reported.<sup>34,35</sup> Interestingly, Hu et. al, tested the tensile properties of a particle in hydrogel system, and found that there was no statistical difference between the moduli of hydrogels with and without particles, an opposite finding to the currently described work.<sup>36</sup>

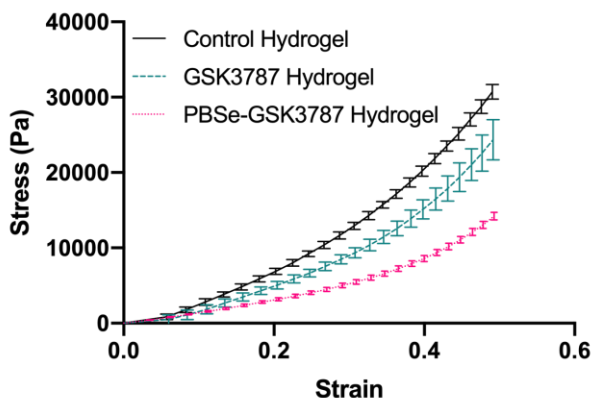


**Figure 4.7: Stress-strain curves of three hydrogel systems, as measured in PBS at 37 °C.** All measurements were performed in triplicates, and the error bars correspond to the standard deviations.

The release of GSK3787 from the **GSK3787 hydrogel** and **PBSe-GSK3787 hydrogel** immersed in PBS at 37 °C was measured over a period of 60 days. Polysorbate 80 was added to the release medium at 2% wt/vol to facilitate the dissolution of the drug.<sup>19, 21, 37-39</sup> Slow release, without any initial burst was observed for both systems. When GSK3787 was loaded into the hydrogel, 44% was released over 60 days, which can likely be attributed in part to hydrogel degradation and in part to slow dissolution and diffusion of the drug from the hydrogel. Release from the **PBSe-GSK3787 hydrogel** was significantly slower, with only 20% released over 60 days. In this case, the drug would need to be first released from the particles, to be released from the hydrogel. Indeed, the release of ~10% of GSK3787 over the first 30 days is in close agreement with the release rate of GSK3787 from the particles themselves (Figure 3.5, Chapter 3). However, it is well established that the release rates of drugs *in vitro* and *in vivo* may be very

different.<sup>21, 22</sup> For example, other factors such as mechanical forces, enzymes, proteins or varying pH levels, could all affect the degradation of the hydrogels and/or the release rates of drugs.<sup>40, 41</sup> Under these conditions, the particle-loaded hydrogel and particles alone may behave quite differently.

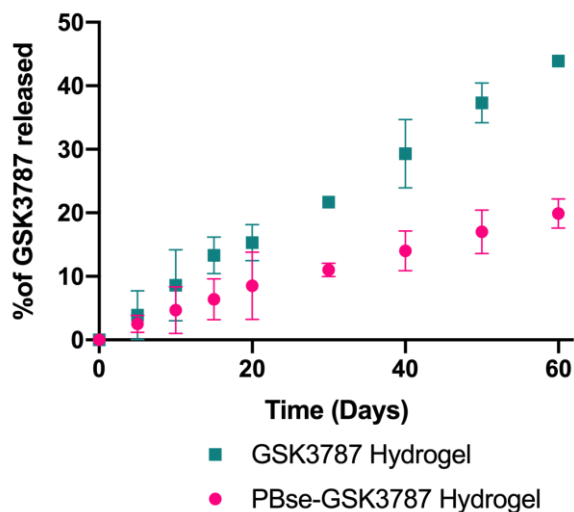


**Figure 4.8: Release of GSK3787 from GSK3787 hydrogel and PBSe-GSK3787 hydrogel in PBS at 37 °C.** Slower release from the particle in hydrogel system is noted. The experiments were performed in triplicate and the error bars correspond to the standard deviations.

#### 4.2.3 Primary cell toxicity from hydrogel systems

IMAC cells were harvested and used for the cell toxicity studies in this work because their phenotype is very close to that of articular chondrocytes.<sup>42</sup> By plating the cells and not passaging them, the IMAC cells are less likely to de-differentiate into fibroblasts, an issue that is very common with other cell lines such as ATDC5, that are used to study cartilage.<sup>43</sup> The cytotoxicity study was performed as a leachate study, in which the hydrogels were soaked in media for 14 days at 37 °C to allow any potentially toxic species to leach from the hydrogels and then this media was added to the cells. After 48 h, an MTT assay was performed to assess cell metabolic activity. None of the three hydrogel compositions, the **control hydrogel**, **GSK3787 hydrogel** and **PBSe-GSK3787**

hydrogel showed significant toxicity from their degradation byproducts as the observed metabolic activities were not statistically different than the control (Figure 4.9).

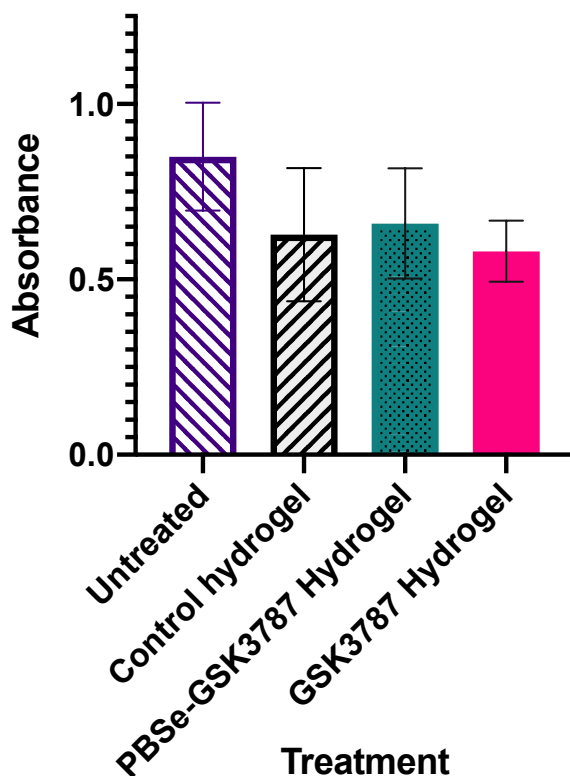


**Figure 4.9:** Metabolic activity of IMAC cell cultures when treated with leachate media from three different hydrogel preparations. Control hydrogel, GSK3787 hydrogel and PBSe-GSK3787 were soaked in media for 14 days before being added to cells for 48 hours. Metabolic activity was tested by MTT assay. All samples were performed with three biological replicates, and six technical replicates per plate. Plotted as mean absorbance  $\pm$  standard error (N = 4).

### 4.3 Conclusions

This work resulted in the development a promising intra-articular drug delivery system that combined two previously described drug delivery technologies: a thermos-responsive hydrogel and poly(ester amide) particles. Hydrogels that were loaded with particles could be prepared in the same manner as control and drug-loaded hydrogels, and showed similar physiochemical characteristics. Inclusion of GSK3787 directly into the hydrogel

resulted in increased syneresis, more rapid degradation, and a lower Young's modulus relative to the control hydrogel, likely due to its incorporation into the hydrophobic PCLA domains and disruption of crystallinity. Incorporation of PBSe-GSK3787 particles into the hydrogel did not significantly affect syneresis, but did result in more rapid degradation and a lower Young's modulus relative to the control hydrogel, likely due to some interference with covalent crosslinking. However, these effects were relatively modest, and these hydrogels are still more stable and much stiffer than physically crosslinked thermo-responsive hydrogels that have been explored *in vivo*.<sup>21, 22</sup> Drug was released more slowly from the PBSe-GSK3787 hydrogel than from the GSK3787 hydrogel due to the requirement for the drug to be first released from the particles, then from the hydrogel. Although the release rate for the PBSe-GSK3787 hydrogel was similar to that reported in Chapter 3 for PBSe-GSK3787 particles *in vitro*, differences are expected *in vivo* due to the ability of the hydrogel to mechanically shield the particles and to retain the particles in the joint. *In vitro* cell toxicity assays showed that the hydrogels do not release harmful byproducts over 14 days, and that they appear to be well tolerated biologically. In future work, it will be important to evaluate whether the particle in hydrogel system serves to provide sustained drug release in the joints of large and small animals. In addition, the efficacy of these GSK3787-loaded hydrogels in preventing or slowing the progression of OA in a model of post-traumatic OA should be evaluated. Overall, the development of more drug delivery systems for IA use can help to overcome some of the persistent challenges that IA drug delivery systems face, and can lead to a system that can have a beneficial effect on the treatment of OA.

## 4.4 References

1. Glyn-Jones, S.; Palmer, A. J. R.; Agricola, R.; Price, A. J.; Vincent, T. L.; Weinans, H.; Carr, A. J., Osteoarthritis. *The Lancet* **2015**, 386, 376-387.
2. Appleton, C. T., Osteoarthritis year in review 2017: biology. *Osteoarthritis Cartilage* **2018**, 26, 296-303.
3. Various Authors. Osteoarthritis: A Serious Disease. OARSI White Paper **2016**.
4. Kelly, S.; Chapman, R. J.; Woodhams, S.; Sagar, D. R.; Turner, J.; Burston, J. J.; Bullock, C.; Paton, K.; Huang, J.; Wong, A.; McWilliams, D. F.; Okine, B. N.;

- Barrett, D. A.; Hathway, G. J.; Walsh, D. A.; Chapman, V., Increased function of pronociceptive TRPV1 at the level of the joint in a rat model of osteoarthritis pain. *Ann Rheum Dis* **2015**, 74, 252-259.
5. Da Costa, B.; Nüesch, E.; Reichenbach, S.; Jüni, P.; Rutjes, A. W., Doxycycline for osteoarthritis of the knee or hip. *The Cochrane Collaboration* **2012**.
  6. Ratneswaran, A.; LeBlanc, E. A.; Walser, E.; Welch, I.; Mort, J. S.; Borradaile, N.; Beier, F., Peroxisome proliferator-activated receptor delta promotes the progression of posttraumatic osteoarthritis in a mouse model. *Arthritis Rheumatol* **2015**, 67, 454-64.
  7. Ratneswaran, A.; Sun, M. M.; Dupuis, H.; Sawyez, C.; Borradaile, N.; Beier, F., Nuclear receptors regulate lipid metabolism and oxidative stress markers in chondrocytes. *J Mol Med (Berl)* **2017**, 95, 431-444.
  8. Shearer, B. G.; Wiethe, R. W.; Ashe, A.; Billin, A. N.; Way, J. M.; Stanley, T. B.; Wagner, C. D.; Xu, R. X.; Leesnitzer, L. M.; Merrihew, R. V.; Shearer, T. W.; Jeune, M. R.; Ulrich, J. C.; Willson, T. M., Identification and characterization of 4-chloro-N-(2-([5-trifluoromethyl]-2-pyridyl)sulfonyl)ethyl)benzamide (GSK3787), a selective and irreversible peroxisome proliferator-activated receptor delta (PPARdelta) antagonist. *J Med Chem* **2010**, 53, 1857-1861.
  9. Maudens, P.; Jordan, O.; Allemann, E., Recent advances in intra-articular drug delivery systems for osteoarthritis therapy. *Drug Discov Today* **2018**, 0, 1-15.
  10. Evans, C. H.; Kraus, V. B.; Setton, L. A., Progress in intra-articular therapy. *Nature Reviews Rheumatology* **2013**, 10, 11-22.
  11. MA., M.; N, K.; A., W., Intra-Articular Steroids; How Soon and How Often after the First Injection? *SM. J. Community Med.* **2016**, 21.
  12. Rovati, L. C.; Girolami, F.; Persiani, S., Crystalline glucosamine sulfate in the management of knee osteoarthritis: efficacy, safety, and pharmacokinetic properties. *Ther. Adv. Musculoskelet. Dis.* **2012**, 4, 167-180.
  13. Bagsby, D. T.; Ireland, P. H.; Meneghini, R. M., Liposomal bupivacaine versus traditional periarticular injection for pain control after total knee arthroplasty. *J. Arthroplasty* **2014**, 29, 1687-1690.

14. Dong, J.; Jiang, D.; Wang, Z.; Wu, G.; Miao, L.; Huang, L., Intra-articular delivery of liposomal celecoxib-hyaluronate combination for the treatment of osteoarthritis in rabbit model. *Int. J. Pharm.* **2013**, 441, 285-290.
15. El-Refaie, W. M.; Elnaggar, Y. S.; El-Massik, M. A.; Abdallah, O. Y., Novel Self-assembled, Gel-core Hyalurosomes for Non-invasive Management of Osteoarthritis: In-vitro Optimization, Ex-vivo and In-vivo Permeation. *Pharm. Res.* **2015**, 32, 2901-2911.
16. Chen, Z.; Liu, D.; Wang, J.; Wu, L.; Li, W.; Chen, J.; Cai, B. C.; Cheng, H., Development of nanoparticles-in-microparticles system for improved local retention after intra-articular injection. *Drug Deliv.* **2014**, 21, 342-350.
17. Kavanaugh, T. E.; Werfel, T. A.; Cho, H.; Hasty, K. A.; Duvall, C. L., Particle-based technologies for osteoarthritis detection and therapy. *Drug Deliv. Transl. Res.* **2016**, 6, 132-147.
18. Whitmire, R. E.; Wilson, D. S.; Singh, A.; Levenston, M. E.; Murthy, N.; Garcia, A. J., Self-assembling nanoparticles for intra-articular delivery of anti-inflammatory proteins. *Biomaterials* **2012**, 33, 7665-7675.
19. Villamagna, I. J.; Gordon, T. N.; Hurtig, M. B.; Beier, F.; Gillies, E. R., Poly(ester amide) particles for controlled delivery of celecoxib. *J Biomed Mater. Res. A* **2019**, 1235-1243.
20. Mountziaris, P. M.; Sing, D. C.; Mikos, A. G.; Kramer, P. R., Intra-articular microparticles for drug delivery to the TMJ. *J. Dent. Res.* **2010**, 89, 1039-1044.
21. Prince, D. A.; Villamagna, I. J.; Borecki, A.; Beier, F.; de Bruyn, J. R.; Hurtig, M.; Gillies, E. R., Thermoresponsive and Covalently Cross-Linkable Hydrogels for Intra-Articular Drug Delivery. *ACS Applied Bio Materials* **2019**, 2, 3498-3507.
22. Petit, A.; Redout, E. M.; van de Lest, C. H.; de Grauw, J. C.; Muller, B.; Meyboom, R.; van Midwoud, P.; Vermonden, T.; Hennink, W. E.; Rene van Weeren, P., Sustained intra-articular release of celecoxib from in situ forming gels made of acetyl-capped PCLA-PEG-PCLA triblock copolymers in horses. *Biomaterials* **2015**, 53, 426-436.

23. Kumar, A.; Bendele, A. M.; Blanks, R. C.; Bodick, N., Sustained efficacy of a single intra-articular dose of FX006 in a rat model of repeated localized knee arthritis. *Osteoarth. Cartilage* **2015**, *23*, 151-160.
24. Janssen, M.; Timur, U. T.; Woike, N.; Welting, T. J.; Draaisma, G.; Gijbels, M.; van Rhijn, L. W.; Mihov, G.; Thies, J.; Emans, P. J., Celecoxib-loaded PEA microspheres as an auto regulatory drug-delivery system after intra-articular injection. *J. Controlled Release* **2016**, *244*, 30-40.
25. Paik, J.; Duggan, S. T.; Kean, S. J., Triamcinolone Acetonide Extended-Release: A Review in Osteoarthritis Pain of the Knee. *Drugs* **2019**, *79*, 455-462.
26. Beck, E. C.; Barragan, M.; Tadros, M. H.; Gehrke, S. H.; Detamore, M. S., Approaching the compressive modulus of articular cartilage with a decellularized cartilage-based hydrogel. *Acta Biomater.* **2016**, *38*, 94-105.
27. Petit, A.; Muller, B.; Meijboom, R.; Bruin, P.; van de Manakker, F.; Versluijs-Helder, M.; de Leede, L. G.; Doornbos, A.; Landin, M.; Hennink, W. E.; Vermonden, T., Effect of polymer composition on rheological and degradation properties of temperature-responsive gelling systems composed of acyl-capped PCLA-PEG-PCLA. *Biomacromolecules* **2013**, *14*, 3172-3182.
28. Petit, A.; Sandker, M.; Muller, B.; Meyboom, R.; van Midwoud, P.; Bruin, P.; Redout, E. M.; Versluijs-Helder, M.; van der Lest, C. H.; Buwalda, S. J.; de Leede, L. G.; Vermonden, T.; Kok, R. J.; Weinans, H.; Hennink, W. E., Release behavior and intra-articular biocompatibility of celecoxib-loaded acetyl-capped PCLA-PEG-PCLA thermogels. *Biomaterials* **2014**, *35*, 7919-7928.
29. Sandker, M. J.; Petit, A.; Redout, E. M.; Siebelt, M.; Muller, B.; Bruin, P.; Meyboom, R.; Vermonden, T.; Hennink, W. E.; Weinans, H., In situ forming acyl-capped PCLA-PEG-PCLA triblock copolymer based hydrogels. *Biomaterials* **2013**, *34*, 8002-8011.
30. Knight, D. K.; Gillies, E. R.; Mequanint, K., Strategies in functional poly(ester amide) syntheses to study human coronary artery smooth muscle cell interactions. *Biomacromolecules* **2011**, *12*, 2475-2487.
31. Gosset, M.; Berenbaum, F.; Thirion, S.; Jacques, C., Primary culture and phenotyping of murine chondrocytes. *Nat. Protoc.* **2008**, *3*, 1253-1260.

32. Prince, D. A.; Villamagna, I. J.; Hopkins, C. C.; de Bruyn, J. R.; Gillies, E. R., Effect of drug loading on the properties of temperature-responsive polyester–poly(ethylene glycol)–polyester hydrogels. *Polymer International* **2019**, 68, 1074-1083.
33. Liu, Q.; Yuan, S.; Guo, Y.; Narayanan, A.; Peng, C.; Wang, S.; Miyoshi, T.; Joy, A., Modulating the crystallinity, mechanical properties, and degradability of poly( $\epsilon$ -caprolactone) derived polyesters by statistical and alternating copolymerization. *Polymer Chemistry* **2019**, 10, 2579-2588.
34. Li, X.; Rombouts, W.; van der Gucht, J.; de Vries, R.; Dijkstra, J. A., Mechanics of composite hydrogels approaching phase separation. *PLoS One* **2019**, 14, e0211059.
35. Sukarto, A.; Amsden, B. G., Low melting point amphiphilic microspheres for delivery of bone morphogenetic protein-6 and transforming growth factor-beta3 in a hydrogel matrix. *J Control Release* **2012**, 158, 53-62.
36. Hu, X.; Qu, S., Inclusion Size Effect on Mechanical Properties of Particle Hydrogel Composite. *Acta Mechanica Solida Sinica*. **2019**.
37. Abouelmagd, S. A.; Sun, B.; Chang, A. C.; Ku, Y. J.; Yeo, Y., Release kinetics study of poorly water-soluble drugs from nanoparticles: are we doing it right? *Mol Pharm* **2015**, 12, 997-1003.
38. Gomez-Gaete, C.; Retamal, M.; Chavez, C.; Bustos, P.; Godoy, R.; Torres-Vergara, P., Development, characterization and in vitro evaluation of biodegradable rhein-loaded microparticles for treatment of osteoarthritis. *Eur. J. Pharm. Sci.* **2017**, 96, 390-397.
39. Kim, S. R.; Ho, M. J.; Kim, S. H.; Cho, H. R.; Kim, H. S.; Choi, Y. S.; Choi, Y. W.; Kang, M. J., Increased localized delivery of piroxicam by cationic nanoparticles after intra-articular injection. *Drug Des., Dev. Ther.* **2016**, 10, 3779-3787.
40. Lin, C. C.; Metters, A. T., Hydrogels in controlled release formulations: network design and mathematical modeling. *Adv. Drug. Deliv. Rev.* **2006**, 58, 1379-1408.
41. Liu, H.-Y.; Lin, C.-C., A Diffusion-Reaction Model for Predicting Enzyme-Mediated Dynamic Hydrogel Stiffening. *Gels* **2019**, 5, 1-10.
42. Lamplot, J. D.; Liu, B.; Yin, L.; Zhang, W.; Wang, Z.; Luther, G.; Wagner, E.; Li, R.; Nan, G.; Shui, W.; Yan, Z.; Rames, R.; Deng, F.; Zhang, H.; Liao, Z.;

Liu, W.; Zhang, J.; Zhang, Z.; Zhang, Q.; Ye, J.; Deng, Y.; Qiao, M.; Haydon, R. C.; Luu, H. H.; Angeles, J.; Shi, L. L.; He, T. C.; Ho, S. H., Reversibly Immortalized Mouse Articular Chondrocytes Acquire Long-Term Proliferative Capability While Retaining Chondrogenic Phenotype. *Cell Transplant* **2015**, 24, 1053-1066.

43. Yao, Y.; Wang, Y., ATDC5: an excellent in vitro model cell line for skeletal development. *J. Cell. Biochem.* **2013**, 114, 1223-1229.

## Chapter 5

### 5 Conclusions and Future Work

#### 5.1 Conclusions

Osteoarthritis (OA) continues to be a disease that affects a large number of people worldwide, causing pain and disability. The prevalence of the disease continues to rise annually, due in part to increasing lifespan and obesity around the world. Despite its prevalence, disease modifying agents are still unavailable to treat OA, and most pharmacologic therapies rely on pain reduction through systemic administration. Systemic administration of pharmacologic therapy is well documented to lead to side effects that can be life-threatening. In addition to systemic pain medications, a number of new molecules have been developed that could potentially serve as disease modifying agents in OA. GSK3787 is a potent peroxisome proliferator activated receptor (PPAR) $\delta$  inhibitor that has been implicated as a potential disease modifying agent for OA. Inhibition of the PPAR $\delta$  receptor in a mouse model has shown the attenuation of OA after surgical induction of post-traumatic OA. However, GSK3787 cannot be delivered systemically, due to concerns about potential adverse side effects.

Intra-articular (IA) drug delivery has become increasingly recognized as a potential strategy for the administration of OA drugs.<sup>1</sup> IA injections can potentially deliver a higher dosage of drug directly at the target tissue, while reducing systemic exposure to the drug and potential adverse side effects. However, the removal of free drugs from the IA space through lymphatic drainage remains a challenge. Drug molecules are typically cleared within a few hours, so they often cannot reach their targets at sufficient levels over the required period of time to achieve a therapeutic effect.<sup>2</sup> Furthermore, it is essential to minimize the frequency of IA injections (ideally  $\leq$  once every 3 months) in order to minimize discomfort for patients as well as potential complications associated with injection.<sup>3, 4, 5</sup>

Drug delivery systems developed for IA use have been proposed for achieving a prolonged release of drug in the joint. To date, while a number of systems have been investigated, challenges remain.<sup>1</sup> Naturally derived hydrogels, based on hyaluronic acid,<sup>6</sup> elastin-like peptides,<sup>7</sup> or synthetically derived hydrogels based on poly(caprolactone-co-lactide)(PCLA)-poly(ethylene glycol)(PEG)-PCLA<sup>8,9</sup> have not exhibited sufficient retention of drugs in the joint, and in many cases led to a burst release of loaded drug. Nanoparticles based on block copolymers have also been explored,<sup>10,11</sup> but they have short retention times in the joint. Microparticles have been most extensively investigated. Flexion Therapeutics has recently gained FDA approval for the use of Zilretta for the treatment of OA.<sup>12</sup> Zilretta is composed of poly(lactic acid-co-glycolic acid) (PLGA) microparticles loaded with triamcinolone. While data from clinical trials has proven the safety of Zilretta, the efficacy is still debated, with studies showing that the release from the particles was not much longer than the effect of injections of corticosteroids to the joint alone. Furthermore, there remain concerns with microparticle formulations for IA delivery systems because of the potential for the particle degradation products to induce adverse inflammatory reactions in the joint,<sup>13,14</sup> or for the particles to cause joint irritation if their mechanical properties are not compatible with surrounding joint tissues.<sup>15</sup> While significant progress has been made towards the development of IA drug delivery systems, a highly effective drug combined with a delivery system capable of drug release over 3 months does not currently exist.

In **Chapter 2**, celecoxib, a commonly used non-steroidal anti-inflammatory drug (NSAID) for OA treatment, was encapsulated in poly(ester amide) (PEA) particles. Two different PEAs that had very similar chemical structures were investigated and compared. Phenylalanine butanediol sebacic acid (PBSe) and phenylalanine octanediol sebacic acid (POSe) only differ by four carbons in the diol component of the polymer, but the effects of this small structural difference on the particles were significant. POSe had a lower glass transition temperature, which made the particles more susceptible to agglomeration and degradation. High loadings of celecoxib, greater than 20 wt% were achieved from particles composed of both PBSe and POSe. However, the release of celecoxib *in vitro* was much faster from POSe particles than from PBSe particles. Overall, these results highlight that small differences in polymer structure can have profound effects on the

properties of a delivery system, so polymers require careful structural tuning and characterization of physicochemical properties.

Based on the physicochemical and drug release properties, PBSe particles were selected for further evaluation as a drug delivery system. Two different cell lines, ATDC5 cells, as well as C2C12 cells were studied. Toxicity was induced with a dose dependent manner from celecoxib, but no significant cytotoxicity was noted from the particles alone. An ovine model was used for *in vivo* studies. The injection of celecoxib loaded particles yielded minimal host response, to the extent that was expected from the injection process itself, suggesting that the particles were well tolerated. Furthermore, it was found that particles had migrated into the synovial membrane. Overall, it could be concluded from this work that PBSe particles warranted further investigated as an IA drug delivery system.

**Chapter 3** further explored the PBSe particle drug delivery system for encapsulation of the PPAR $\delta$  inhibitor GSK3787. To our knowledge, this is the first instance in which a PPAR $\delta$  inhibitor has been incorporated into a drug delivery system. The particles were characterized physiochemically. The GSK3787 loaded particles were ~200 nm smaller in diameter, and the incorporated GSK3787 existed in crystalline domains in the particles, as evidenced by the presence of a melting transition for the drug. In addition, it was only possible to load GSK3787 at 8.1 wt%, as compared to the 23 wt% for celecoxib. 8.1 wt% should be sufficient to deliver a therapeutic dose *in vivo* due to the drug's expected high potency due to the non-reversible binding method of the GSK3787. From these results it can be concluded that the application of a particle delivery platform to a different drug is not always straightforward and optimization is required on a case by case basis.

Mechanical properties of individual particles were measured using atomic force microscopy (AFM), and it was determined that the particles had a Young's modulus close to that of native cartilage tissue within the joint. The particles exhibited a slow release of the loaded drug, and did not cause significant toxicity to IMAC cells, further leading to the conclusion that PEA particles warranted further investigation as an intra-articular delivery system. One limitation of the work was the absence of ovine controls that did not have particles injected into the joints. This was not possible due to the nature of the large

animal model as other joints in the animals had been used for other experiments in the Hurtig lab. However our collaborator is experienced in evaluating the joints of sheep, so was still able to make qualitative assessments based on the known histological results for a normal joint.

While *in vitro* release of both celecoxib and GSK3787 from the particles were slow, unpublished results in sheep measuring celecoxib concentration suggested that drug concentrations were undetectable by 1 week and that drug release would not be sufficiently sustained *in vivo*. The difference between the *in vitro* and *in vivo* results was thought to arise from either trafficking of the particles out of the joint cavity to the synovial membrane, or from mechanical or biochemical degradation of the particles. It was proposed that encapsulation of the drug-loaded particle in a hydrogel would afford protection and facilitate particle retention in the joint cavity. **Chapter 4** described the use of a thermo-responsive, covalently crosslinked hydrogel to encapsulate GSK3787 or GSK3787-loaded particles. Physicochemical characterization led to the conclusion that the incorporation of drug or particles within the hydrogel led to only modest changes in their degradation rate and Young's modulus. The release of drug was studied *in vitro* and when drug loaded particles were embedded within the hydrogel, the amount of drug that was released over 60 days was cut by roughly half as compared to hydrogels loaded with drug directly. Based on these results, these hydrogel systems warrant further investigation for IA delivery.

Though the studies encompassed in this thesis were designed with care and intended to be comprehensive, limitations of the aforementioned work remain. Foremost, animal studies that were performed in chapter 2 of this thesis were done in the absence of controls. The use of a large animal model can pre-empt the ability to utilize all joints, and control over sacrifice of the animals, leaving the study without a usable joint for a control. Furthermore, release studies that were performed in this work were done in the absence of degradative enzymes and biological factors that could have a large effect on the release rate of the system. In this thesis, release studies were designed to show the slowed release from a free release system, to compare between different compositions of particles or hydrogels, or to serve as a model for prolonged release. The studies were not

designed to make claims about the *in vivo* applicability of the aforementioned release systems.

Overall, the research described here laid the groundwork for future testing to be done to determine whether PPAR $\delta$  antagonists can slow or halt the progression OA. If successful, these therapeutics can potentially serve as the first disease-modifying treatment for OA. In addition, the platform delivery systems developed in this thesis can be used for the IA delivery of other existing drugs ranging from NSAIDs to new potential therapeutics that are currently under development in our lab and in other labs.

## 5.1 Future Directions

The proposed future research stemming from this project will first and foremost determine the potential for PPAR $\delta$  antagonists to slow or halt the progression of post-traumatic OA. Studies of GSK3787-loaded hydrogel and GSK3787-loaded particles in hydrogel utilizing a rat model that has OA surgically induced are planned, to determine if the system provide a disease modifying response. If successful, further studies will be performed in large animals, such as sheep, where the biomechanics more closely mimic those of humans. It is expected that due to the nature of the studies required with examining the efficacy of GSK3787, it would be advantageous to use a small animal model that would be available for a larger amount of studies, such as sectioning, dissection and testing of tissues. Larger animal studies will be reserved for *in vivo* release studies and biocompatibility, both of which can be much easier to test in larger animal models due to the larger size.

From a materials standpoint, particles have already shown promise for use in IA drug delivery, and the PEA particles described in this thesis are still of interest for future studies. In particular, it would be worthwhile to continue to screen different PEAs for use in particle delivery systems. PEAs are known for their tunability, and changing the polymer structures would allow for new drug delivery systems with significantly different properties to be developed. In 2018, Bajpayee and Grodzinsky suggested that more research be done on the utilization of electrostatic interactions in order to penetrate into the cartilage tissue before releasing drug.<sup>16</sup> The ability to develop systems that are

charged, and are able to interact with the anionic surface of the cartilage is feasible, and can provide new areas of research. PEAs provide an excellent opportunity for this, as they have the ability to incorporate charges pendant to the polymer backbone<sup>17</sup> which could help move the particles through the charged tissues of the joint, thereby further targeting the release of drug to more specific tissues.

In addition, the hydrogel platform delivery system can be further optimized, both chemically and physically. Chemical modification would allow for new formulations that can lead to “smart”, stimuli-responsive drug delivery systems. Further modification of the properties of these delivery systems is proposed to develop the selective release of drugs in response to chemical triggers associated with OA, such as enzymes, changes in pH or reactive oxygen species. The development of systems that exhibit altered properties in response to the aforementioned triggers opens up the possibility of “patient specific” OA treatment, in which different amounts of medication will be released at different rates, depending on the severity of disease in individual patients.

## 5.2 References

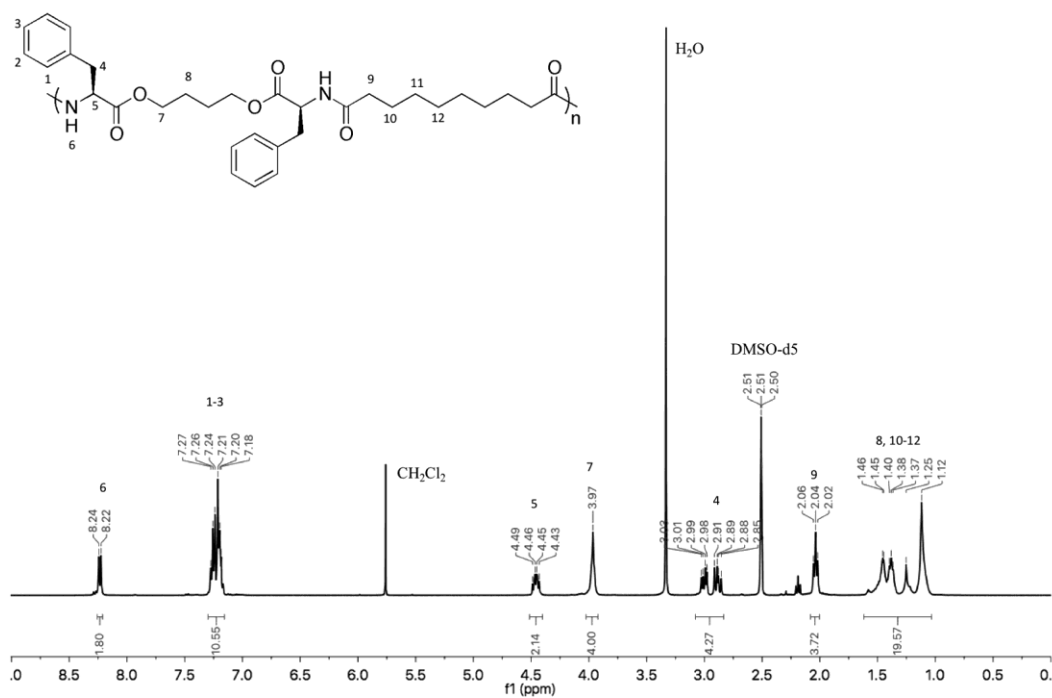
1. Maudens, P.; Jordan, O.; Allemann, E., Recent advances in intra-articular drug delivery systems for osteoarthritis therapy. *Drug Discov. Today* 2018, 23 (0), 1761-1775.
2. Larsen, C.; Østergaard, J.; Larsen, S. W.; Jensen, H.; Jacobsen, S.; Lindegaard, C.; Andersen, P. H., Intra-articular depot formulation principles: Role in the management of postoperative pain and arthritic disorders. *J. Pharm. Sci.* 2008, 97 (11), 4622-4654.
3. Malone, M. A.; Kaushik, N.; Waheed, A., Intra-articular steroids: How soon and how often after the first injection? *SM J Community Med* 2016, 2 (1), 1014.
4. Stephens, M. B.; Beutler, A. I.; O'Connor, F. G., Musculoskeletal injections: A review of the evidence. *Am. Family Phys.* 2008, 78 (8), 970-976.
5. Cheng, J.; Abdi, S., Complications of joint, tendon, and muscle injections. *Tech. Reg. Anesth. Pain Manag.* 2007, 11, 141-147.
6. Shan-Bin, G.; Yue, T.; Ling-Yan, J., Long-term sustained-released in situ gels of a water-insoluble drug amphotericin B for mycotic arthritis intra-articular administration: preparation, in vitro and in vivo evaluation. *Drug Dev. Ind. Pharm.* 2015, 41 (4), 573-582.
7. Betre, H.; Liu, W.; Zalutsky, M. R.; Chilkoti, A.; Kraus, V. B.; Setton, L. A., A thermally responsive biopolymer for intra-articular drug delivery. *J. Controlled Release* 2006, 115 (2), 175-182.
8. Petit, A.; Redout, E. M.; van de Lest, C. H.; de Grauw, J. C.; Muller, B.; Meyboom, R.; van Midwoud, P.; Vermonden, T.; Hennink, W. E.; Rene van Weeren, P., Sustained intra-articular release of celecoxib from in situ forming gels made of acetyl-capped PCLA-PEG-PCLA triblock copolymers in horses. *Biomaterials* 2015, 53, 426-36.

9. Petit, A.; Sandker, M.; Müller, B.; Meyboom, R.; van Midwoud, P.; Bruin, P.; Redout, E. M.; Versluijs-Helder, M.; van der Lest, C. H. A.; Buwalda, S. J.; de Leede, L. G. J.; Vermonden, T.; Kok, R. J.; Weinans, H.; Hennink, W. E., Release behavior and intra-articular biocompatibility of celecoxib-loaded acetyl-capped PCLA-PEG-PCLA thermogels. *Biomaterials* 2014, 35 (27), 7919-7928.
10. Thakkar, H.; Sharma, R. K.; Murthy, R. S. R., Enhanced retention of celecoxib-loaded solid lipid nanoparticles after intra-articular administration. *Drugs R & D* 2007, 8 (5), 275-285.
11. Morgen, M.; Tung, D.; Boras, B.; Miller, W.; Malfait, A.-M.; Tortorella, M., Nanoparticles for improved local retention after intra-articular injection into the knee joint. *Pharm. Res.* 2013, 30, 257-268.
12. Kumar, A.; Bendele, A. M.; Blanks, R. C.; Bodick, N., Sustained efficacy of a single intra-articular dose of FX006 in a rat model of repeated localized knee arthritis. *Osteoarthr. Cartil.* 2015, 23, 151-160.
13. Martin, C.; Winet, H.; Bao, J. Y., Acidity near eroding polylactide-polyglycolide in vitro and in vivo in rabbit tibial bone chambers. *Biomaterials* 1996, 17 (24), 2373-2380.
14. Suganuma, J.; Alexander, H., Biological response of intramedullary bone to poly-L-lactic acid. *J. Appl. Biomater.* 1993, 4 (1), 13-27.
15. Sukarto, A.; Amsden, B. G., Low melting point amphiphilic microspheres for delivery of bone morphogenetic protein-6 and transforming growth factor-beta3 in a hydrogel matrix. *J. Controlled Release* 2012, 158, 53-62.
16. Bajpayee, A. G.; Grodzinsky, A. J., Cartilage-targeting drug delivery: can electrostatic interactions help? *Nat Rev Rheumatol* 2017, 13 (3), 183-193.
17. De Wit, M. A.; Wang, Z.; Atkins, K. M.; Mequanint, K.; Gillies, E. R., Syntheses, characterization, and functionalization of poly(ester amide)s with pendant

amine functional groups. *Journal of Polymer Science Part A: Polymer Chemistry* 2008, 46 (19), 6376-6392.

## 6 Appendices

## 6.1 Appendix A: Supplemental Information for Chapter 2

Figure A.1:  $^1\text{H}$  NMR spectrum of PBSe ( $\text{DMSO-}d_6$ , 400 MHz).

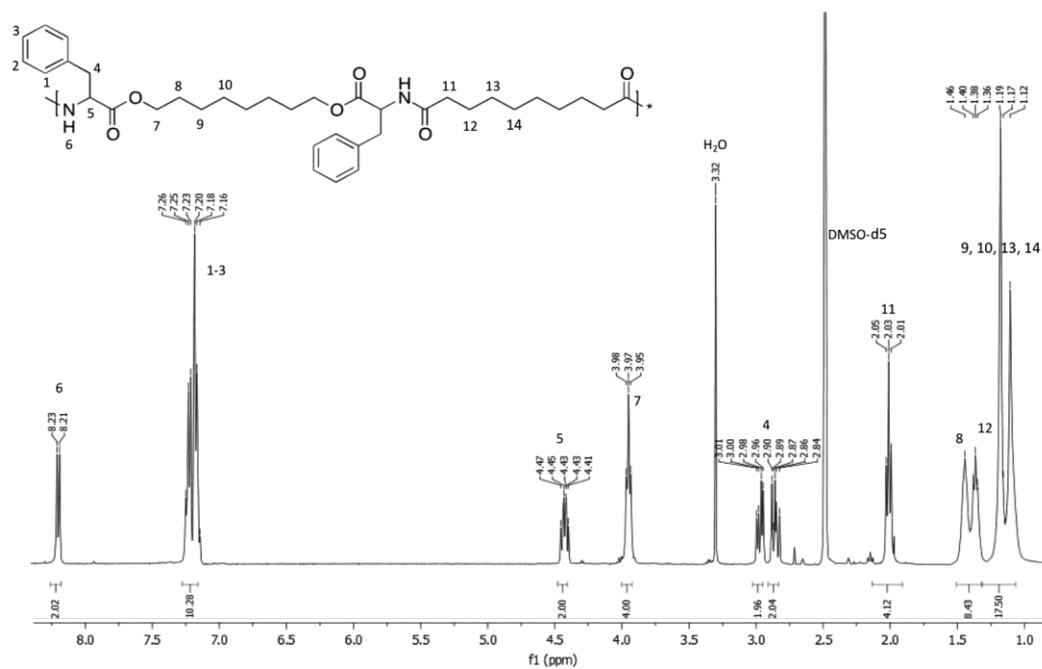


Figure A.2:  $^1\text{H}$  NMR spectrum of POSe (DMSO- $d_6$ , 400 MHz).

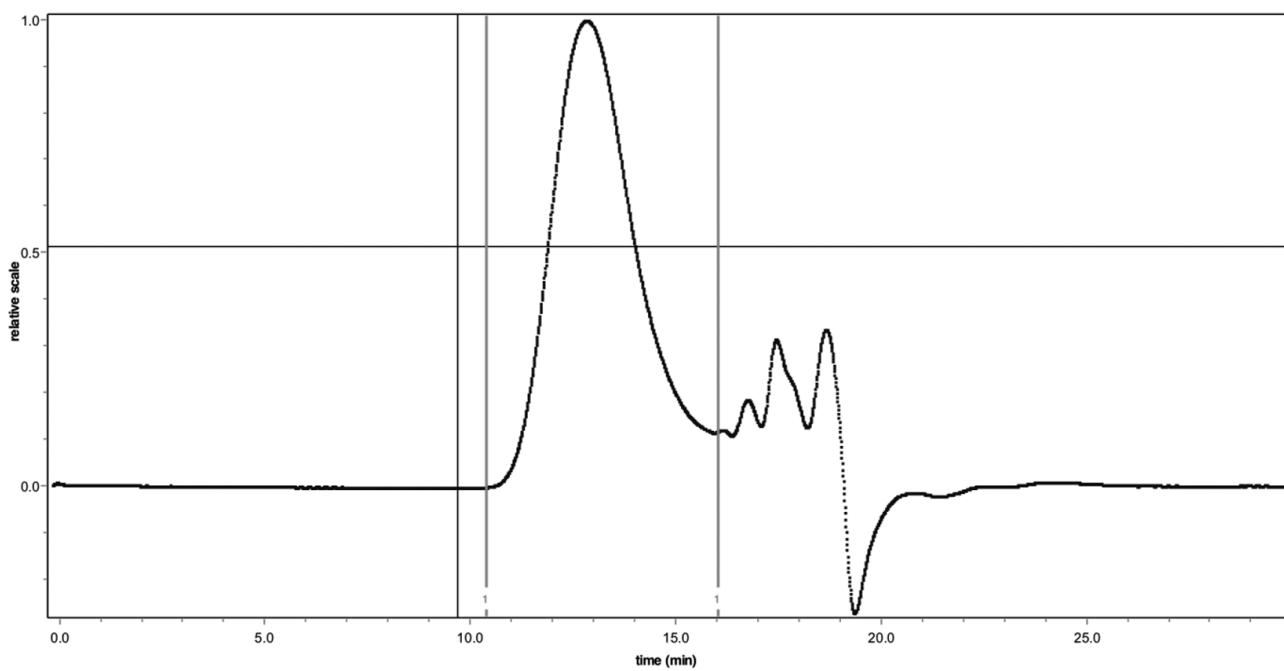


Figure A.3: SEC trace (DMF eluent containing 10 mM LiBr, refractive index detection) for PBSe ( $M_n = 30$  kg/mol and  $D = 2.0$ ).

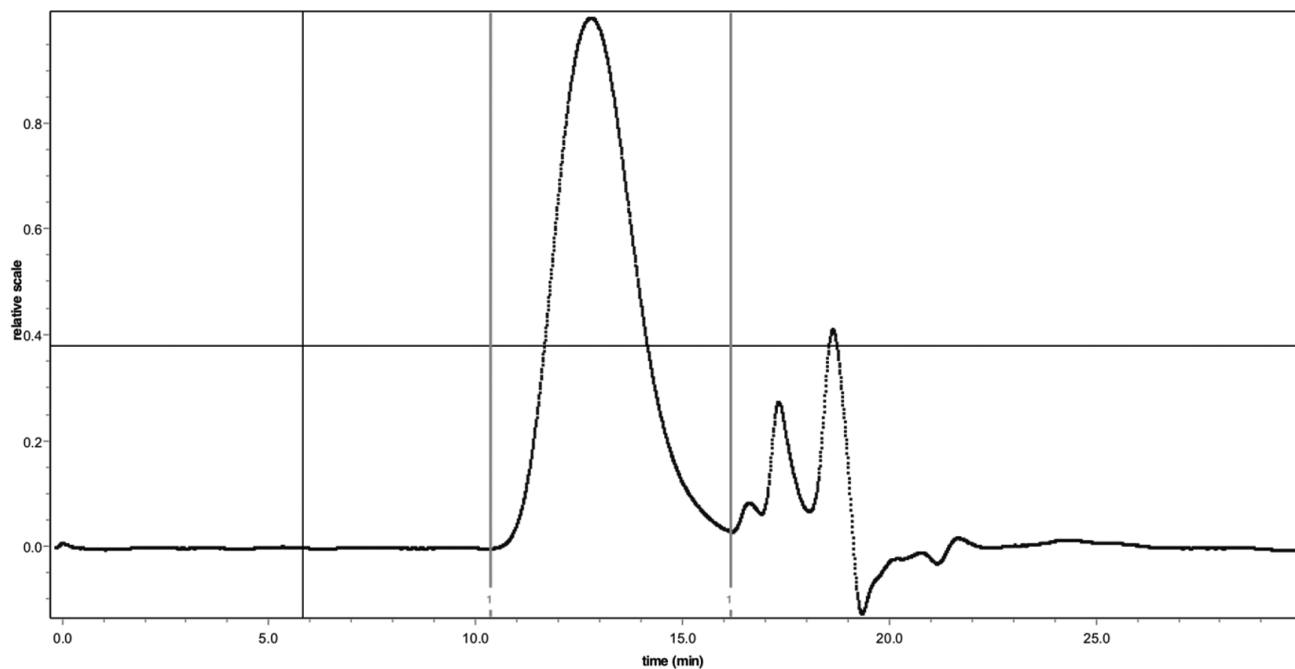


Figure A.4: SEC trace (DMF eluent containing 10 mM LiBr, refractive index detection) for POSe ( $M_n = 18$  kg/mol and  $D = 1.9$ ).

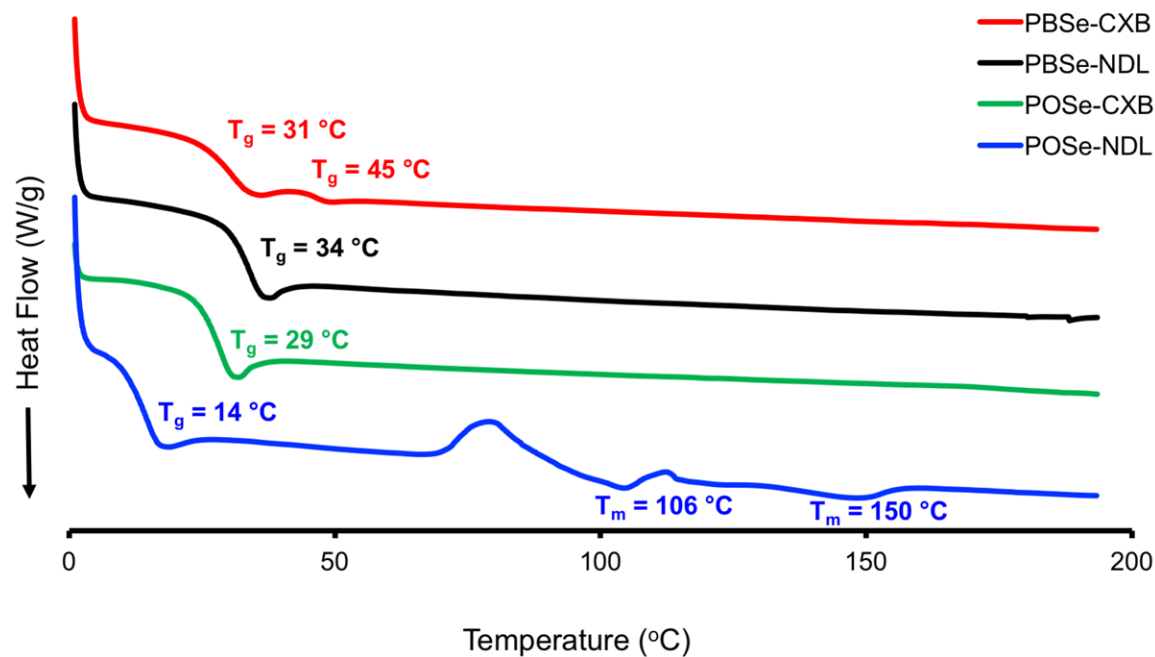


Figure A.5: DSC thermograms of the drug-loaded and non-drug-loaded bulk polymers that were prepared by the same melt pressing procedure as the samples for tensile testing

described in the manuscript. The multiple melting peaks for POSe-NDL have been commonly observed for PEAs and were attributed to the formation of different crystalline domains.<sup>1</sup> The exothermic peak preceding the melting transitions corresponds to cold crystallization.

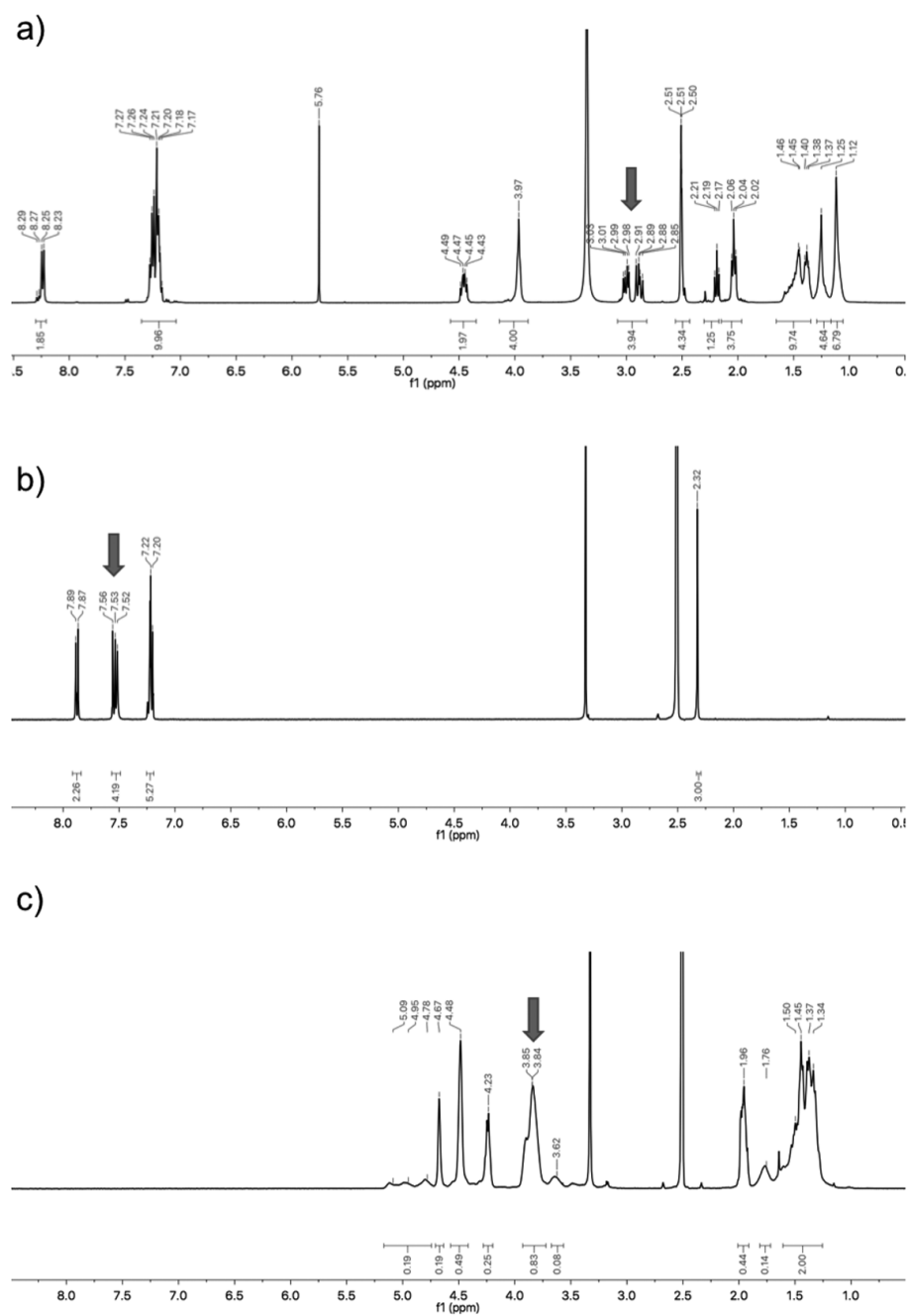


Figure A.6:  $^1\text{H}$  NMR spectra of a) PBSe, b) CXB and c) PVA ( $\text{DMSO-}d_6$ , 400 MHz).

Peaks used in the calculation of CXB loading are indicated with arrows. The same peaks were used for calculation of POSe drug loading and encapsulation efficiency.

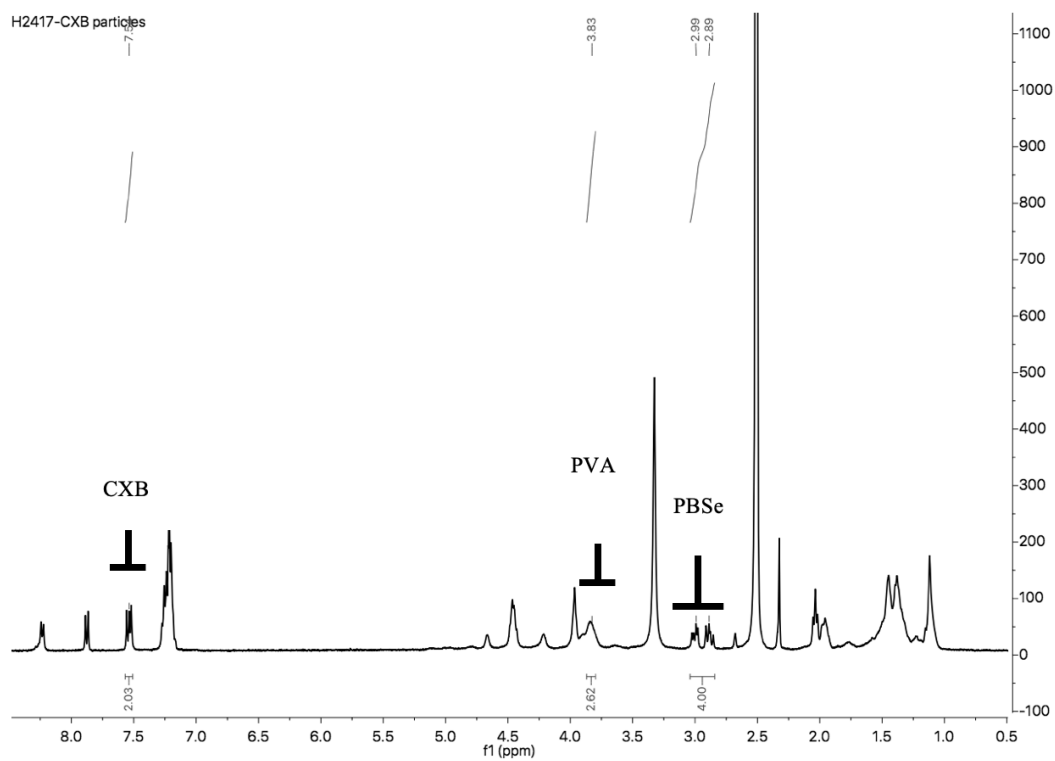
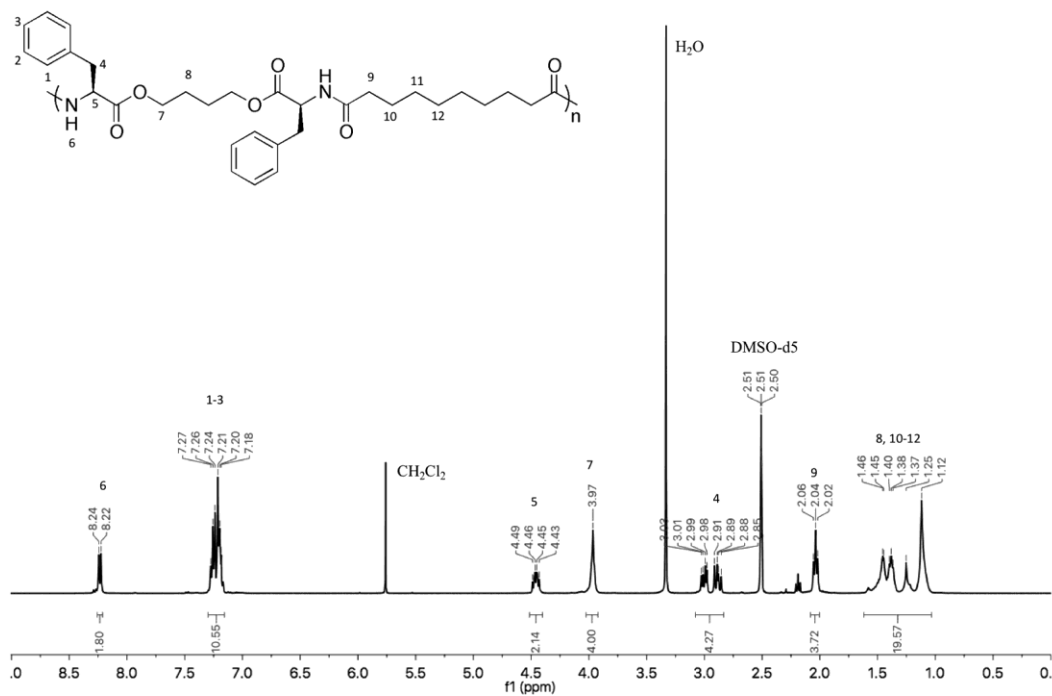


Figure A.7: Representative  $^1\text{H}$  NMR spectra of PBSe-CXB particles. Three peaks are identified and integrated for their use in calculation of CXB loading percentage and encapsulation efficiency.

## 6.2 Appendix B: Supplemental Information for Chapter 3

Figure B.1:  $^1\text{H}$  NMR spectrum of PBSe ( $\text{DMSO-}d_6$ , 400 MHz). As used in Chapter 3.

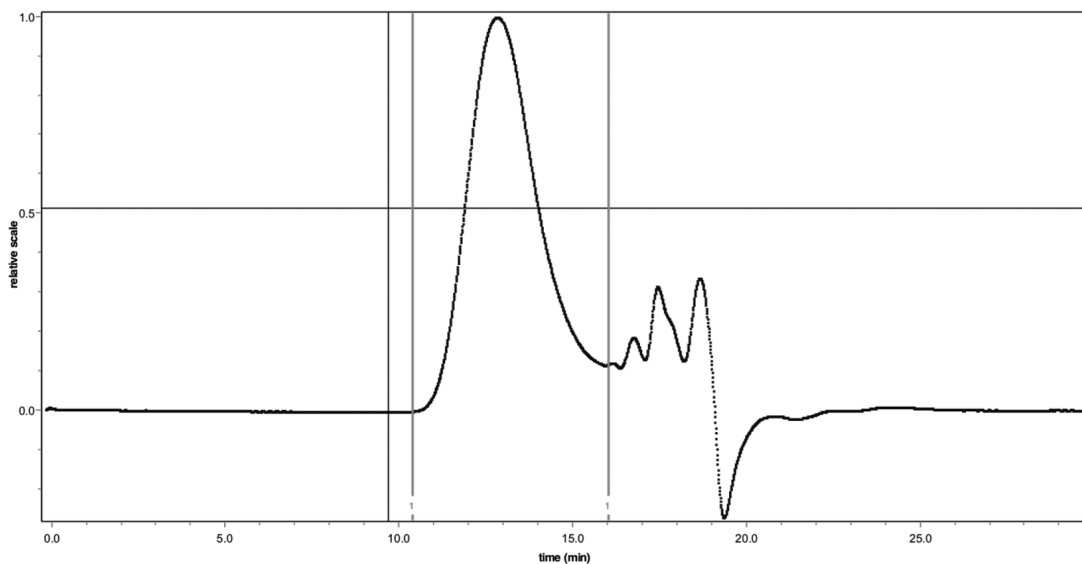


Figure B.2: SEC trace (DMF eluent containing 10 mM LiBr, refractive index detection) for PBSe ( $M_n = 30$  kg/mol and  $D = 2.0$ ). As used in chapter 3.

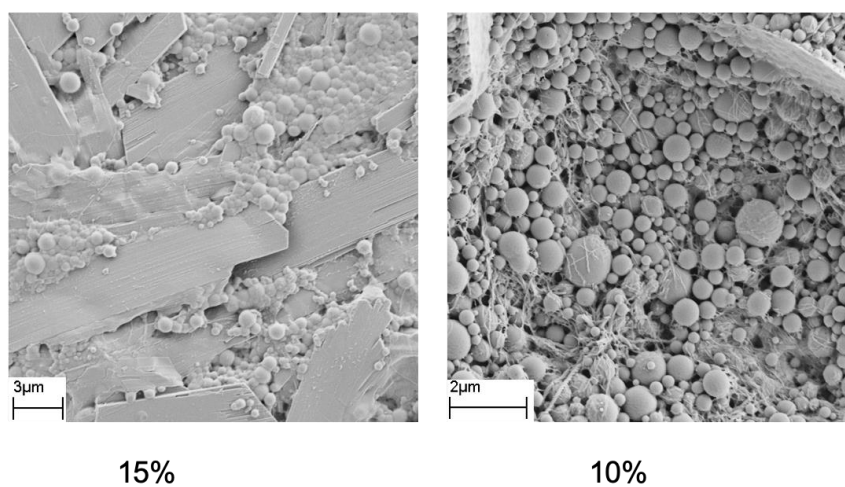


Figure B.3: Scanning electron micrographs of particle formations with varying amounts of theoretical GSK3787 drug loading percentages. Particles with 15 wt% of GSK3787 added to the dispersed phase of the emulsion did form, but in small numbers and with large amounts of excess, non particle, material (left). Particles with 10 wt% of GSK3787 did form, and were of spherical morphology and had a good size distribution, but had visible polymer remaining in the samples (right). Scanning electron micrographs of

PBSe-GSK3787 (A) and PBSe-NDL (B) particle preparations were taken using a Leo 1530 scanning electron microscope at a working distance of 6mm, at 2kV.

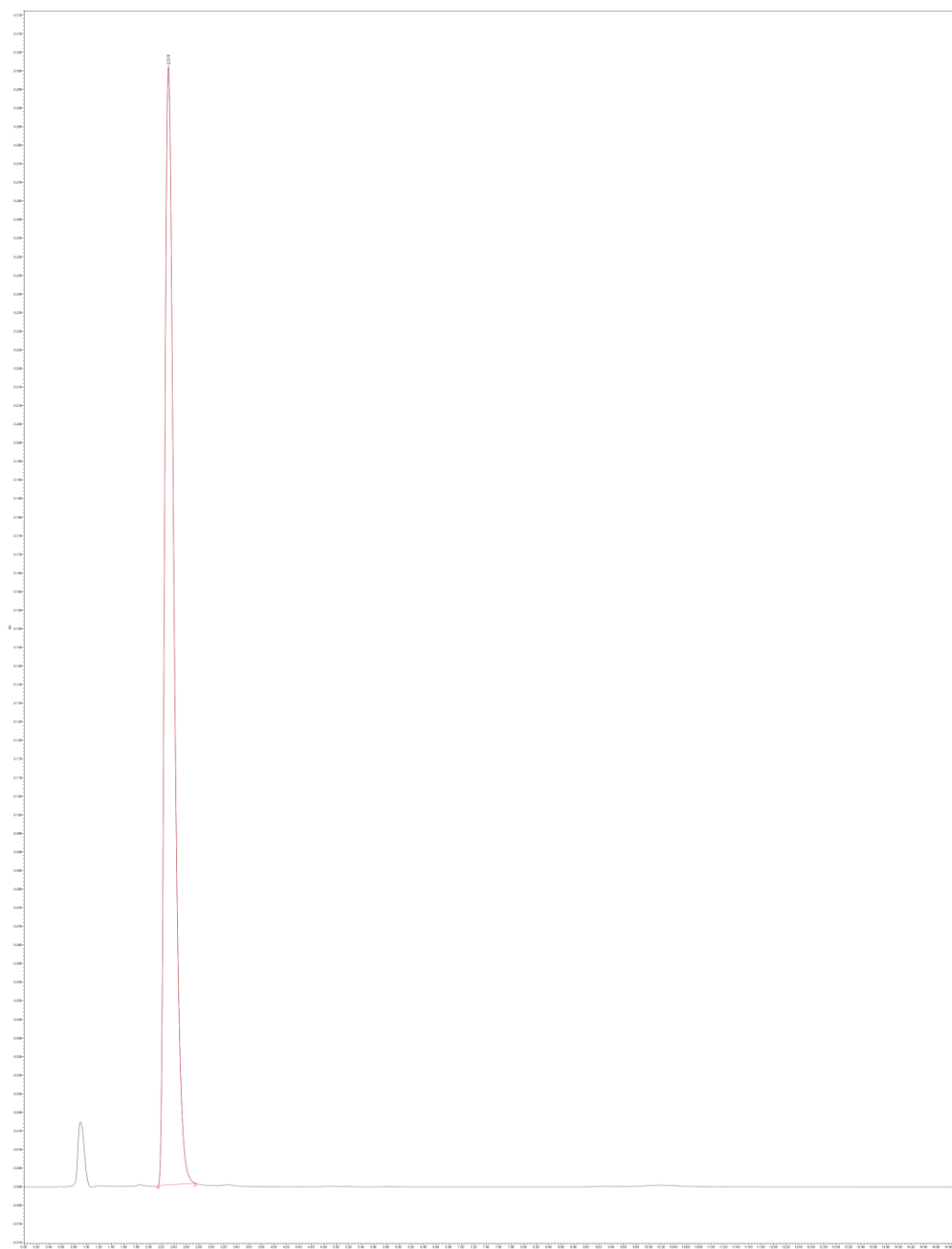


Figure B.4: Representative HPLC trace of GSK3787 as measured for drug loading and encapsulation efficiency of particles.

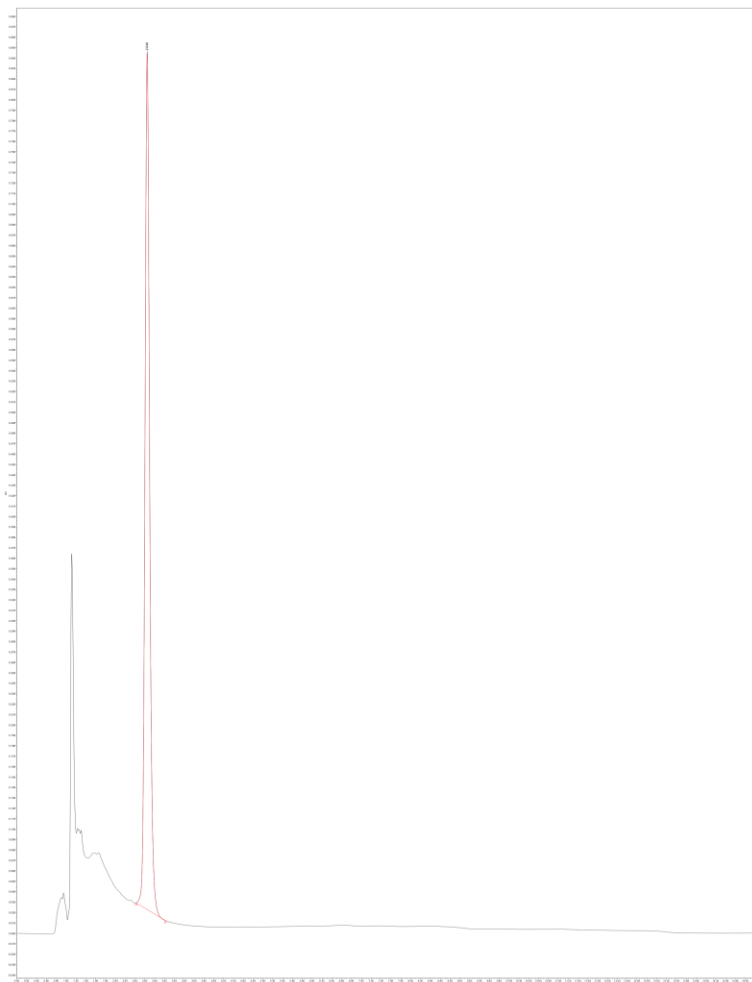


Figure B.5: Representative HPLC trace of GSK3787 release in PBS from PBSe-GSK3787, as measured for drug release studies from particles.

## 6.3 Appendix C: Supplemental Information for Chapter 4

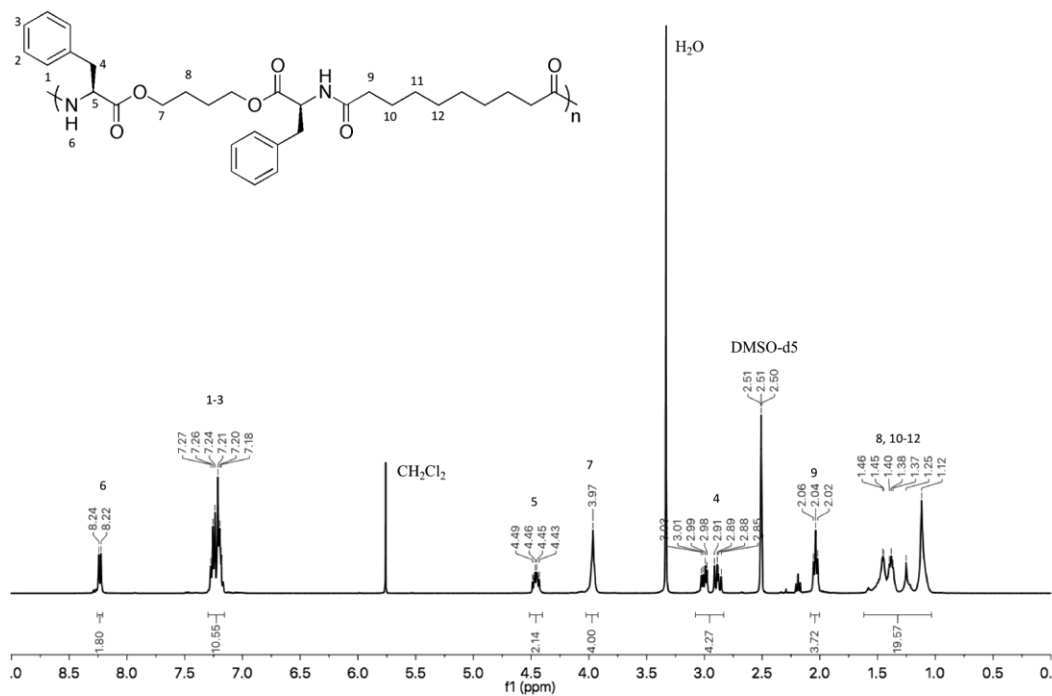


Figure C.1:  $^1\text{H}$ NMR spectrum of PBSe (400 Hz,  $\text{DMSO-}d_6$ ). As used in chapter 4.

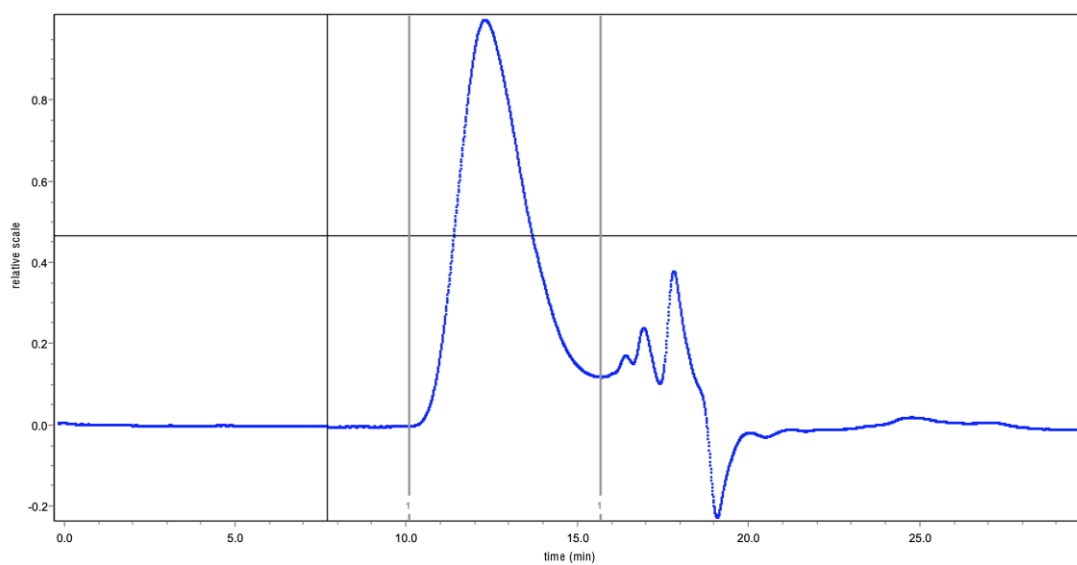


Figure C.2: SEC trace (DMF eluent containing 10 mM LiBr, refractive index detection) for PBSe ( $M_n = 28 \text{ kg/mol}$  and  $D = 2.1$ ). As used in chapter 4.

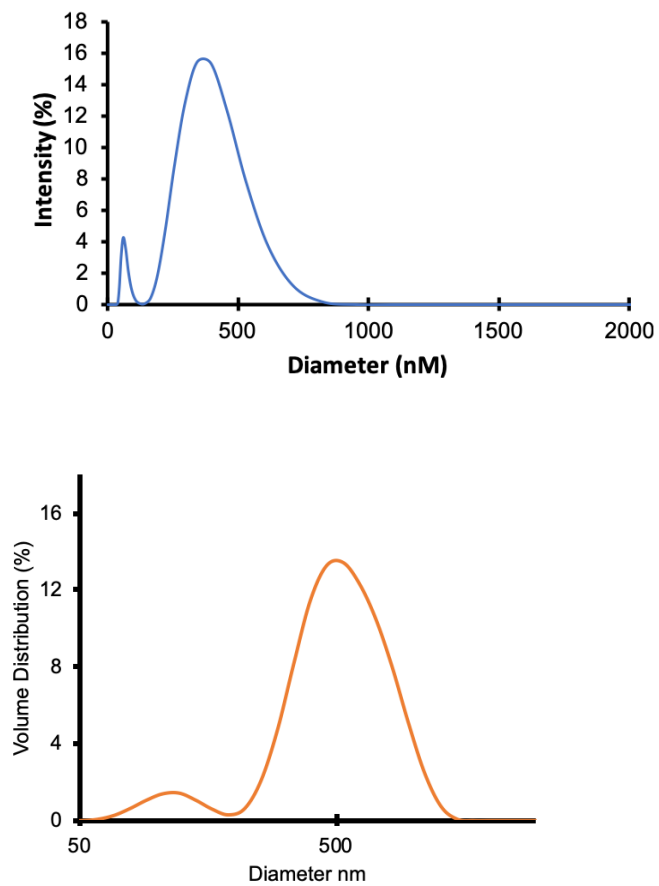


Figure C.3: Volume and intensity distributions of PBSe-GSK3787 particle diameters as measured by DLS. Intensity is shown on the top, volume distribution bottom. As used in chapter 4.

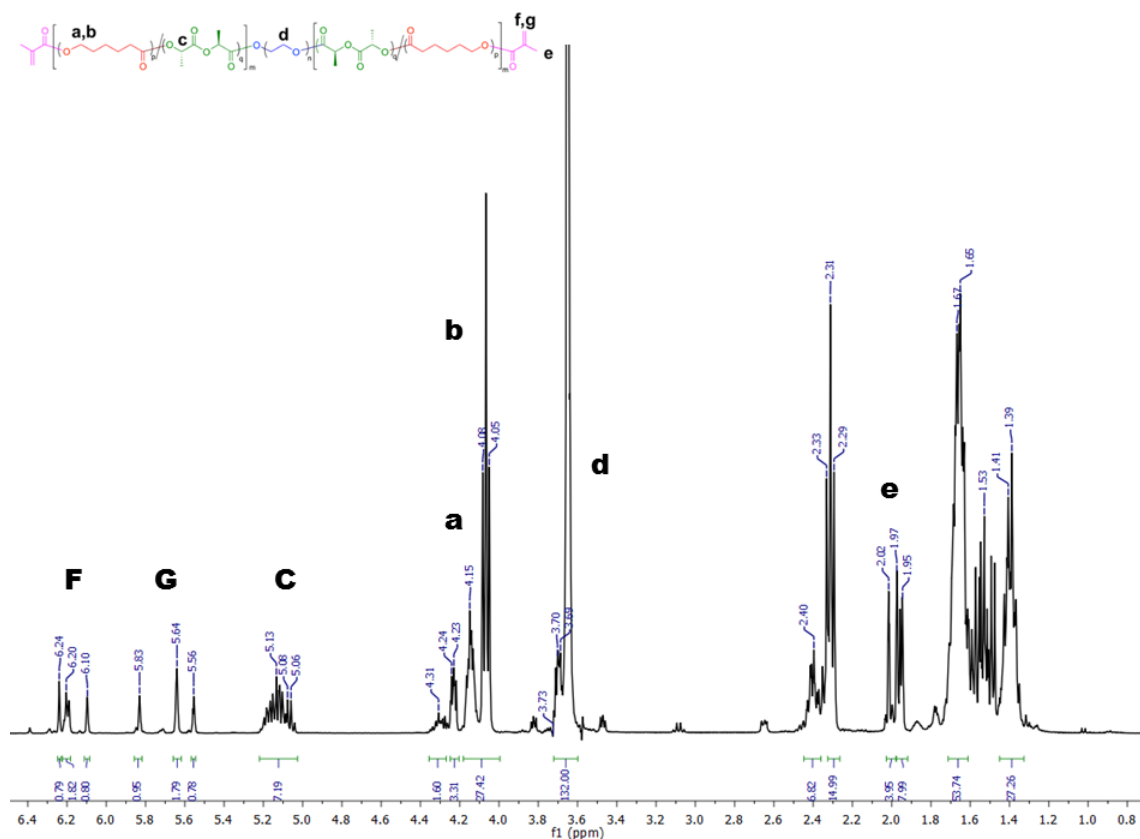
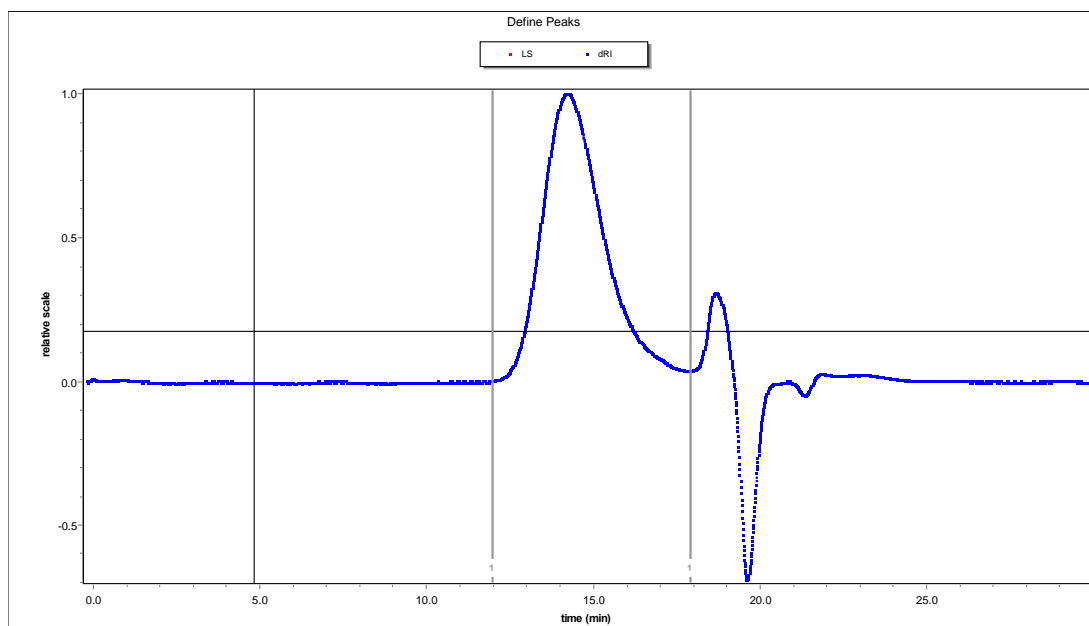
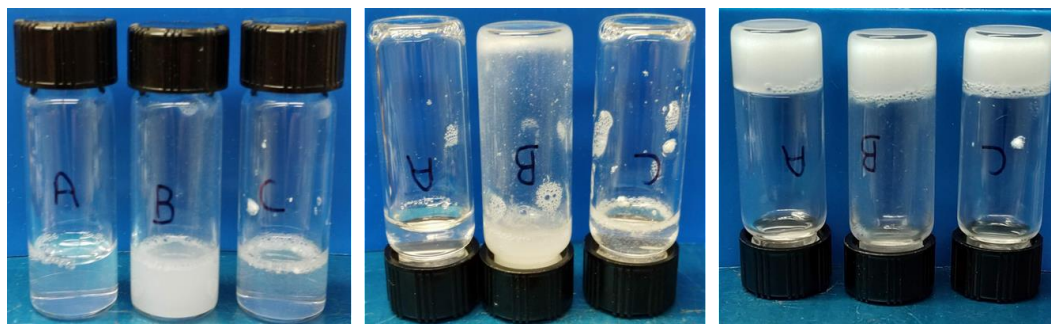


Figure C.4: <sup>1</sup>H NMR spectrum of MA-PCLA-PEG<sub>1500</sub>-PCLA-MA (400 Hz, CDCl<sub>3</sub>).

Assignment of peaks used in the calculation of the composition of the polymer are denoted by “a” which denotes the CH<sub>2</sub> adjacent to the lactide group, “b” denotes the CH<sub>2</sub> adjacent to a caprolactone unit, and “e” denotes a methacrylate unit. The PEG peak (d) was set to 132 corresponding to 1500 g/mol. The number of LA units was determined from the integration of the peak at 5.1 ppm and the number of CL units was calculated as the sum of the integrations of peaks at 4.03 and 3.98 ppm divided by 2 protons per repeat unit. Methacrylation % was calculated by comparing the integration of peaks labeled “e” to that of PEG “d”.



**Figure C.5.** SEC trace of MA-PCLA-PEG<sub>1500</sub>-PCLA-MA (DMF eluent containing 10 mM LiBr, refractive index detection) for PBSe ( $M_n = 5.4$  kg/mol and  $D = 2.2$ ). As used in chapter 4.



**Figure C.6:** Vial inversion tests of hydrogel systems. Vial A corresponds to control hydrogel, vial B corresponds to 10 wt% particle-in-hydrogel and vial C corresponds to 10 wt% GSK3787 in hydrogel. Left: Three hydrogel systems after the addition of KPS and TEMED, at 4 degrees. Center: Three hydrogel systems pre-gelation. Right: Three hydrogel systems with the addition of KPS and TEMED for physical crosslinking, post incubation for 30 minutes at 37 °C.

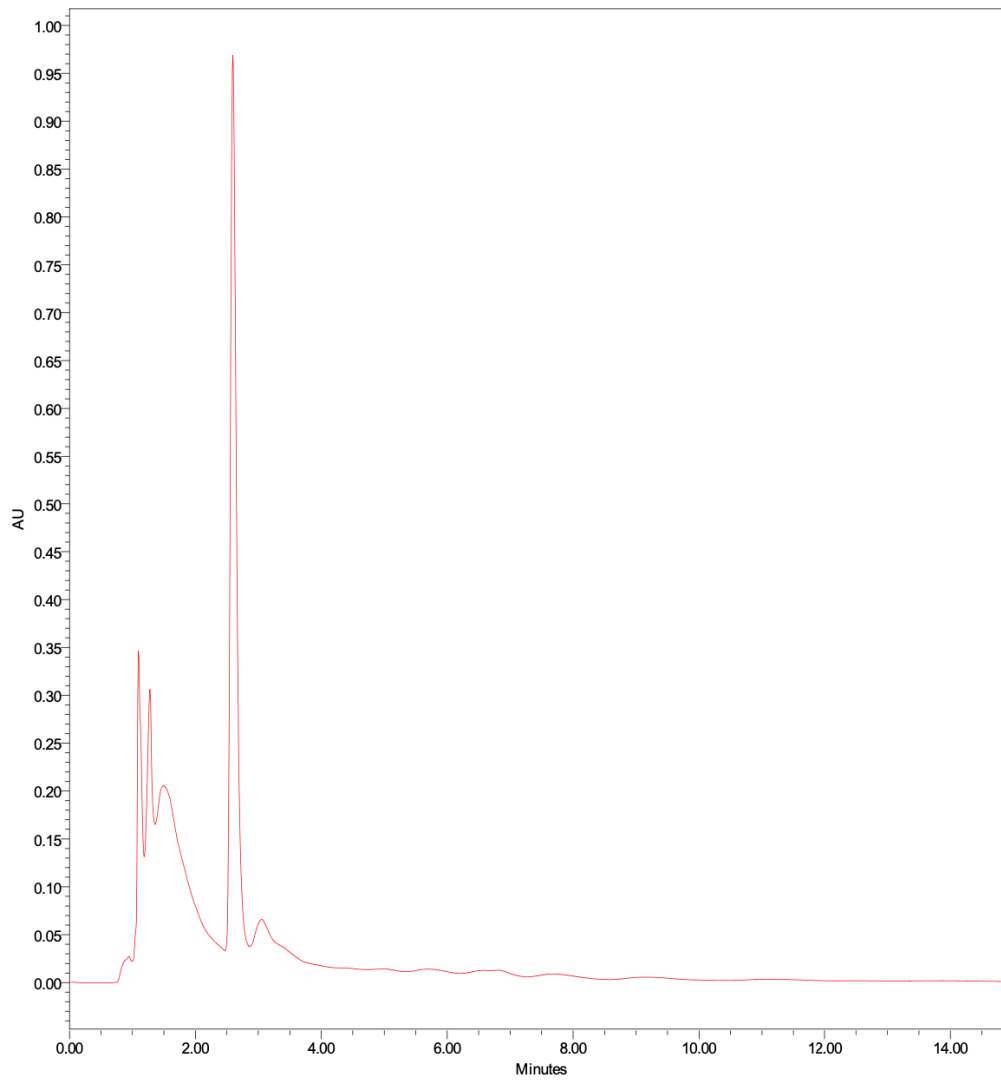


**Figure C.7:** Representative HPLC trace showing GSK3787 at 2.25 minutes retention time.

## 6.4 Appendix D: Permissions

### ELSEVIER LICENSE TERMS AND CONDITIONS

Dec 02, 2019

This Agreement between Ian Villamagna ("You") and Elsevier ("Elsevier") consists of your license details and the terms and conditions provided by Elsevier and Copyright Clearance Center.

License Number	4720811372875
License date	Dec 02, 2019
Licensed Content Publisher	Elsevier
Licensed Content Publication	Best Practice & Research Clinical Rheumatology
Licensed Content Title	Biomechanical factors in osteoarthritis
Licensed Content Author	Farshid Guilak
Licensed Content Date	Dec 1, 2011
Licensed Content Volume	25
Licensed Content Issue	6
Licensed Content Pages	9
Start Page	815
End Page	823
Type of Use	reuse in a thesis/dissertation
Portion	figures/tables/illustrations
Number of figures/tables/illustrations	1
Format	both print and electronic
Are you the author of this Elsevier article?	No
Will you be translating?	No
Title	Preparation of Intra-Articular Drug Delivery Systems
Institution name	University of Western Ontario
Expected presentation date	Jan 2020
Portions	Figure 1

Total **0.00 USD**  
Terms and Conditions

INTRODUCTION

**Figure D.1:** Permission for figure 1.1

## ELSEVIER LICENSE TERMS AND CONDITIONS

Dec 02, 2019

This Agreement between Ian Villamagna ("You") and Elsevier ("Elsevier") consists of your license details and the terms and conditions provided by Elsevier and Copyright Clearance Center.

License Number	4720820808927
License date	Dec 02, 2019
Licensed Content Publisher	Elsevier
Licensed Content Publication	Osteoarthritis and Cartilage
Licensed Content Title	Should subchondral bone turnover be targeted when treating osteoarthritis?
Licensed Content Author	M.A. Karsdal,D.J. Leeming,E.B. Dam,K. Henriksen,P. Alexandersen,P. Pastoureau,R.D. Altman,C. Christiansen
Licensed Content Date	Jun 1, 2008
Licensed Content Volume	16
Licensed Content Issue	6
Licensed Content Pages	9
Start Page	638
End Page	646
Type of Use	reuse in a thesis/dissertation
Portion	figures/tables/illustrations
Number of figures/tables/illustrations	1
Format	both print and electronic
Are you the author of this Elsevier article?	No
Will you be translating?	No
Title	Preparation of Intra-Articular Drug Delivery Systems
Institution name	University of Western Ontario
Expected presentation date	Jan 2020
Portions	Figure 1

Total	<b>0.00 USD</b>
Terms and Conditions	

**Figure C.2:** Permission for figure 1.3.

## ELSEVIER LICENSE TERMS AND CONDITIONS

Dec 02, 2019

This Agreement between Ian Villamagna ("You") and Elsevier ("Elsevier") consists of your license details and the terms and conditions provided by Elsevier and Copyright Clearance Center.

License Number	4718370002513
License date	Nov 29, 2019
Licensed Content Publisher	Elsevier
Licensed Content Publication	Carbohydrate Polymers
Licensed Content Title	Thermo-sensitive injectable hydrogel based on the physical mixing of hyaluronic acid and Pluronic F-127 for sustained NSAID delivery
Licensed Content Author	Young-seok Jung,Wooram Park,Hyejin Park,Deok-Keun Lee,Kun Na
Licensed Content Date	Jan 20, 2017
Licensed Content Volume	156
Licensed Content Issue	n/a
Licensed Content Pages	6
Start Page	403
End Page	408
Type of Use	reuse in a thesis/dissertation
Portion	figures/tables/illustrations
Number of figures/tables/illustrations	1
Format	both print and electronic
Are you the author of this Elsevier article?	No
Will you be translating?	No
Title	Preparation of Intra-Articular Drug Delivery Systems
Institution name	University of Western Ontario
Expected presentation date	Jan 2020
Portions	Scheme 1 (a) and (b) on page 404

Total **0.00 USD**  
Terms and Conditions

**Figure C.3:** Permission for figure 1.10.

12/2/2019

RightsLink - Your Account

## ELSEVIER LICENSE TERMS AND CONDITIONS

Dec 02, 2019

This Agreement between Ian Villamagna ("You") and Elsevier ("Elsevier") consists of your license details and the terms and conditions provided by Elsevier and Copyright Clearance Center.

License Number	4718370600456
License date	Nov 29, 2019
Licensed Content Publisher	Elsevier
Licensed Content Publication	Colloids and Surfaces B: Biointerfaces
Licensed Content Title	Injectable hydrogels for treatment of osteoarthritis – A rheological study
Licensed Content Author	Benjamin von Lospichl,Shabnam Hemmati-Sadeghi,Pradip Dey,Tilo Dehne,Rainer Haag,Michael Sittinger,Jochen Ringe,Michael Gradzielski
Licensed Content Date	Nov 1, 2017
Licensed Content Volume	159
Licensed Content Issue	n/a
Licensed Content Pages	7
Start Page	477
End Page	483
Type of Use	reuse in a thesis/dissertation
Portion	figures/tables/illustrations
Number of figures/tables/illustrations	1
Format	both print and electronic
Are you the author of this Elsevier article?	No
Will you be translating?	No
Title	Preparation of Intra-Articular Drug Delivery Systems
Institution name	University of Western Ontario
Expected presentation date	Jan 2020
Portions	Figure 1

Total **0.00 USD**  
Terms and Conditions

**Figure C.4:**Permission for Figure 1.11

License Number	4722230442104
License date	Dec 04, 2019
Licensed Content Publisher	John Wiley and Sons
Licensed Content Publication	JOURNAL OF BIOMEDICAL MATERIALS RESEARCH PART A
Licensed Content Title	Poly(ester amide) particles for controlled delivery of celecoxib
Licensed Content Author	Ian J. Villamagna, Trent N. Gordon, Mark B. Hurtig, et al
Licensed Content Date	Feb 22, 2019
Licensed Content Volume	107
Licensed Content Issue	6
Licensed Content Pages	9
Type of Use	Dissertation/Thesis
Requestor type	Author of this Wiley article
Format	Print and electronic
Portion	Full article
Will you be translating?	No
Title of your thesis / dissertation	Preparation of Intra-Articular Drug Delivery Systems
Expected completion date	Jan 2020
Expected size (number of pages)	1

Publisher Tax ID	EU826007151
Total	<b>0.00 USD</b>
Terms and Conditions	

**Figure C.5:** Permission to reprint “Poly(ester amide) particles for controlled delivery of celecoxib”, as seen in chapter 2.

## Curriculum Vitae

**Name:** Ian Villamagna

**Post-secondary Education and Degrees:** University of Nevada, Las Vegas  
Las Vegas, Nevada, USA  
2009-2013 B.S. Biology

Midwestern University  
Glendale, Arizona, USA  
2013-2015 Master of Biomedical Science

The University of Western Ontario  
London, Ontario, Canada  
2015- Ph.D. Biomedical Engineering

**Honours and Awards:** Western Graduate Research Scholarship  
2015-2019

NSERC Create CONNECT! Scholarship  
2015-2019

Western Bone and Joint Transdisciplinary Award  
2014-2018

**Related Work Experience** Graduate Teaching Assistant  
The University of Western Ontario  
2015-2019

Internship  
Eupraxia Pharmaceuticals  
Victoria, British Columbia, Canada  
2017

**Publications:**

1. **Villamagna, I. J.**; Gordon, T. N.; Hurtig, M. B.; Beier, F.; Gillies, E. R., Poly(ester amide) particles for controlled delivery of celecoxib. *J Biomed Mater Res A* **2019**, *107*, 1235-1243.
2. Prince, D. A.; **Villamagna, I. J.**; Hopkins, C. C.; de Bruyn, J. R.; Gillies, E. R., Effect of drug loading on the properties of temperature-responsive polyester–poly(ethylene glycol)–polyester hydrogels. *Polymer International* **2019**, *68*, 1074-1083.
3. Prince, D. A.; **Villamagna, I. J.**; Borecki, A.; Beier, F.; de Bruyn, J. R.; Hurtig, M.; Gillies, E. R., Thermoresponsive and Covalently Cross-Linkable Hydrogels for Intra-Articular Drug Delivery. *ACS Applied Bio Materials* **2019**, *2*, 3498-3507.
4. **Villamagna, I. J.**; McRae, D. M., Borecki, A.; Lagune-Labarthet, F.; Beier, F.; Gillies, E.R., (In Press) GSK3787-loaded Poly(ester amide) particles for Intra-articular Drug Delivery. *Polymers* **2019**.